2900-121-T

Report of Project MICHIGAN

POLARIZATION, MICROWAVE DISPERSION, AND LOSS IN HIGH-PERMITTIVITY FERROELECTRICS

HOWARD DIAMOND

January 1960

Willow Run Laboratories
THE UNIVERSITY OF MICHIGAN
Ann Arbor, Michigan

DISTRIBUTION OF REPORTS

Distribution control of Project MICHIGAN Reports has been delegated by the U. S. Army Signal Corps to:

Commanding Officer
U. S. Army Liaison Group Project MICHIGAN
Willow Run Laboratories
Ypsilanti, Michigan

It is requested that information or inquiry concerning distribution of reports be addressed accordingly.

The work reported herein was carried on by the Willow Run Laboratories for the U. S. Army Signal Corps under Project MICHIGAN, Contract No. DA-36-039 SC-78801. The experimental work was initially supported by the U. S. Air Force Office of Scientific Research and The National Science Foundation. University contract administration is provided to the Willow Run Laboratories through The University of Michigan Research Institute.

PREFACE

Project MICHIGAN is a continuing research and development program for advancing the Army's long-range combat-surveillance and target-acquisition capabilities. The program is carried out by a full-time Willow Run Laboratories staff of specialists in the fields of physics, engineering, mathematics, and psychology, by members of the teaching faculty, by graduate students, and by other research groups and laboratories of The University of Michigan.

The emphasis of the Project is upon basic and applied research in radar, infrared, acoustics, seismics, information processing and display, navigation and guidance for aerial platforms, and systems concepts. Particular attention is given to all-weather, long-range, high-resolution sensory and location techniques, and to evaluations of systems and equipments both through simulation and by means of laboratory and field tests.

Project MICHIGAN was established at The University of Michigan in 1953. It is sponsored by the U. S. Army Combat Surveillance Agency of the U. S. Army Signal Corps. The Project constitutes a major portion of the diversified program of research conducted by the Willow Run Laboratories in order to make available to government and industry the resources of The University of Michigan and to broaden the educational opportunities for students in the scientific and engineering disciplines.

Progress and results described in reports are continually reassessed by Project MICHIGAN. Comments and suggestions from readers are invited.

Robert L. Hess
Technical Director
Project MICHIGAN

FOREWORD

Large-scale electronic systems in the past decade have made increasing demands on the circuit designer to produce better high-frequency amplifier devices, especially of the low-noise microwave type. Recent techniques have emphasized the development of the so-called solid-state amplifiers, of which the ruby maser is an example. Many investigators in this country have explored the possibility of applying semiconductor diodes, ferrites, and ferroelectrics to parametric amplifiers, and some limited success has already been obtained with the diodes. Success with the ferroelectrics has been somewhat marginal, partially because presently available materials appear to dissipate too much energy for application at microwave frequencies. In order for more rapid progress to be made in improving ferroelectric materials, a more thorough understanding of the nonlinear processes and loss mechanisms for these substances is required. Moreover, there is a need for more data on the microwave dielectric properties of the ferroelectric materials. It is the purpose of this investigation to obtain such microwave data and also to study the mechanisms of the change in permittivity with electric field in certain types of ferroelectrics. It is this later property which is fundamental in the parametric devices.

This investigation as a doctoral thesis was initially suggested by Dr. H. W. Welch, formerly of the Electrical Engineering Department at The University of Michigan. The problem as originally stated was to investigate the rather pronounced microwave dispersion of the permittivity observed in $BaTiO_3$ ceramics. (This is shown in Fig. 5 of this report.) Upon considering the possible reasons for this effect, the question of the role of ferroelectric domains was raised. Subsequent investigations, both experimental and analytical, indicated that the nonlinear processes involving the large-field permittivity in ferroelectric ceramics could not be made consistent with the idea of domain growth or alignment. The work on a theory of the nonlinearity of this class of ferroelectrics was expanded, and consequently what originally appeared to be a side issue became a rather extensive research activity. This investigation constitutes Sec. 1 and 2 of the report.

Professor Gunnar Hok, who served as chairman of the doctoral committee, contributed active support and helpful discussions during this work. Dr. Betzalel Avitzur aided in programming an IBM 650 electronic computer for numerically

evaluating some of the integrals which appear in Sec. 3. Miss Viola Chang deserves special mention for her invaluable aid in the preparation of ceramics and single crystals used for the experiments, and also for her help in reducing the microwave data. The many discussions with Miss Chang served as a basis for formulating several of the experiments on the ferroelectric ceramics.

CONTENTS

FIGURES

FIGURES (Continued)

TABLES

ABSTRACT

The purpose of this study is to investigate, by analysis of experimental data, polarization, dispersion, and loss processes in high-permittivity ferroelectrics. The study proceeds from the observation that, according to published data, polycrystalline $BaTiO_3$ and similar compositions show strong relaxation in permittivity at microwave frequencies. This phenomenon is shown to be generally related to polarization and loss properties of the dielectric. Processes of particular interest in accounting for the microwave relaxation are: (a) domain effects, (b) possible dipolar or molecular polarization, and (c) mechanical effects produced by piezoelectric and electrostrictive coupling.

In connection with category (a), measurements were made of hysteresis properties and experiments were conducted on ceramic samples, in which the permittivity was measured parallel and transverse to strong electric fields. It is concluded that domains are immobile in the ceramic grains. In order to account for nonlinearity in the permittivity under the action of an electric field, a phenomenological theory is postulated. Each grain in the ceramic is presumed to be described by a free-energy function of the form given by Devonshire for $BaTiO_3$ single crystals. The free-energy function takes into account a transition between a ferroelectric and a nonferroelectric state at a critical temperature (the Curie temperature). For a polycrystalline ferroelectric the transition temperatures of the crystallites are assumed to be given by a Gaussian distribution about some operating temperature. The domains are presumed immobile in those grains in the distribution which are ferroelectric. The free-energy function predicts that a ferroelectric state will be induced by the field in those grains which are not ferroelectric, and it is assumed that the polar axis is induced along the field direction. This model, when analyzed, leads to theoretical results which correlate remarkably well with experimental data.

In connection with category (b), measurements were made of the permittivities of single crystals of $BaTiO_3$ at microwave frequencies with the polar axis both parallel and transverse to the signal fields. In contrast with the results for ceramics, the single crystals showed no relaxation at microwave frequencies.

In connection with category (c), mechanical effects on the permittivity were analyzed. These effects are important because at sufficiently high frequencies a dielectric may behave as if it were mechanically clamped. Single crystals and

polycrystalline samples have been measured on a dielectric spectrometer over a frequency range from 0.5 mc to 200 mc. Dimensional resonnances were observed at the low-frequency end of the spectrum. Above frequencies where dimensional resonances are significant, the permittivity was reduced to about one half of that at the low-frequency limit. This result is consistent with predictions based on Devonshire's free-energy function. It is further shown that a loss mechanism can result in a significant dielectric relaxation. The losses are considered to result from mechanical interactions at domain walls and grain boundaries.

The conclusions that may be drawn from this work are as follows.

(1) The field sensitivity of the incremental permittivity of polycrystalline ferroelectrics is not a domain effect, but results from an induced ferroelectric state in nonferroelectric grains.

(2) Nonlinear permittivity under electric fields must necessarily be accompanied by substantial thermal sensitivity.

(3) Orientation of the domains does not contribute to microwave dispersion.

(4) Molecular or dipolar relaxation does not occur at microwave frequencies for $BaTiO_3$ single crystals. Therefore, this is not a mechanism for dispersion in the ceramic.

(5) Dielectric loss as well as piezoelectric and electrostrictive activity would result in microwave dispersion in high-permittivity ferroelectrics.

1
INTRODUCTION

1.1. OBJECTIVES

The objectives of this investigation are twofold: (1) to investigate both experimentally and theoretically the mechanism by which the small-signal permittivity changes with electric field and temperatures; the analysis is carried out using essentially a macroscopic model; and (2) to investigate the microwave relaxation in the permittivity which is observed for several ferroelectric ceramics. The question of a dielectric loss mechanism is also considered with regard to an explanation for the observed microwave relaxation. Attention is centered on those ferroelectrics of the high-permittivity type – typically the so-called perovskite class of ferroelectrics of which $BaTiO_3$ is the most familiar member.

The terms introduced in the present subsection are defined and clarified in the succeeding subsections. The reader already familiar with these terms and with the general concepts of the classical dielectric theories may proceed immediately to Sec. 2 of this report.

1.2. REVIEW OF SOME FERROELECTRIC PROPERTIES

Ferroelectricity is defined as that property of certain dielectric materials of exhibiting a spontaneous electric polarization in the absence of an external field. In addition, there is a further condition that must be fulfilled if a given dielectric is to be regarded as a ferroelectric, and this condition is that the direction of spontaneous polarization may be reversed upon the application of an external field of sufficient intensity and reversed polarity. Some classes of dielectrics, such as pyroelectrics and the so-called "electrets," show a spontaneous polarization, but this polarization cannot be changed or switched by an external electric field; i.e., the polarization is in a sense "frozen in"; therefore, these materials are not classified as ferroelectrics. As a consequence of the property of the polarization direction switching under the influence of a suitable electric field, the ferroelectrics display a dielectric hysteresis loop in polarization, P vs. electric field E. This effect, together with the property in most of these substances of having a rather large permittivity, has resulted in the coining of the term "ferroelectricity" to describe the analogue to some of the properties of magnetic substances (i.e., ferromagnetic properties).

Ferroelectricity was first observed in Rochelle salt ($NaKC_4H_4O_6 \cdot 4H_2O$) as early as 1921 by Valasek (Ref. 1). The discovery, by independent investigators in the U. S. (Ref. 2) and U. S. S. R. (Ref. 3) during World War II, of the remarkable dielectric properties of the ferroelectric, barium titanate ($BaTiO_3$), stimulated the active research seen in this field today. $BaTiO_3$ belongs to the class of ferroelectrics known as the perovskites, since all members of this class have the crystal structure of the mineral perovskite ($CaTiO_3$). The crystal structure for the members of this class is shown in Fig. 1 with the definitions of the crystallographic directions relative to the polarization direction shown on the figure (it will be necessary to refer constantly to these definitions in the course of this report). It is important to note that the barium titanate structure is the simplest of any known ferroelectric, and this imparts to this material an especially significant role in the development of theories of ferroelectricity.[1] In addition to the existence of dielectric hysteresis loops and the large permittivities mentioned above, there are some further properties of ferroelectrics which

[1] The structure of WO_3 is even simpler and consists of the $BaTiO_3$-type lattice with the Ba sites vacant. However, WO_3 is actually an antiferroelectric; that is, the structure has alternate lines or cells of opposite spontaneous polarization. The net result is cancellation of any externally observable polarization. This is similar to the antiferromagnetic state of some magnetic materials.

have to be taken into account in this study. All ferroelectric materials contain at least one ion in an asymmetric position in the crystal lattice, and, since these dielectrics are also polar, they are consequently strongly piezoelectric. (In fact, one of the largest technological applications of $BaTiO_3$-type ceramics is the utilization of the piezoelectric effects in transducer elements such as phono pickups, submarine detectors, etc.) Even in the symmetric nonferroelectric phase where permittivities are rather large but the crystal is not piezoelectric, one would expect large values of electrostriction, since large polarizability in an ionic lattice implies large displacements of ions, and electrostriction and piezoelectric effects thus would be salient factors in an analysis of dielectric losses in these ferroelectrics. Due to the piezoelectric effect in the ferroelectric state, the permittivity for a free crystal is expected to be considerably different from that for a mechanically clamped crystal. For fields of frequency much higher than the mechanical resonant modes, the crystal would then behave as if it were effectively mechanically "clamped."

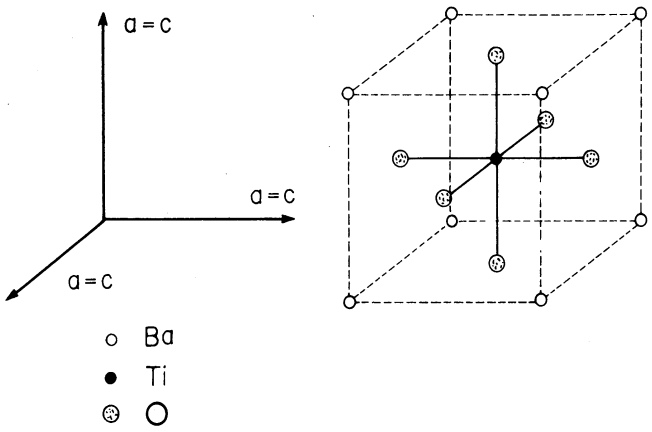

The Crystal Structure of $BaTiO_3$ and Similar Perovskite-Type Ferroelectrics in the Cubic (Nonferroelectric) Phase

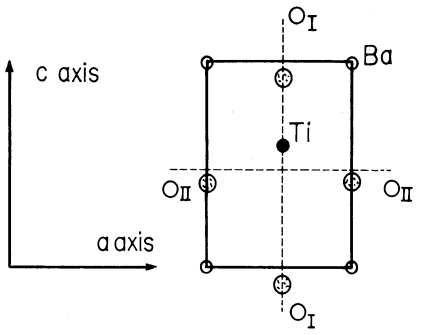

$\delta Ti = + 0.06$ Angstrom

$\delta O_I = - 0.09$ Angstrom

$\delta O_{II} = - 0.06$ Angstrom

The c Crystalographic Axis is the Polar Axis

Schematic of Shift in Ionic Positions of $BaTiO_3$ in the Tetragonal (Ferroelectric) Phase (After Neutron Diffraction Data of Frazer, Danner, and Pepinsky, Ref. 4)

FIG. 1. CRYSTAL STRUCTURES OF $BaTiO_3$

Figure 2 shows the effects of temperature on the lattice dimensions in the perovskite-like structure of $BaTiO_3$ and also on the values of permittivity along specific crystalline axes. Comparison of the two curves shows a rather remarkable effect. The tetragonal distortion from the perfect cubic structure amounts to only about 1% at room temperature. That is, the difference between the c-dimension and the a-dimension at room temperature is only 0.04 angstrom, with a unit-cell dimension of about 4 angstroms. At the same time, the isotropic permittivity observed in the cubic state becomes in the ferroelectric tetragonal phase extremely

anisotropic, the permittivity in the c-direction being only of the order of 100 while the permittivity in the a-direction (i.e., transverse to the polar axis) is about 4000. And this happens with only a 1% distortion of the unit cell from the nonferroelectric phase.

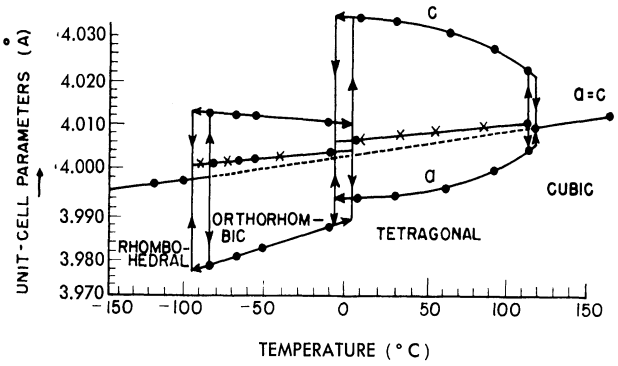

(a)

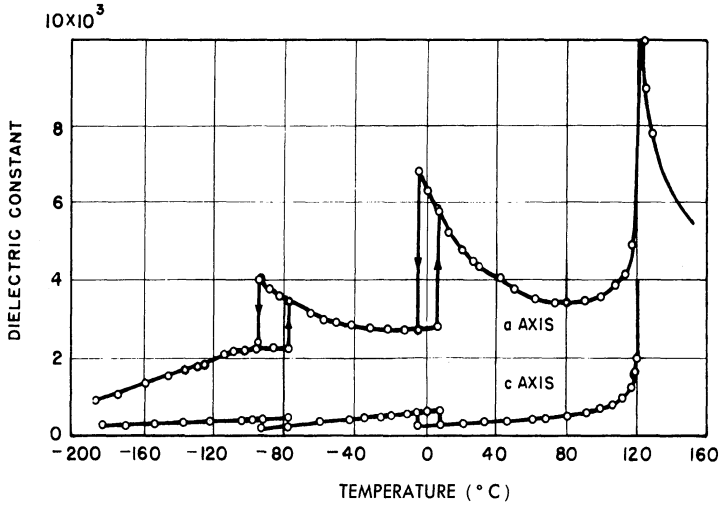

(b)

FIG. 2. EFFECT OF TEMPERATURE ON THE LATTICE DIMENSIONS AND PERMITTIVITY OF $BaTiO_3$. (a) Lattice dimensions (after Kay and Vousden, Ref. 5). (b) Dielectric constants of a single crystal (after Merz, Ref. 6 and 7). The transition from tetragonal ferroelectric to cubic nonferroelectric at 120°C is called the Curie point as for magnetic materials. The dielectric constant above 120°C follows a Curie-Weiss law.

One further property of the ferroelectrics that must be noted is that a given crystal tends to break up into many domains. A domain is defined as a region within a ferroelectric crystal in which the direction of the spontaneous polarization is the same throughout. This behavior is similar to that of the ferromagnetic materials; however, there are some very striking differences between the ferromagnetic and ferroelectric domains. Since there are no isolated magnetic poles, ferromagnetic domains tend to form in such a way that they provide paths of

closed flux. Both 90° and 180° walls exist, and the transition from one wall orientation to another takes place over hundreds or thousands of lattice constants. In ferroelectric domains, isolated charges are possible, and the domains do not necessarily have to form closed flux linkages. The domains tend to be thin and needle-like with both 90° and 180° walls possible. The ferroelectric domain walls are only one or two lattice constants thick.

In the above discussion we have considered some properties of the ferroelectrics, especially in regard to those characteristics in which they differ from the usual dielectric materials. These properties certainly have to be taken into account when dealing with the polarization or permittivity of the ferroelectrics, for both small-field and large-field effects. Indeed, the question arises as to just how one can define a permittivity for these materials when not only is the relationship between D (the electric displacement) and E (the electric field) strongly nonlinear, but the D is not a single-valued function of E because of the dielectric hysteresis. As has been pointed out by Jaynes (Ref. 8), one has to be extremely careful to define what is meant by the term linearity when time-varying fields are applied. Also, the notions of nonlinearity and dispersion have to be distinguished. In the following paragraphs, the definitions of these concepts essential to this study are established.

Since $BaTiO_3$ is anisotropic, D is related to E via a tensor permittivity.

$$D_i = \epsilon_{ij} E_j, \tag{1.1}$$

where the convention of summation over repeated indices is used. For the case of $BaTiO_3$ in the tetragonal ferroelectric state, as for other perovskite-like dielectrics in corresponding states, the $\epsilon_{11} = \epsilon_{22} = \epsilon_a$, and $\epsilon_{33} = \epsilon_c$, the off-diagonal terms being zero. This is referred to the crystal axes defined in Fig. 1. From classical theory the polarization is related to the field[2] via

$$P = D - E = (\epsilon_r - 1)\epsilon_o E. \tag{1.2}$$

It is often convenient to define P in terms of the field directly through the electric susceptibility, χ. Thus the relationship corresponding to Eq. (1.1) between polarization and field is

$$P_i = \chi_{ij} E_j, \tag{1.3}$$

where

$$\chi_{ij} = (\epsilon_{ij} - 1)\epsilon_o \cong \epsilon_{ij}\epsilon_o, \tag{1.4}$$

[2] In the notation in this section we use ϵ_r as the relative permittivity and ϵ_o as the permittivity of vacuum.

for $\epsilon_{ij} >> 1$. One takes the point of view here that, at least for the study of crystalline lattice, (i.e., from the so-called microscopic viewpoint), the variables P (the dipole moment per unit volume) and E are the most convenient to use and are open to direct physical interpretation.[3] Now the relationships expressed by Eq. (1.1) and (1.3) have meaning for the case where E is time dependent only if P or D is related to E linearly. The linearity requirement is usually expressed in the frequency domain as follows: a dielectric is linear if a unique $\epsilon(\omega)$ or $\chi(\omega)$ exists such that

$$D(\omega) = \epsilon(\omega)E(\omega)$$

or

$$P(\omega) = \chi(\omega)E(\omega). \tag{1.5}$$

That is, given a cyclic field $E(\omega)$ at some frequency ω_o, there is some constant ϵ for this value of frequency ω_o such that D will be proportional to $E(\omega_o)$ and contain only ω_o for its frequency component. This does not require that ϵ or χ be independent of frequency for linear dielectrics. Whenever $\epsilon = \epsilon(\omega)$ or $\chi = \chi(\omega)$, dielectric dispersion is said to exist in the medium; this can be taken as the definition of dispersion.

Equations (1.5) imply the principle of linear superposition in the time domain. That is, if $E_1(t)$ produces a $D_1(t)$ and $E_2(t)$ produces a $D_2(t)$, then $E_1(t) + E_2(t)$ produces $D_1(t) + D_2(t)$. The proof that this property follows from Eq. (1.5) is left to the Appendix, where it is also shown that a necessary condition is that $\epsilon(\omega)$ or $\chi(\omega)$ be independent of the field. This last result is more or less expected by intuition. The fact that $D(\omega)$ and $E(\omega)$ are simply related through $\epsilon(\omega)$ does not mean that a similarly simple relationship must exist between D(t) and E(t), for by considering the Fourier integrals

$$E(t) = \int_{-\infty}^{\infty} E(\omega)e^{i\omega t}\,d\omega, \tag{1.6}$$

where

$$E(\omega) = \frac{1}{2\pi}\int_{-\infty}^{\infty} E(x)e^{-i\omega x}\,dx, \tag{1.7}$$

and

$$P(t) = \int_{-\infty}^{\infty} P(\omega)e^{i\omega t}\,d\omega, \tag{1.8}$$

we can derive a general relationship between P(t) and E(t) by substituting $P(\omega) = \chi(\omega)E(\omega)$ into Eq (1.8). We get

[3] Accordingly, we note that the Devonshire theory of ferroelectrics, a macroscopic thermodynamic theory, uses the variables P and E rather than D and E. P serves as the intensive thermodynamic variable and E as the extensive one. P can be visualized as a measure of atomic "stretching" or distortion upon the application of the field E.

$$P(t) = \int_{-\infty}^{\infty} \chi(\omega) E(\omega) e^{i\omega t} d\omega = \int_{-\infty}^{\infty} \chi(\omega) e^{i\omega t} \left[\int_{-\infty}^{\infty} E(t) e^{-i\omega t} dt \right] d\omega \qquad (1.9)$$

as a general formula relating P(t) and E(t). It is noted that if no dispersion is present, i.e., if χ is independent of frequency, then Eq. (1.9) becomes:

$$P(t) = \chi E(t). \qquad (1.10)$$

This means that the polarization will follow the applied field only to the extent that ϵ or χ are frequency independent. This is expected, because in order for P(t) to be precisely the same function as E(t), all Fourier (frequency) components in one must appear in the other and in the same proportions. For the case where dispersion is present, as it is for many high-permittivity ferroelectrics, there is no simple algebraic relationship between P(t) and E(t). Definitions of the small-signal susceptibility, spontaneous polarization, coercive field, etc., and how these are related to the hysteresis loop are shown in Fig. 3.

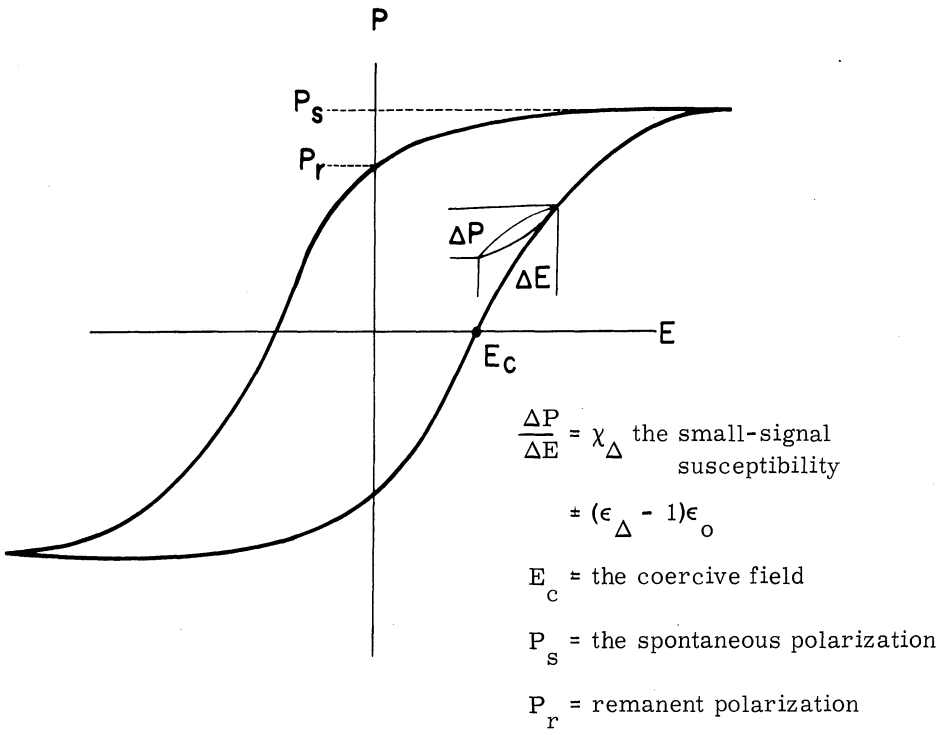

FIG. 3. DEFINITIONS RELATING TO FERROELECTRIC HYSTERESIS LOOP

Table I, a schematic, may aid in clarifying some of the more prominent dielectric properties of the materials under investigation in the frequency-field domain. This schematic is divided into four regions, based on the magnitudes of the electric fields and on the frequencies involved. The divisions are made arbitrarily to coincide with some physical process in a single crystal of the ferroelectric. Thus, we take as a small field an electric field which is

much smaller than the coercive field of the crystal (i.e., $\Delta E \ll E_c$ for a small field). Under such conditions, domain nucleation and growth effects should not exist nor contribute to the small-signal or incremental polarizability of the material. The division between low frequency and high frequency is made on the basis of whether or not the crystal behaves as if it were mechanically clamped. Frequencies in excess of the elastic dimensional resonances are considered high frequencies. Frequencies in the neighborhood of the piezoelectric modes and lower are considered low frequencies. For $BaTiO_3$ single crystals, E_c is of the order of 1000 volts/cm, and in most crystals the highest elastic resonance frequency observed is of the order of 15 mcs (Ref. 9), so that one may use about 100 volts/cm and 50 mcs as the dividing points. These figures vary from crystal to crystal, of course, but they give a rough idea of what constitutes large and small quantities in field and frequency for the purposes of this study.

TABLE I. SOME DIELECTRIC PROPERTIES OF $BaTiO_3$-LIKE FERROELECTRICS

Low Frequencies, Small Fields	High Frequencies, Small Fields
Incremental P and E are taken as linearly related via $\epsilon_\Delta \cong \frac{4\pi\Delta P}{\Delta E}$.	Incremental values of P and E are taken as linearly related via $\epsilon_\Delta \cong \frac{4\pi\Delta P}{\Delta E}$.
Piezoelectric effects observed.	Piezoelectric effects clamped out.
Domain nucleation and growth not expected.	No domain effects expected.
Low Frequency, Large Fields	**High Frequencies, Large Fields**
Major hysteresis loops. No unique relationship between P and E.	Properties largely unknown.
Some heating by cyclic fields.	Domain nucleation and growth not expected on the basis of present knowledge.
Large piezoelectric effects.	Dielectric heating expected.
Domain nucleation and growth effects.	Some nonlinearity in ϵ expected.

1.3. THE CLASSICAL THEORY OF DIELECTRICS[4]

The classical theory of dielectrics will be used as the starting point in the analysis of the small-field polarizability in the perovskite-like ferroelectrics. This theory, therefore, will be very briefly reviewed at this point. If a homogeneous dielectric material is placed in a uniform electric field, the molecules or atoms become polarized. By this it is meant, for example, that a physical charge separation occurs due to a separation of the center of gravity

[4] As a matter of convenience the cgs system of units, the most useful for the thermodynamic analysis, will be used for the analysis in the succeeding sections. On the other hand, when data are reported, they will be displayed and discussed in terms of the familiar practical units.

of positive (the nucleus) and negative (the electrons) charge within an atom, or that a polar molecule is oriented. The polarization vector, P, is really a measure of the charge separation in that it is defined as the electric dipole moment per unit volume of the material. The dipole moment is given by

$$\bar{\mu} = \sum_i e_i \bar{r}_i, \tag{1.11}$$

where the sum is taken over all charges e_i, and $\bar{r}_i$ is the position vector. In a substance which is electrically neutral,

$$\sum_i e_i = 0, \tag{1.12}$$

so that the expression for the dipole moment, μ, is independent of the origin taken for the position vector $\bar{r}_i$.

The field effective in polarizing an atom at a lattice point in a dielectric is not necessarily the same as the applied macroscopic field. This results from the fact that as the applied field polarizes the dielectric, the dipoles thus created give rise to fields which in turn affect the effective field at any point in the dielectric. In addition, if the dielectric placed in the field is of certain configurations, say an ellipsoid, the induced charges appearing at the surfaces give rise to fields which tend to oppose the applied field. This results in the so-called depolarization field. The net result of these effects is in general an electric field far different from that applied, especially in the case of the high-permittivity ferroelectrics. The resultant field at a point within the dielectric is called the local field.

One of the earliest calculations of the local field was worked out by Lorentz (Ref. 10). His method is to assume that at sufficient distances from the point at which one wishes to derive the effective field, the medium is treated in a completely macroscopic way, that is, as a continuous medium. In a spherical region or cavity about the point in question, the medium is assumed to consist of its particular atomic structure. In this manner the local field is broken up into a sum of the contributions of fields external to the spherical cavity and the fields due to the induced dipoles within the cavity.

$$\bar{E}_\ell = \bar{E}_e + \bar{E}_i, \tag{1.13}$$

where $\bar{E}_\ell$ is the local or effective field, $\bar{E}_e$ is the external contribution, and $\bar{E}_i$ is the internal contribution. The external contribution is the sum of the effects of the applied field, $\bar{E}$, the depolarization field, and the fields produced by the surface charges on the walls of the cavity. The internal contribution is the field felt at the center of the cavity as a result of all the dipoles within the cavity. For the case where the dielectric is placed between electrodes such that the depolarization field is zero, one obtains the expression for the famous Lorentz field:

$$\bar{E}_\ell = \bar{E} + \frac{4\pi}{3}\bar{P} + \sum_i \frac{3(\bar{\mu}_i \cdot \bar{r}_i)\bar{r}_i - r_i^2 \bar{\mu}_i}{r_i^5}, \tag{1.14}$$

where $\bar{E}$ is the applied field, $\bar{P}$ is the polarization, $\bar{\mu}$ is the dipole moment of each dipole within the cavity, and $\bar{r}$ is its position vector relative to the origin at the center of the cavity. The summation in the above is over all dipoles in the cavity except the one taken at the origin. For substances having cubic structure such as NaCl and for those with random structure such as a gas or nonpolar liquid, the above reduces to

$$\bar{E}_\ell = \bar{E} + \frac{4\pi}{3}\bar{P}. \tag{1.15}$$

The perovskite structure does not have cubic symmetry for each ion so that an evaluation of the Lorentz field proceeds with Eq. (1.14).

Equation (1.2) with Eq. (1.15) becomes

$$\bar{E}_\ell = \frac{(\epsilon_s + 2)}{3}\bar{E}, \tag{1.16}$$

where ϵ_s is the static (zero-frequency) permittivity. This shows that a very large "amplification" is possible in the Lorentz local field if a high-permittivity dielectric is considered. Viewed conversely, a favorable local field could cause a large polarization which in turn enhances the local field. Thus one can visualize a situation occurring under favorable circumstances in which the material as a whole can become spontaneously polarized, i.e., ferroelectric.

The Lorentz field leads to the Clausius-Mosotti formula

$$\chi = \frac{P}{\bar{E}} \frac{\sum_i N_i \alpha_i}{1 - \frac{4\pi}{3}\sum_i N_i \alpha_i}, \tag{1.17}$$

where N_i is the number of atoms of the i-th species per cubic centimeter and α_i is the polarizability[5] of the atoms of the i-th species. This seems to correlate well with experimental data for gases and some liquids. Its application to solids has not been particularly successful, especially for those containing polar molecules as part of their structure. The Lorentz formula was derived under the assumption that the induced dipoles in the medium are parallel. This would be expected of a symmetrical structure at sufficiently low temperatures, but not of a polar substance at elevated temperatures. Moreover, the Lorentz field leads to predictions of ferroelectricity far too easily, for when the denominator of Eq. (1.17) approaches zero,

[5] Polarizability is defined as the induced dipole moment per atom per unit local field.

the susceptibility becomes greater and greater, that is, the amplification in local field becomes stronger. An analysis of the Lorentz field results in a prediction of ferroelectricity in such substances as water and other polar liquids above their boiling points – clearly an impossible situation. It can be seen that the Lorentz local field is too strong a correction to the applied field and that further modifications have to be made.

There are two objections to the use of the Lorentz field. The first is that although in principle the Lorentz correction may be used to compute the local field for an array of permanent dipoles, provided that these dipoles are all aligned along the macroscopic polarization direction, in practice, it does not work successfully because the thermal agitation of the dipoles disturbs their alignment. The same is true of induced dipoles. The second objection is that if a given dipole is rotated out of alignment from the polarization direction it has the tendency to pull neighboring dipoles out of alignment as well because of coupling between the dipolar fields.

In order to meet the objections mentioned above, Onsager (Ref. 11) has developed an expression for the local field based on the following model. The dipole in the material is replaced by a small uniformly polarized sphere which is free to rotate in a cavity cut out of the gross media of fixed uniform polarization. By the solution of an electrostatic boundary value problem, the resultant field in the neighborhood of the dipole is found as the superposition of the uniform field of the medium and the field of the sphere which may be rotated to some angle θ, with respect to the polar direction of the rest of the material. The interaction energy V of a dipole in a field E is given by

$$V = -\bar{\mu} \cdot \bar{E} = -|\bar{\mu}||\bar{E}| \cos\theta, \tag{1.18}$$

and from the Boltzmann distribution one has for the average value of $\cos\theta$,

$$\overline{\cos\theta} = \frac{\int \cos\theta \, e^{-\frac{V}{kT}} d\Omega}{\int e^{-\frac{V}{kT}} d\Omega}, \tag{1.19}$$

where the integration is carried over the solid angle $\Omega = 4\pi$. If the integration of Eq. (1.19) is carried out, one obtains the well-known Langevin function:

$$\overline{\cos\theta} = \coth\left(\frac{\mu E}{kT}\right) - \frac{1}{\left(\frac{\mu E}{kT}\right)} \cong \frac{\mu E}{3kT}, \tag{1.20}$$

(for $\mu E \ll kT$). Since the polarizability is given by

$$\alpha = \frac{\mu \cos \theta}{E}, \tag{1.21}$$

the dipolar contribution to the polarizability is

$$\alpha_{d.p.} = \frac{\mu^2}{3kT}. \tag{1.22}$$

The result of an analysis of Onsagers' model using the dipolar contribution to polarizability, Eq. (1.22) is that the local field

$$E_{loc.} = E + \frac{4\pi P}{2\epsilon + 1}, \tag{1.23}$$

and

$$\epsilon = \frac{1}{4}\left[1 + \frac{4\pi\mu^2 N}{kT} + 3\left(1 + \frac{8\pi\mu^2 N}{9kT} + \frac{16\pi^2\mu^4 N^2}{9k^2T^2}\right)^{1/2}\right]. \tag{1.24}$$

This result[6] shows that there is no critical point for the dielectric constant. Consequently, the exact onset of ferroelectricity cannot be determined from the Onsager model. If one were to write, after Jaynes (Ref. 12), the expressions for the local fields in the form

$$E_\ell = E + \beta P, \tag{1.25}$$

the factor β takes on the character of a "general Lorentz factor." For the Lorentz fields, $\beta = \frac{4\pi}{3}$, and for the Onsager model, $\beta = \frac{4\pi}{2\epsilon + 1}$, as is seen from Eq. (1.23). From this it is evident that the Onsager field is always smaller than the Lorentz field with the former approaching the latter as $\epsilon \to 1$. Whereas the Lorentz field turned out to provide an excessive correction to the applied field, the Onsager field represents an insufficient correction, since it results in the prediction that a material will never become ferroelectric. Calculations of the local fields in $BaTiO_3$ have been carried out by Slater (Ref. 13) and Triebwasser (Ref. 14), but both have based their calculations on the validity of the Lorentz fields. All the theories for internal fields are beset with great difficulties, and the above examples are to be considered as rather rough idealizations. The study of dielectric properties and the onset of ferroelectricity is very important to an understanding of the nature of chemical bonding. On the other hand, the dielectric behavior depends, as shown here, very strongly on the nature of the local fields, the derivation

[6] The result given here assumes no displacement polarizability. If the latter is taken into account, one obtains

$$\epsilon \cong \epsilon_\infty + (\epsilon_\infty + 2)^2 \frac{4\pi N\mu^2}{27kT} + \ldots.$$

of which assumes some knowledge of the chemical bond. The local fields and chemical binding play the central roles in the theory of dielectrics. Further discussion on this topic is adequately available in the literature.

From the chemical-bond point of view, the contributions to the total polarizability or susceptibility is usually taken as a linear superposition of electronic, ionic, and dipolar terms. That is, one writes

$$\chi_{tot} = \chi_e + \chi_i + \chi_{d.p.} . \tag{1.26}$$

In this expression the χ_e is the susceptibility due to distortions in the electronic shells as a result of the action of the field, χ_i is the displacement of one ion against another, for example, in an ionic crystal, and $\chi_{d.p.}$ is the contribution from the alignment of dipoles in polar substances. Strictly speaking, these terms are not completely independent. For example, in an ionic crystal such as NaCl, as the ions shift with an applied field, one would expect a distortion of the electronic shells as a result of the ionic displacement. For this reason one often finds the first two terms in Eq. (1.26) grouped together as the total induced susceptibility, as distinct from the susceptibility due to rotations of permanent dipole moments, $\chi_{d.p.}$. Whether each of the terms in Eq. (1.26) contributes to the total susceptibility depends on the chemical and crystalline composition of the substance in question. The ionic structure of NaCl, for example, would not be expected to contribute a dipolar term, i.e., $\epsilon_{d.p.} = 0$.

An examination of Eq. (1.26) term by term will show in greater detail how each contribution affects the total susceptibility in the light of classical theory. For χ_e, the electronic susceptibility, experimental evidence indicates the validity of the Clausius-Mosotti law and the Lorentz field for those dielectrics whose major contribution to the susceptibility is electronic in origin. This is the case, for example, in nonpolar gases and covalent solids. According to classical theory, an electron bound elastically to a nucleus has the properties of a harmonic oscillator with a resonant frequency $\omega_o = \sqrt{R/m}$, where R is the restoring force constant and m is the mass of the electron. This results in an electronic polarizability which is given classically by

$$\alpha_e = \frac{e^2/m}{\omega_o^2 - \omega^2} . \tag{1.27}$$

For most dielectrics the resonant frequencies ω_o are in the optical frequency range or higher. For dielectrics in the optical region and for frequencies sufficiently removed from absorption or resonance, the relationship between the index of refraction and the dielectric constant is given by Maxwell's formula:

$$n^2 = \epsilon_\infty .$$

The notation ϵ_∞ will be used to indicate the dielectric constant at the highest frequency of interest. It is thus possible to measure the index of refraction of certain dielectrics and from this information to determine the contribution of electronic displacement to the dielectric constant. Table II shows the dielectric constants of various types of dielectrics for three frequency regions, the low-frequency or audio range, the high-frequency or microwave range, and finally the optical frequencies. The compositions shown in the table represent different types of chemical binding. Diamond and sulfur are typical of the covalent bond, and for these materials the atomic nuclei are tightly bound in their equilibrium positions by strongly directed electron bonds. It is seen that almost all of the polarizability of these solids results from electronic displacements.[7] On the other hand, NaCl and LiF, which are ionic salts, have, in addition to electronic displacements, polarizability as a result of harmonic displacements of the ions in the electric field. For the case of a polar liquid such as H_2O there is, in addition to the ionic and electronic polarization described above, the possibility

TABLE II. DIELECTRIC CONSTANTS FOR VARIOUS DIELECTRICS

	H_2O liquid	C (diamond)	S	NaCl	LiF	TiO_2 $\parallel$	TiO_2 $\perp$	$BaTiO_3$ $\parallel$	$BaTiO_3$ $\perp$
ϵ_{audio}	81	5.7	4.1	5.9	9.0	170	86	200	4000
$\epsilon_{\mu wave}$	35*	5.5	4.1	5.9	9.0	170	86	100**	2000**
ϵ_∞	1.78	5.8	4.0	2.4	1.9	8.5	6.9	5.5	5.8
% ϵ_∞ of total	2%	~100%	100%	40%	20%	5%	8%	5%	0.3%
% χ_∞ of total	1%	~100%	97%	29%	11%	4.4%	7%	4.5%	0.2%

$\parallel$ and $\perp$ indicate, respectively, parallel and perpendicular to the optical or polar axis.

*The microwave behavior in water is a relaxation phenomenon. This figure is at 25°C and 2.4×10^{10} cps.

**These values are taken at frequencies higher than that for elastic resonances. The differences between ϵ_{audio} and $\epsilon_{microwave}$ appear largely as a result of mechanical clamping.

[7] At extremely high frequencies, e.g., in the optical range, only the electrons follow the field. Atomic nuclei and molecules cannot follow the optical fields because of their inertia.

of alignment of the dipolar molecule H_2O with the electric field. In water, the low-frequency permittivity of 81 is mostly a result of the dipolar mechanism. It is further seen that as far as small fields are concerned, the permittivities in TiO_2 and $BaTiO_3$ have even smaller contributions from the electronic polarizability than the ionic salts.

Theoretical expressions for the ionic polarizability have been developed by Born (Ref. 15) and others (e. g., Fröhlich, Ref. 16) based on vibrations and normal modes in ionic lattices. For a simple one-dimensional crystal containing two types of ions of mass m and M and charges $\pm e$, Born obtains the equations

$$P = \frac{e^2 E}{2\omega_o^2 a^3}\left(\frac{1}{m} + \frac{1}{M}\right), \tag{1.28}$$

from which

$$\chi_i = \frac{e^2}{\delta\omega_o^2 a^3}\left(\frac{1}{m} + \frac{1}{M}\right), \tag{1.29}$$

or

$$\Delta\epsilon = \frac{2\pi e^2}{\omega_o^2 a^3}\left(\frac{1}{m} + \frac{1}{M}\right), \tag{1.30}$$

where $\Delta\epsilon$ is the difference between the optical dielectric constant and the dielectric constant due to ionic displacements, ω_o is the infrared absorption frequency, and a is the nearest neighbor distance in the one-dimensional crystal. The development of the Born equations above neglects the effect of the local fields. If the parameters for NaCl are substituted in the above equations, the theoretical value of $\Delta\epsilon = 2.7$ is obtained as compared to that observed of about 3.4. This is a difference of approximately 30%. It is interesting to note the effect of the local field on the Born equations above. Consider $E = E_o + \beta P$ as we have done in Eq. (1.25) where E_o here is the applied external field, E is the local field, and β is the generalized "Lorentz factor." If this is substituted into Eq. (1.28) one may easily obtain an expression analogous to Eq. (1.30). We will call the quantities on the right-hand side of Eq. (1.30) identically $(\Delta\epsilon)_o$, that is, the ionic permittivity, under the assumption that the local field is the same as the applied field. Thus we obtain:

$$\Delta\epsilon = \frac{(\Delta\epsilon)_o}{1 - \beta\frac{(\Delta\epsilon)_o}{4\pi}}. \tag{1.31}$$

If we use the $(\Delta\epsilon)_o = 2.7$ and $\beta = \frac{4\pi}{3}$ for the Lorentz field, then $\Delta\epsilon = 27$, an order of magnitude too large! On the other hand, if $\beta = \frac{4\pi}{2\epsilon + 1}$ as for the case of the Onsager field where we take $\epsilon = \epsilon_s$, the static permittivity, which is 5.9, then we obtain $\Delta\epsilon = 3.4$, exactly the value obtained via experiment. The above is a rather striking example of the overcompensation which results from the Lorentz field. As the reader may recall, the basic assumptions of the derivation by Lorentz were that the induced dipoles all had the same constant moment and that there were to be no thermal agitation effects. The Onsager field takes these effects and the close-range dipole-dipole interactions into account. Although Onsager's derivation proceeded with the assumption of permanent dipoles, one would expect similar behavior for the case of a lattice of induced dipoles under the action of thermal agitation – especially in the static or infinite wavelength limit where the disorientation of one dipole will evidently affect its neighbors. A recent paper by Toupin and Lax (Ref. 17) shows that the Onsager result is valid in a lattice of dipoles which are in part induced and in part permanent. The treatment of ionic polarizability here is in reality quite crude but is intended to illustrate the concepts and methods of attack. The theory of ionic polarizability plays a very important role in infrared spectra, or more precisely, the converse may be said. Extensive treatments of the subject abound in the literature.

The dipolar or orientational contribution to the electric susceptibility was first introduced in connection with the Onsager field, and this led to Eq. (1.24). This equation gives the electric susceptibility due to dipoles as:

$$\chi_{d.\,p.} = \frac{N\mu^2}{3kT}, \tag{1.32}$$

with the notation being the same as in Eq. (1.24). These results were derived in a general way for dipoles which were free to rotate. If one were to view the situation, with Kittel, Fröhlich and others, of a solid polar crystal in which the dipoles had but two orientations – either parallel or antiparallel to the applied electric field, then a result similar to Eq. (1.32) holds. If a and b are the parallel and antiparallel sites, respectively, and n_a and n_b are the number of dipoles in each site, one obtains the following via the Boltzmann distribution:

$$n_a = \frac{N}{2} e^{\frac{\mu E}{kT}},$$

and

$$n_b = \frac{N}{2} e^{-\frac{\mu E}{kT}};$$

and normalization requires $N_a + n_b = N$, i.e., the total number of dipoles per unit volume. Thus the excess aligned with the field is

$$n_a - n_b = \frac{N}{2}\left(e^{\frac{\mu E}{kT}} - e^{-\frac{\mu E}{kT}}\right) = N \cdot \frac{\mu E}{kT},$$

for $\frac{\mu E}{kT} \ll 1$. Now $n_a - n_b$ is the net number of dipoles per unit volume so the $\mu(n_a - n_b)$ is the total dipole moment per unit volume or P. Thus

$$\chi_{d.\,p.} = \frac{P}{E} = \frac{N\mu^2}{kT}, \tag{1.33}$$

a polar susceptibility three times as great as for the freely rotating molecule but of the same general form.

1.4. MECHANISMS OF DIELECTRIC LOSS AND THEIR RELATIONSHIP TO POLARIZATION

Whenever a dielectric medium is polarized, work must be done. To the extent that the work done in polarizing a substance can never be completely reclaimed, the dielectric is said to have losses. The source of the energy may be the battery which charges a capacitor and thus polarizes the dielectric, or some electromagnetic wave such as a microwave field propagating in a dielectric medium.

In the preceding discussion of polarization, the total susceptibility of a dielectric was taken as a superposition of several components – ionic, electronic, and dipolar. It seems natural to treat the question of dielectric losses in a similar manner. That is, it may be said that each particular contribution to the total polarizability has associated with it a specific loss mechanism. Again, it must be understood that the electronic and ionic components are not strictly independent. Compared with the abundance of literature on dielectric polarization there is surprisingly little analysis available on dielectric losses. Most of the analysis is phenomenological or macroscopic in approach.

One can conceive of at least five distinct ways in which a dielectric material may exhibit losses. These are:

(1) Acoustical Loss. All dielectrics show some degree of electrostriction and one could expect, for the most part, that the greater the polarizabilities, the greater would be the electrostriction. This should be even more evident for small fields in the ferroelectrics which are piezoelectric; i.e., the mechanical extension is a linear function of field in contrast to the quadratic extension for the electrostrictive substances. As a consequence of electrostrictive or piezoelectric "pumping" of the atmosphere or environment, an acoustical wave might be initiated. The energy in this wave is lost from the dielectric system.

(2) Joule Heat Loss. Because no dielectric is a perfect insulator, there will be an i^2R loss due to the conduction. The magnitude of this conduction depends on the type of dielectric, the number of carriers available, etc., but one would expect this type of loss to be restricted to fairly low frequencies for most dielectrics.

(3) Frictional Loss. Along grain boundaries, domain walls, fissures, etc., one may assume relative motion of one part of the dielectric with respect to another part as a consequence of electrostrictive or piezoelectric activity. The total loss from friction would be a function of the net wall area. In isotropic ceramics, for example, one would expect this loss to be much lower than for a ceramic composed of nonisotropic grains, because in the former the electrostriction affects each grain in the same way; thus there would be little relative motion of one grain against another. For the nonisotropic media, there will be a distribution of orientations of grains, and each orientation has in general a different electrostrictive or piezoelectric coefficient; therefore, comparatively large relative motions of one grain (or domain) against its neighbor would be expected.

(4) Radiative Effects. The polarization of the dielectric as a whole under the influence of a high-frequency field can be considered an oscillating dipole. If a dimension of the dielectric approaches one-half wavelength, then a coherent electromagnetic radiation from the dielectric may result.

(5) Molecular Loss. The effects listed in items (1) to (4) above are macroscopic in nature. The molecular loss contribution is taken from a more microscopic viewpoint. The atoms, ions, and molecules in a dielectric are in a state of thermal agitation. For an ionic lattice there are certain characteristic modes or frequencies in the infrared which represent vibrations of the ions or groups of ions against one another. A polarizing field or wave in the dielectric in the interaction with the ions can excite these infrared vibrations and therefore lose energy from the original fields. Similarly, a polar molecule can be thought of an continually interacting or colliding with its surroundings and energy can be exchanged as a result of these interactions. Thus all the interactions which lead to losses occurring on the molecular or microscopic scale during electronic, ionic, or molecular polarization can be grouped under the general heading of "molecular loss."

Specific models will be formulated for the above mechanisms of loss in Sec. 4, where the particular ferroelectrics are considered. For now, we will examine the relationship between the polarizability and loss. With the macroscopic approach the loss is usually taken into account by defining a complex permittivity:

$$\epsilon = \epsilon' - i\epsilon'', \tag{1.34}$$

with ϵ'' being proportional to the dielectric loss and $\tan \delta = \frac{\epsilon''}{\epsilon'}$ defining the loss tangent. A complex frequency variable is defined such that

$$p \equiv \sigma + i\omega,$$

with σ and ω being the real and imaginary components of the complex frequency, respectively. If ϵ is then considered as an analytic function of a complex frequency variable $\sigma + i\omega$, then it follows from the theory of complex variables that $\epsilon'(\sigma, \omega)$ and $\epsilon''(\sigma, \omega)$ are not independent of one another in the frequency plane. Fröhlich (Ref. 16) arrives at the same conclusion through the use of superposition and the convolution integral. He defines a decay function $\alpha(t)$ that takes into account the inertia of the polarization within a dielectric upon the sudden application or removal of an electric field. The α relates the D and E of a dielectric in the following way on the sudden removal of the field E, at the time t = u:

$$D(t - u) = \alpha(t - u)E(u),$$

for $t > u$, and

$$\alpha(t - u) \longrightarrow 0$$

as $t \longrightarrow \infty$.

By an integration of the above for the case of sinusoidally periodic fields Fröhlich writes:

$$\epsilon'(\omega) - \epsilon_\infty = \int_0^\infty \alpha(X) \cos \omega X \, dX, \tag{1.35}$$

$$\epsilon''(\omega) = \int_0^\infty \alpha(X) \sin \omega X \, dX, \tag{1.36}$$

and since the $\alpha(X)$ is a parameter appearing in both Eq. (1.35) and (1.36) it may be eliminated, upon which:

$$\epsilon'(\omega) - \epsilon_\infty = \frac{2}{\pi} \int_0^\infty \epsilon''(\mu) \frac{\mu}{\mu^2 - \omega^2} d\mu, \tag{1.37}$$

and

$$\epsilon''(\omega) = \frac{2}{\pi} \int_0^\infty (\epsilon'(\mu) - \epsilon_\infty) \frac{\omega}{\mu^2 - \omega^2} d\mu. \tag{1.38}$$

Here ϵ_∞ has the meaning of the permittivity at the highest frequency of interest, and for the present case this will be the optical values, i.e., $\epsilon_\infty \simeq n^2$. In order for the derivation to be valid it is necessary to assume that D and E are linearly related – an approximation that must be made for very small fields in ferroelectrics.

These equations indicate that once either the losses or the real part of the permittivity are specified as functions of frequency, the other part must be completely specified. These equations will be used in the analysis of the high-frequency behavior of the ferroelectrics. Equations (1.35) and (1.36) are particularly useful when considering molecular models of polarization, since the term $\alpha(t)$ can be derived on the basis of a statistical analysis. The $\alpha(t)$, therefore, provides a link between the microscopic and macroscopic phenomena in the dielectric. If in a particular dielectric the $\alpha(t)$ is exponential in character, that is, if upon the sudden removal or application of the field, the time average of the polarization decays or grows exponentially, then Eq. (1.35) and 1.36) or (1.37) and 1.38) lead to the famous Debye equations. Let $\alpha(t) = ke^{-\frac{t}{\tau}}$, where k is some constant and τ is a time constant. Using this form of $\alpha(t)$ in Eq. (1.35) and 1.36) gives

$$\epsilon'(\omega) - \epsilon_\infty = \int_0^\infty k e^{-t/\tau} \cos \omega t \, dt = k\tau \frac{1}{1 + \omega^2 \tau^2}, \tag{1.39}$$

and

$$\epsilon''(\omega) = \int_0^\infty k e^{-t/\tau} \sin \omega t \, dt = k\tau \frac{\omega\tau}{1 + \omega^2 \tau^2}. \tag{1.40}$$

Equations (1.39) and (1.40) may be written in a slightly different form by noting that if $\omega = 0$ in Eq. (1.39) one obtains $\epsilon_s' - \epsilon_\infty = k\tau$, where ϵ_s' is the static value of the permittivity. Thus we arrive at the Debye equations for dielectric relaxation in the following form:

$$\epsilon'(\omega) - \epsilon_\infty = \frac{\epsilon_s' - \epsilon_\infty}{1 + \omega^2 \tau^2}, \tag{1.41}$$

and

$$\epsilon''(\omega) = \frac{(\epsilon_s' - \epsilon_\infty)\omega\tau}{1 + \omega^2 \tau^2}. \tag{1.42}$$

It may easily be shown from electrical network analysis that the following equivalent circuit gives the same type of equations:

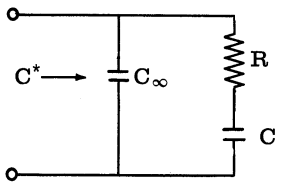

with $C^* = C' - jC''$

$\epsilon \longrightarrow C'$

$\epsilon'' \longrightarrow C''$

$\epsilon_\infty \longrightarrow C_\infty$

$\tau \longrightarrow RC$

$\epsilon_s \longrightarrow C + C_\infty$

$k \longrightarrow \frac{1}{R}$

1.5. SUMMARY

In the preceding sections some of the properties of the high-permittivity ferroelectrics were reviewed, with primary attention on $BaTiO_3$. General concepts of the local field and polarizability for a dielectric were introduced, and polarizability was further examined in connection with electronic, ionic, and dipolar individual contributions. It was demonstrated that, under the assumption of a linear dielectric, the real and imaginary parts of the complex permittivity are not independent of each other. The ferroelectrics are distinctly nonlinear with regard to large fields. The exact mechanism of this large-field nonlinearity is still being investigated in

several laboratories, and at this time it is not completely understood. However, for small time-dependent fields this study takes the point of view that the substances dealt with are linear dielectrics, the permittivity of which is "set" by the instantaneous value of the large field. This study is basically concerned with the small-field polarizability. Small fields are considered those whose magnitudes are much smaller than the coercive fields of the particular ferroelectric crystal. The question of the onset of ferroelectricity in dielectrics is not a primary concern here. The approach is rather: given a particular ferroelectric or high-permittivity substance, what may be said of the small-signal polarizability and losses as a function of biasing fields and of frequency?

Experimentally, the various contributions to the polarizability are separated by measurements of the permittivity as a function of frequency over very wide frequency ranges. As the frequency is increased, the various polarization processes, one at a time, no longer follow the time-varying field because of the inertia of the dipoles or ions, etc. (Fig. 4). The dipolar part of the spectrum, as can be seen in Fig. 4, shows a relaxation spectrum rather than the resonance absorption exhibited by the ionic or electronic mechanisms. This is explained on the basis that the dipoles have no restoring forces in the same sense that ions or electrons have in the crystalline lattice.

Soon after the discovery of the properties of $BaTiO_3$ and other isomorphic high-permittivity ferroelectrics, experiments of the type described above were initiated in Great Britian by Powles and Jackson (Ref. 18) and in this country by Von Hippel and his co-workers (Ref. 19). These measurements mainly covered the low-frequency to microwave range and the data were taken for polycrystalline (i. e., ceramic) samples of $BaTiO_3$. The data have been smoothed and reported by Kittel in his textbook (Ref. 20) and the results are shown in Fig. 5. One notices a rather marked relaxation of the permittivity in the two decades between 10^8 and 10^{10} cps. In this frequency range there is a drop in permittivity of about one order of magnitude. To date, two explanations of this effect have been put forward. Kittel, in discussing the data in his textbook, suggests that the relaxation is caused by the inertia of ferroelectric domain boundaries, and Von Hippel has suggested that elastic resonances in the ceramic are the cause. The first explanation seems untenable, first, because the fields under which the relaxation was presumably measured were very much smaller than the coercive field of the crystal so that significant domain motion would not take place, and second because the ferroelectric domain, according to present knowledge, does not have the gradual wall transition that is ascribed to magnetic materials so that the concept of a wall inertia here has questionable meaning. Moreover, and this should be the coup de grace to both explanations, the relaxation has been reported by Von Hippel (Ref. 21) and others (e. g., Sharpe and Brockus, Ref. 22) for ceramic ferroelectrics at temperatures higher than their Curie point where the ceramic is not ferroelectric, domains do not exist, and the material is not piezoelectric.

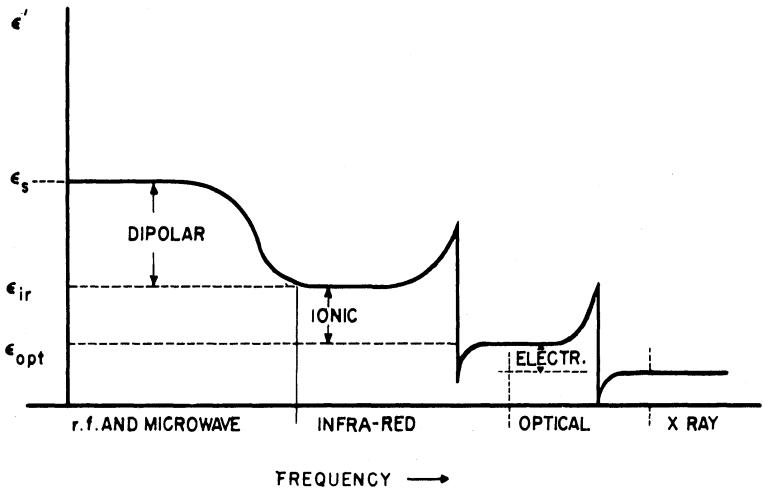

FIG. 4. SCHEMATIC OF CONTRIBUTIONS TO PERMITTIVITY IN A DIELECTRIC

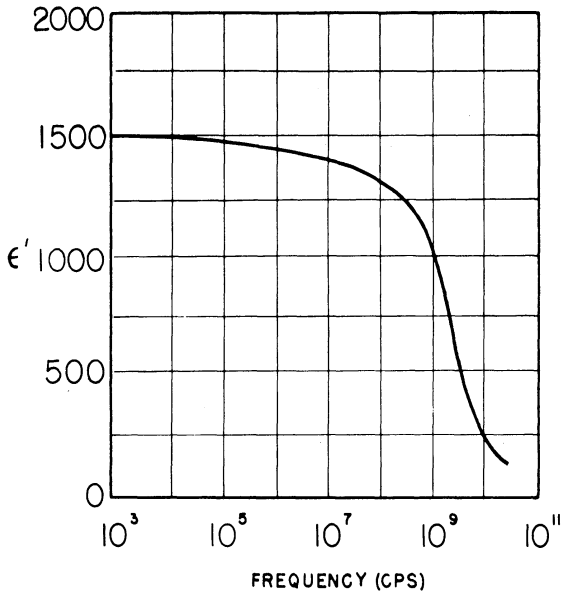

FIG. 5. THE SMALL-FIELD PERMITTIVITY VS. FREQUENCY FOR CERAMIC $BaTiO_3$. From the data by Powles and Jackson (Ref. 18) and Von Hippel (Ref. 19) — smoothed by Kittel (Ref. 20).

There are certainly other explanations possible for the observed relaxation, two of which will be considered, namely, the possibility of a molecular relaxation of the dipolar type described in the preceding sections, and the possibility of a relaxation primarily caused by a loss mechanism. That is, since real and imaginary parts of the permittivity are not independent, anything which produces a significant loss term must also affect the real part.

To arrive at an explanation, it was thought desirable first to attempt to reproduce experimentally the observed high-frequency behavior cited by Kittel for ceramics and then to examine the high-frequency behavior for single crystals of $BaTiO_3$ with the high-frequency fields oriented both parallel and perpendicular to the polar axis. If the reported relaxation is basically a molecular phenomenon, one could expect that with the single crystal the relaxation would be extremely sharp and well defined, perhaps even being a resonance phenomenon. The type of model chosen for an analysis of the polycrystalline material would then depend on the results of the latter experiment. In the experiments performed, the single crystals did not exhibit any substantial relaxation at frequencies up to 4000 mcs. Therefore, since no particular molecular phenomenon need be invoked, it was found most convenient to base an analysis on a phenomenological or thermodynamic framework.

2
The POLARIZABILITY and LOSSES in the PEROVSKITE STRUCTURE

2.1. THERMODYNAMIC APPROACH

One may study dielectrics with either a macroscopic phenomenological approach or with a model theory or microscopic approach. No new basic information is provided by the former approach, but rather various relationships are derived among the different parameters of the system in question. A thermodynamic "equation of state" is postulated, and from this equation and the laws of thermodynamics, the behavior of the system is derived. Provided that the fundamental equation of state is "correct," the success of this method is guaranteed. It is the task of a model or microscopic theory or direct experiment to provide the equation of state.

The method of applying thermodynamics to dielectrics is to write the combined forms of the first and second laws. Assuming reversibility for small fields and for the lossless case,

$$T\,dS = dU - E_m\,dP_m + X_i\,dx_i, \tag{2.1}$$

where the summation convention is used for repeated indices, S is the entropy, U is the internal energy, E_m is the externally applied field, P_m the polarization, and X_i and x_i are the stress and strain components, respectively. Then the thermodynamic potentials used are defined as

$$\begin{aligned} A &= U - TS, \text{ the Helmholtz free energy,} \\ G &= H - TS, \text{ the Gibbs free energy,} \\ H &= U + X_i x_i - E_m P_m, \text{ the enthalpy.} \end{aligned} \tag{2.2}$$

According to the phenomenological theory presented by Devonshire (Ref. 23), one assumes that it is possible to express the Gibbs or Helmholtz free energy as a power-series expansion in the polarization and stresses or strains. Also, from Eq. (2.1) and (2.2) it can be seen that

$$dA = E_m\,dP_m - X_i\,dx_i - S\,dT,$$

and (2.3)

$$dG = P_m\,dE_m + x_i\,dX_i - S\,dT.$$

For the particular case of the stress-free crystal with one direction of polarization (as with $BaTiO_3$ in the tetragonal ferroelectric state), Devonshire writes:

$$A(P,T) = A_0' + \frac{1}{2}a'P^2 + \frac{1}{4}b'P^4 + \frac{1}{6}c'P^6 + \ldots, \tag{2.4}$$

where A_0', a', b', and c' are empirically determined constants which may be, and in fact are, temperature dependent. The primes indicate that the constants are for a free crystal. The expansion is taken in only the even powers of P, since the free energy is independent of the algebraic sign of the polarization.

It then follows that

$$E = \left(\frac{\partial A}{\partial P}\right)_{T, X=0} = a'P + b'P^3 + c'P^5 + \ldots . \tag{2.5}$$

For zero electric field, if P^7 and higher powers are neglected,

$$a'P + b'P^3 + c'P^5 = 0,$$

in which P = 0 is one solution, as in the paraelectric state. However, P need not be zero and is in fact finite in the ferroelectric state. For this case,

$$P^2 = \frac{-b' \pm \sqrt{b'^2 - 4a'c'}}{2c'} = \frac{-b' \pm \left(b' - \frac{2a'c'}{b'}\right)}{2c'} . \tag{2.6}$$

The constant a' can be interpreted as the inverse isothermal susceptibility at P = 0 by noting from Eq. (2.5) that

$$\left(\frac{\partial E}{\partial P}\right)_T = \frac{1}{\chi} = a' + 3b'P^2 + 5c'P^4 + \ldots . \tag{2.7}$$

If one considers temperatures above T_0, the Curie temperature, where there is no spontaneous polarization, the limit for the small-signal susceptibility from Eq. (2.7) is

$$\chi = \frac{1}{a'} = \frac{C}{T - T_0} . \tag{2.8}$$

The last term is the Curie-Weiss law and is determined experimentally. This in turn allows the evaluation of a'. C is the Curie constant. Several workers have made measurements in order to determine the constants a'b'c' and C. A tabulation of the more recent values is shown in Table III. It is noticed that the latest value of b' is temperature dependent. The free-energy function of Devonshire allows the prediction, at least qualitatively, of most of the observed experimental data for $BaTiO_3$ crystals.

Some criticism has been raised as to the use of the same function on both sides of Curie transition. The justification of its use, however, is that the free-energy function does in fact allow a prediction of the results determined experimentally for $BaTiO_3$ in both the ferroelectric and nonferroelectric states. This point is also tied in with the question as to whether the phase transition at 120°C, the Curie point, is a first- or second-order thermodynamic transition. In a first-order transition, the free-energy function is continuous, but its derivative with temperature (the entropy) has a discontinuity at the transition. For a second-order

effect, both the free energy and the entropy are continuous, but the derivative of the entropy (which is proportional to the heat capacity) is discontinuous. Experiments indicate that $BaTiO_3$ undergoes a phase change of the first kind at 120°C but with such a small change in entropy that it practically behaves as if the change were of the second order. This may account for the success of the use of a smooth free-energy function on both sides of the upper Curie temperature.

TABLE III. SOME RECENT EVALUATIONS OF THE COEFFICIENTS IN DEVONSHIRE'S FREE-ENERGY FUNCTION

[Values taken from table given by Devonshire (Ref. 23)]

c	a'	b'	c'	Worker
10^4	$\frac{T - T_0}{10^4}$	-1.1×10^{-12}	2.8×10^{-22}	Merz (Ref. 24)
10^4	$\frac{T - T_0}{10^4}$	-1.2×10^{-12}	3.5×10^{-22}	Devonshire (Ref. 23) and recalculated by Merz (Ref. 24)
1.4×10^4	$\frac{T - T_0}{1.4 \times 10^4}$	-0.68×10^{-12}	2.3×10^{-22}	Merz (Ref. 24)
2.7×10^4	$\frac{T - T_0}{2.7 \times 10^4}$	$-4.5 \times 10^{-15}(T_2 - T)$	9×10^{-23}	Huibregtse and Young (Ref. 25)

$T_0 = 110°C$

$T_2 = 175°C$

It is instructive to examine the free-energy function in Eq. (2.4) for various values of the coefficients a', b', and c'. The value of $a' = \frac{T - T_0}{C}$ is determined experimentally. Stability demands that $\frac{\partial^2 A}{\partial P^2} > 0$ as $P \rightarrow \infty$, so that $c' > 0$ is a necessary condition. The coefficient b' may be greater than or less than zero. Figure 6 shows a schematic of A vs. P for varying values of T (and therefore for varying a') for the cases where $b' > 0$ and for $b' < 0$. The system is in equilibrium under the condition that the free energy is a minimum. For the free-energy function in which $b' > 0$, it is seen that the minimum occurs at $P = 0$ for temperatures greater than or equal to the critical temperature T_0. As the temperature is lowered below T_0, the minimum smoothly and continuously shifts to finite values of P, corresponding to the

onset of ferroelectricity. Since for $b' > 0$ there is no discontinuity in P and hence no discontinuity in the entropy, the case in which $b' > 0$ represents a second-order transition. For $b' < 0$, the minimum in A jumps discontinuously from $P = 0$ for $T \geq T_0$ to some finite value of P. Hence $b' < 0$ represents a first-order transition.

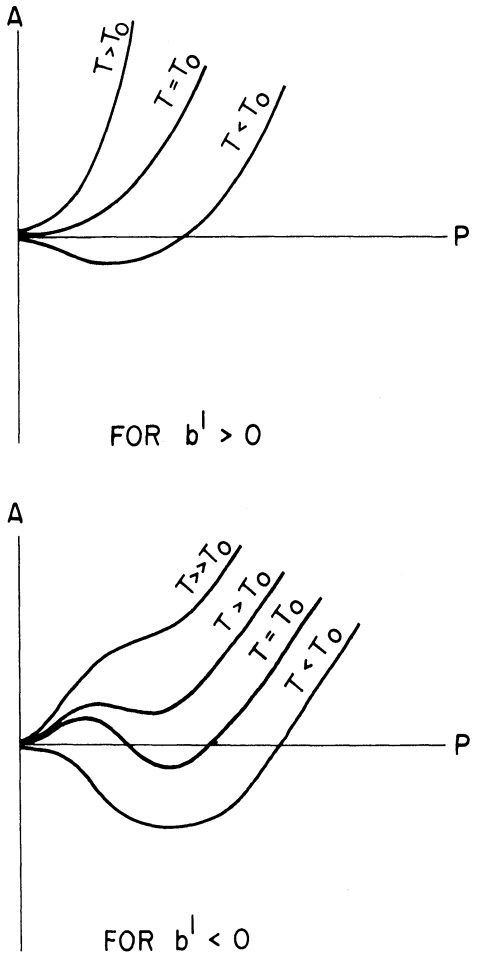

FIG. 6. FREE ENERGY VS. POLARIZATION WITH TEMPERATURE AS A PARAMETER

The experimental evidence to date is that $BaTiO_3$ undergoes a first-order transition at its upper Curie point. It may easily be shown that the correct expression for the spontaneous polarization in this case is given by Eq. (2.6) in which the term in parenthesis is taken with the minus sign. Thus in the neighborhood of T_0,

$$P_s^2 = \frac{-b'}{c'} + \frac{a'}{b'}$$

for $T \leq T_c$, and

$$P_s^2 = 0$$

for $T > T_c$ where T_c is the Curie temperature, which is not necessarily equal to T_0 for a first-order transition.

An effect which is predicted from the free-energy function and which is of importance in analyzing the behavior of the ceramic dielectrics, is the shift in transition temperature with an applied field. This can be shown in the following way. The stability requirement demands that at a minimum in free energy

$$\frac{\partial^2 A}{\partial P^2} > 0 .$$

From Eq. (2.5) one has

$$\frac{\partial^2 A}{\partial P^2} = \frac{\partial E}{\partial P} = a' + 3b' P^2 + 5c' P^4 > 0 \qquad (2.9)$$

for stability. If one plots (Ref. 24) P vs. E out of Eq. (2.5), the hysteresis behavior of the single crystal becomes evident and this behavior is shown in Fig. 7. A value of P for a given E is unstable for which $\frac{\partial E}{\partial P} < 0$ and a discontinuous change in P takes place (along the dotted lines) until one has again $\frac{\partial E}{\partial P} > 0$. The free-energy function predicts double hysteresis loops for $T > T_c$, and these have actually been observed by Merz (Ref. 24) and by Diamond and Orr (Ref. 26). These double hysteresis loops come about as a result of the dependence of the coefficient a' on the temperature. For $T > T_0$ the a' term in Eq. (2.9) is positive and the slope $\frac{\partial E}{\partial P}$ of the polarization-field characteristic of Fig. 7 is also positive at E = 0. This means that at E = 0 the material is paraelectric, since P = 0 at E = 0 is a stable solution to Eq. (2.5). Now as E is increased at temperatures $T > T_0$, the second term in Eq. (2.9), i.e., $3b' P^2$, becomes increasingly important. Since b' has a value which is negative, a field is soon reached at which $\frac{\partial E}{\partial P}$ becomes negative. At this value of E the polarization jumps discontinuously to a new value for which $\frac{\partial E}{\partial P}$ is positive and hence stable. This leads to the double hysteresis loops shown in Fig. 7 for $T > T_0$. The double hysteresis loop actually amounts to a shift in the Curie point to higher temperatures with applied field since the single-valued part of the P(E) characteristic is paraelectric and the double-valued part is ferroelectric. It is also interesting to note that at sufficiently high temperatures the crystal will not become ferroelectric even under the strongest of electric fields. This amounts to a change from a first-order transition to a second-order one. This can only be possible if the coefficient b' is a function of temperature as has been found by Huibregtse and Young (see Table III).

Knowledge of the rate at which the Curie point shifts with electric field will be required in a later section and may be estimated from Eq. (2.5). In order to carry out the derivation, the following assumptions will be made.

(a) The double hysteresis loops represent a ferroelectric state induced by the field.

(b) The field at which the ferroelectric state is induced is taken to be the field halfway between the sides of the double loop. The temperature associated with this particular loop is the modified Curie temperature.

(c) This field represents an inflection point on the P vs. E characteristic.

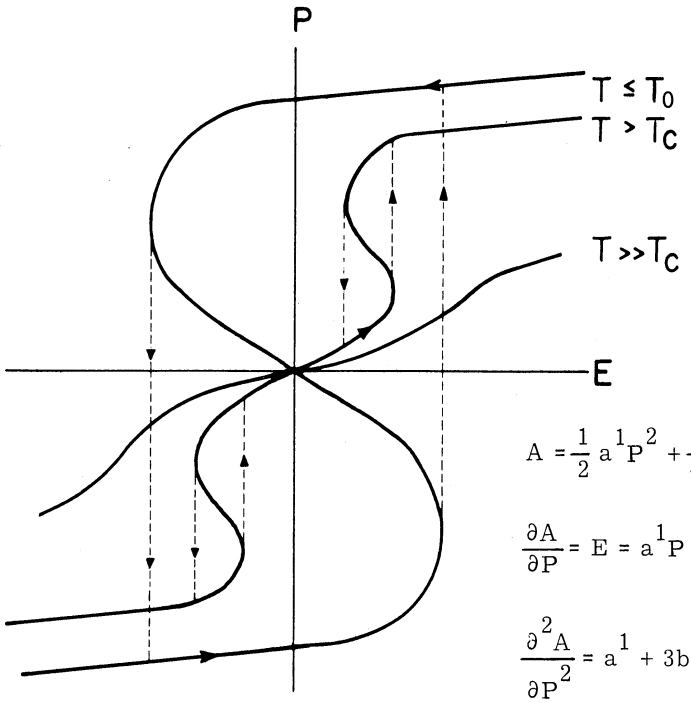

$$A = \frac{1}{2}a^1P^2 + \frac{1}{4}b^1P^4 + \frac{1}{6}c^1P^6 \qquad a^1 \cong \frac{T - T_o}{10^4}$$

$$\frac{\partial A}{\partial P} = E = a^1P + b^1P^3 + c^1P^5 \qquad b^1 \cong -10^{-12}$$

$$\frac{\partial^2 A}{\partial P^2} = a^1 + 3b^1P^2 + 5c^1P^4 \qquad c^1 \cong 3 \times 10^{-22}$$

$$T_0 \cong 110^{\circ}C$$

FIG. 7. THE P VS. E CHARACTERISTIC FOR A FREE $BaTiO_3$ CRYSTAL BASED ON DEVONSHIRE'S FREE-ENERGY FUNCTION. [After Merz (Ref. 24).]

Thus Eq. (2.5) is rewritten as

$$E = a'P + b'P^3 + c'P^5,$$

and the inflection points are

$$\frac{\partial^2 E}{\partial P^2} = 6b'P + 20c'P^3 = 0.$$

The inflection at P = 0 is of no concern here, so that the above becomes

$$3b' + 10c'P^2 = 0,$$

or

$$P^2 = -\frac{3b'}{10c'} \qquad (2.10)$$

for the point of inflection. Recall that b' has a negative value for a first-order transition.

Substituting Eq. (2.10) into Eq. (2.5) gives the dependence of $a' = \frac{T - T_0}{c}$ on E. That is, for convenience, let $-\frac{3b'}{10c'} = \ell^2$, so that

$$E = a'\ell + b'\ell^3 + c'\ell^5$$

and

$$a' = \frac{E - b'\ell^3 - c'\ell^5}{\ell}.$$

Substituting for a' results in

$$T^* - T_0 = \frac{C(E - b'\ell^3 - c'\ell^5)}{\ell}. \qquad (2.11)$$

Here T* is the temperature associated with the inflection point at E and is the modified Curie point. T_0 is the temperature to which $\frac{1}{\chi}$ vs. temperature is extrapolated in the Curie-Weiss law. This is not the same as the observed zero-field Curie temperature. For E = 0 and P $\neq$ 0 the inflection occurs on the P-axis. For this case one has the temperature at which the ferroelectric hysteresis loop just begins to show a double character. This is the observed zero-field Curie temperature, T_c. Therefore, from Eq. (2.11) with E = 0 the following is obtained:

$$T_c - T_0 = C(-b'\ell^2 - c'\ell^4) = c\left(\frac{3b'^2}{10c'} - \frac{9b'^2}{1000c'}\right). \qquad (2.12)$$

Numerically,

$$T_c - T_0 = 10^4\left(\frac{3 \times (1.1)^2 \times 10^{-24} \times 0.7}{10 \times 2.8 \times 10^{-22}}\right) = 10^{\circ}C.$$

T_0 is found experimentally to be 110°C, so that one expects the Curie transition at 120°C — just where it is observed for $BaTiO_3$! By substituting Eq. (2.12) into Eq. (2.11) one obtains the relationship between the zero-field Curie temperature, the "new" Curie temperature, and the field. That is,

$$T^* - T_0 = \frac{CE}{\ell} + T_c - T_0.$$

Hence

$$T^* - T_0 = \frac{CE}{\sqrt{\frac{-3b'}{10c'}}}. \qquad (2.13)$$

This last result is rather important, and we will make use of it later. It shows that the shift in Curie point is a linear function of E. Numerically, using Merz's values of $C = 10^4$, $c' = 2.8 \times 10^{-22}$, $b' = -1.1 \times 10^{-12}$, one obtains $\frac{\Delta T^*}{\Delta E} \simeq 10^{-3}$ °C/volt/cm. If the temperature-

dependent value of b' (Huibregtse and Young's value in Table III) were to be used, the result (Eq. 2.13) would be slightly more complicated. One notes from this relationship that the shift in Curie temperature with field occurs only for $b' < 0$ and $c' > 0$, i.e., for a first-order transition.

Experimentally, the shift in Curie temperature may be measured from the double hysteresis loops. By means of the apparatus shown schematically in Fig. 8 one may display these hysteresis loops at various temperatures. The specimen is placed in a temperature bath of transformer oil and excited by a 60-cycle, 1000-volt power transformer. The x-input to the oscilloscope receives a suitable part of the driving field of the divider R_1R_2. The polarizing current i, which flows through the specimen, is integrated by the capacitor C, producing an output voltage proportional to the polarization. If P is the polarization in coulombs per square centimeter and A is the electroded area of the specimen in square centimeters, then

$$P = \frac{1}{A}\int i\,dt,$$

and since

$$V = \frac{1}{C}\int i\,dt,$$

then

$$P = \frac{C}{A}V.$$

The above enables one to calibrate the oscilloscope for polarization. Figure 9 shows a series of double hysteresis loops which have been traced off the oscillograms for a $BaTiO_3$ single crystal. The zero-field Curie temperature seems about 5° lower than most of the reported data for single crystals. This may be due to impurities in the crystal.[8]

Figure 10 shows the shift in Curie temperature with field, the data being taken from the photographs of Fig. 9. The measured shift in this experiment is 1.2×10^{-3} °C/volt/cm, consistent with the theoretical value predicted by Eq. (2.13).

To recapitulate the preceding section, it has been shown that by starting with the free-energy function for $BaTiO_3$ postulated by Devonshire, it is possible to predict a shift in Curie point with an applied field. An experimental determination of this shift has been made, and the observed value is in fair agreement with that derived from the thermodynamic analysis. This result will be used in a later section in order to explain the observed large-field nonlinearity in the perovskite-type ferroelectrics on the basis of an "induced ferroelectricity." The shift in Curie temperature upward with field implies such an induced ferroelectricity.

[8] The crystals were prepared by the writer in the Solid-State Devices Laboratory at The University of Michigan by growing them out of a high-temperature melt.

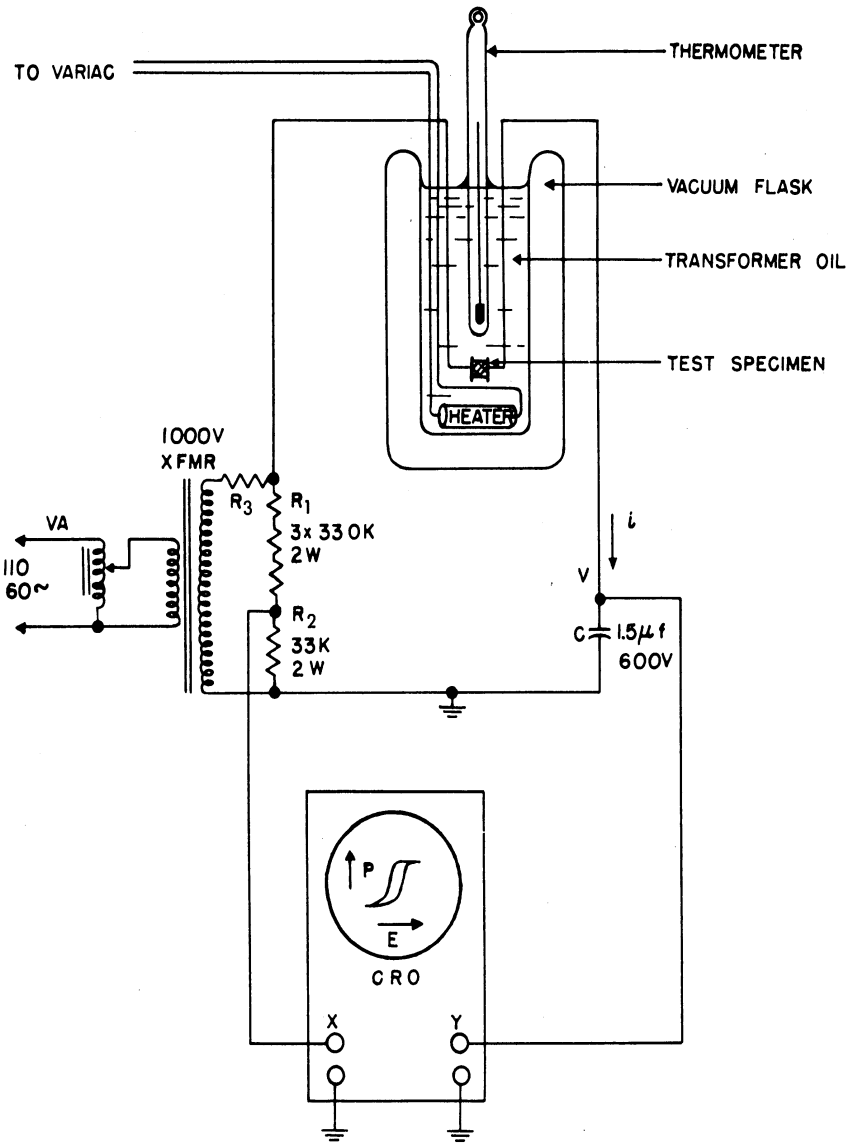

FIG. 8. THE P-E HYSTERESIS LOOP PLOTTER

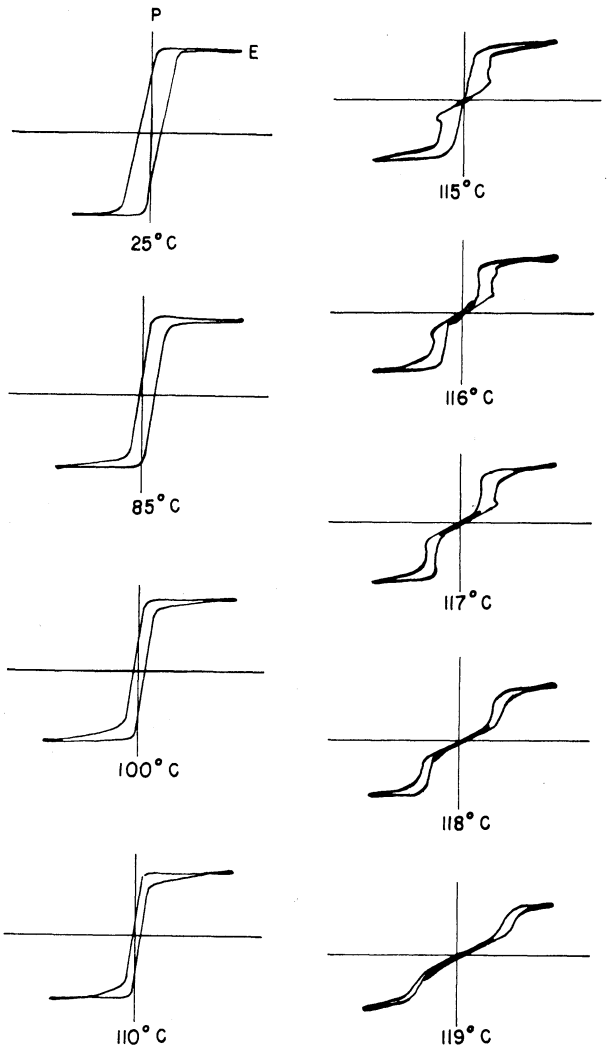

FIG. 9. DOUBLE HYSTERESIS LOOPS IN A c-ORIENTED $BaTiO_3$ CRYSTAL

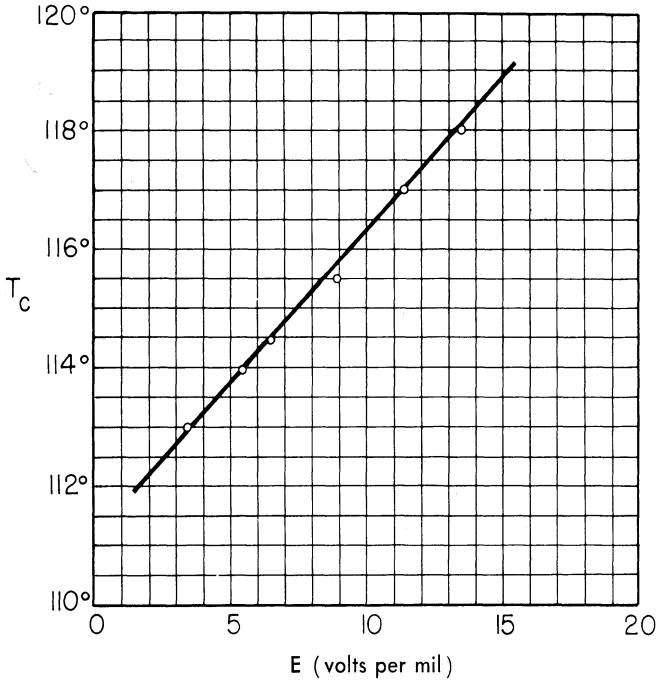

FIG. 10. CURIE TEMPERATURE AS A FUNCTION OF FIELD

2.2. RELATIONSHIP BETWEEN THE FREE AND CLAMPED COEFFICIENTS IN THE FREE-ENERGY, ISOTHERMAL, AND ADIABATIC CONDITIONS

The values for a', b', c', c, T_0, and T_c are all taken under the assumption of zero stresses in Eq. (2.3). This essentially means that the crystal is allowed to strain freely in compliance with an electric field. Experimentally, at sufficiently low frequencies these conditions are met. As will be shown via dynamic spectra in Sec. 3, the crystals of $BaTiO_3$ become effectively clamped at frequencies on the order of 10^7 cps. According to the behavior of these types of ferroelectrics in the uhf and microwave regions, a free-energy function having coefficients obtained under clamped conditions is required.

A more general expansion of the Helmholtz free energy containing terms in the crystal strains has been expressed by Devonshire for the case of the strained cubic crystal as:

$$A = A_0 + \frac{1}{2}a''\left(P_1^2 + P_2^2 + P_3^2\right) + \frac{1}{4}b''_{11}\left(P_1^4 + P_2^4 + P_3^4\right) + \frac{1}{2}b''_{12}\left(P_2^2P_3^2 + P_1^2P_2^2 + P_1^2P_3^2\right) \qquad (2.14)$$

(Continued on page 34)

$$+\frac{1}{2}c_{11}\left(x_1^2 + x_2^2 + x_3^2\right) + c_{12}\left(x_2x_3 + x_1x_3 + x_1x_2\right)$$

(Continued from p. 33)

$$+\frac{1}{2}c_{44}\left(x_4^2 + x_5^2 + x_6^2\right) \qquad (2.14)$$

$$+ q_{11}\left(x_1P_1^2 + x_2P_2^2 + x_3P_3^2\right) + q_{12}\left[x_1\left(P_2^2 + P_3^2\right)\right.$$

$$\left. + x_2\left(P_3^2 + P_1^2\right) + x_3\left(P_1^2 + P_2^2\right)\right]$$

$$+ q_{44}\left(x_4P_2P_3 + x_5P_3P_1 + x_6P_1P_2\right) + \ldots \text{ terms in } P^6$$

etc.

In the above, a'', b'' are defined as the dielectric coefficients for zero strain, analogous to the a' and b' defined for zero stress. The subscripts 1, 2, and 3 on P and x indicate, respectively, the x, y, and z components of the polarization and strain. The components x_4, x_5, and x_6 are shear strains. The q's are electrostrictive coefficients, and the c's represent the elastic coefficients corresponding to the Young's modulus. Gibbs free-energy function, for the stress-free crystal, may be put into a form analogous to Eq. (2.14) by replacing in Eq. (2.14) the double primes by primes and the strains x by the stresses X. This will also involve different elastic coefficients obtained by replacing the c's by new coefficients s, and the q's by Q.

With the free-energy function stated in the form above, one treats the crystal in the ferroelectric state as if it were a cubic isotropic crystal which has been strained under the influence of its own spontaneous polarization or "self field." Under these conditions $P \rightarrow P_s$ in the expression for the free energy. The function as stated in Eq. (2.14) is consistent with the usual equations relating stress to strains and polarization (see also Eq. 2.3):

$$\left(\frac{\partial A}{\partial x_i}\right)_{P,T} = X_i = c_{ij}x_i + q_{ijk}P_jP_k .$$

Because of the symmetry between the two a - axes in the tetragonal structure of $BaTiO_3$,

$$c_{12} = c_{13}; \quad c_{23} = c_{32} = 0.$$

Devonshire further shortens the notation for q_{ijk} to read

$$q_{111} \equiv q_{11}$$

$$q_{122} \equiv q_{12}$$

$$q_{133} \equiv q_{13} = q_{12}$$

$$q_{123} = q_{321} = q_{231} = 0, \text{ etc.},$$

and

$$P_1 \equiv P_s .$$

It is therefore possible to derive piezoelectric coefficients from the electrostrictive coefficients for $P_1 = P_s$ in Eq. (2.14), viz:

$$\left(\frac{\partial A}{\partial x_i}\right)_{P,T} = x_1 = c_{11}x_1 + c_{12}(x_2 + x_3) + q_{11}P_1^2 + q_{12}\left(P_2^2 + P_3^2\right),$$

and

$$\left(\frac{\partial X_1}{\partial P_1}\right)_{xT} \equiv b_{11} = 2q_{11}P_1 .$$

Here b_{11} is a piezoelectric coefficient and may be evaluated from a knowledge of the value of q_{11} and by allowing $P_1 \rightarrow P_s$.

Devonshire relates the coefficients for a free crystal to those of the clamped crystal by noting from Eq. (2.3) that $\left(\frac{\partial A}{\partial x_i}\right)_{P,T} = X_i$ and setting $X_i = 0$, obtaining:

$$\left.\begin{aligned} a' = a'' &= \frac{T - T_0}{10^4} \\ b'_{11} &= b''_{11} + 2\left[\frac{-q_{11}^2(c_{11} + c_{12}) + 4q_{11}q_{12}c_{12} - 2q_{12}^2c_{11}}{(c_{11} + 2c_{12})(c_{11} - c_{12})}\right] \\ b'_{12} &= b''_{12} + 2\left[\frac{-q_{11}^2c_{12} + 2q_{12}q_{11}c_{11} - q_{12}^2(-c_{11} + 2c_{12})}{(c_{11} - c_{12})(c_{11} + 2c_{12})}\right] . \end{aligned}\right\} \qquad (2.15)$$

The derivation of this result is given in the Appendix. These relationships are of importance in that they enable one to relate the behavior of the clamped crystal to that of a free crystal. For example, the relationship between the free and clamped permittivity may be shown.

Let us examine this relationship for a $BaTiO_3$ crystal viewed along its c-axis. It has already been noted from Eq. (2.5) that

$$\left(\frac{\partial A}{\partial P_1}\right)_{X,T} = E_1 = a'P_1 + b'_{11}P_1^3 + \ldots ,$$

where $P_2 = P_3 = 0$ (i.e., there is no polarization along the a-axis). One may also write from the free-energy function

$$\left(\frac{\partial A}{\partial P_1}\right)_{x,T} = E_1 = a''P_1 + b''_{11}P_1^3 + \ldots ,$$

and since $\left(\frac{\partial E_1}{\partial P_1}\right) = \frac{1}{\chi_c}$, it follows that

$$\frac{1}{\chi_c''} = \frac{1}{\chi_c'} + 6\left[\frac{q_{11}^2(c_{11}+c_{12}) - 4q_{11}q_{12}c_{12} + 2q_{12}^2c_{11}}{(c_{11}+2c_{12})(c_{11}-c_{12})}\right]P^2. \tag{2.16}$$

By assuming that the strains along the polar axis are the most significant, one may approximate by saying that $c_{12} = q_{12} \cong 0$, thus obtaining

$$\frac{1}{\epsilon_c(\text{clamped})} - \frac{1}{\epsilon_c(\text{free})} = \frac{6q_{11}^2}{4\pi c_{11}}P^2. \tag{2.17}$$

The latter formula indicates that the small-signal (i.e., for $P \rightarrow 0$) permittivities for the free and clamped crystal above the Curie temperature are the same. For temperatures below the Curie temperature $P \rightarrow P_s$, the spontaneous polarization, and a significant difference in the permittivities is expected.

If the crystal is viewed with a small signal along its a-axis but is polarized in the c-direction, the free and clamped permittivities are found as before from Eq. (2.14) viz:

$$\left(\frac{\partial A}{\partial P_2}\right)_{P_1, X, T} = E_2 = a''P_2 + b_{11}''P_2^3 + b_{12}''P_3^2P_2 + b_{12}''P_1^2P_2$$

$$+ 2q_{11}x_2P_2 + 2q_{12}(x_1 + x_3)P_2 \ldots .$$

For $x = 0$ and $P_3 = 0$,

$$\left(\frac{\partial E_2}{\partial P_2}\right)_{x=0} = \frac{1}{\chi_{a''}} = a'' + b_{12}''\left(+P_1^2\right) + 3b_{11}''P_2^2.$$

For the small-signal limit, $P_2 \rightarrow 0$, and

$$\frac{1}{\chi_{a''}} = a'' + b_{12}''\left(P_1^2\right). \tag{2.18}$$

Similarly for the free crystal:

$$\frac{1}{\chi_{a'}} = a' + b_{12}'\left(P_1^2\right) + \ldots . \tag{2.19}$$

Letting $P_1 = P_s$, the spontaneous polarization along the c-axis, and letting the induced polarization along an a-axis be P_2 with $P_3 = 0$, one obtains with the aid of Eq. (2.15):

$$\frac{1}{\chi_{a''}} = \frac{1}{\chi_{a'}} + 2\left[\frac{-q_{11}^2 c_{12} + 2q_{11}q_{12}c_{11} + q_{12}^2(c_{11} - 2c_{12})}{(c_{11} - c_{12})(c_{11} + 2c_{12})}\right]P_s^2. \qquad (2.20)$$

Here, as for the case for the c-axis, when the spontaneous polarization goes to zero, the free and clamped small-signal permittivities are the same.

In a recent paper, Berlincourt and Jaffe (Ref. 27) have presented some experimental evaluations of the elastic and electrostrictive constants for $BaTiO_3$ single crystals. These data are presented in terms of the elastic compliances s_{ij} rather than in the modulii c_{ij}. Since one set of coefficients forms the inverse matrix of the other set, it is not difficult to compute the c's from Berlincourt and Jaffe's values for s. The electrostrictive coupling constants q and Q are defined by Eq. (2.21).

$$X_h = -c_{hi}x_i + q_{hk\ell}P_kP_\ell,$$

and (2.21)

$$x_i = -s_{ij}X_j + Q_{imn}P_mP_n.$$

Some of these constants are shown in Table IV.

TABLE IV. SOME VALUES OF ELASTIC AND ELECTROSTRICTIVE COEFFICIENTS FOR $BaTiO_3$ SINGLE CRYSTALS

Constant	Value in esu	Investigator
s_{11}	0.725×10^{-12}	Berlincourt and Jaffe (Ref. 27)
s_{12}	-0.315×10^{-12}	Berlincourt and Jaffe (Ref. 27)
$s_{13} = s_{23}$	-0.326×10^{-12}	Berlincourt and Jaffe (Ref. 27)
s_{33}	1.08×10^{-12}	Berlincourt and Jaffe (Ref. 27)
Q_{11}	3.1×10^{-12}	Mean value computed from two values given by Devonshire (Ref. 23)
Q_{12}	-1.23×10^{-12}	Mean value computed from two values given by Devonshire (Ref. 23)
c_{11}	2.4×10^{12}	Mean value computed from above data.
c_{12}	1.7×10^{12}	Mean value computed from above data.
q_{11}	3.2	Mean value computed from above data.
q_{12}	0.28	Mean value computed from above data.

From these equations one has

$$Q_{imn} = s_{ih} q_{hmn},$$

and (2.22)

$$q_{hmn} = c_{hi} Q_{imn} .$$

By substituting the coefficients from Table IV into Eq. (2.16) one obtains for the c-direction:

$$\frac{\epsilon_{cX}}{\epsilon_{cx}} = 1 + \frac{6}{4\pi} \epsilon_{cX} P_s^2 \left[\frac{q_{11}^2 (c_{11} + c_{12}) - 4q_{11}q_{12}c_{12} + q_{12}^2 c_{11}}{(c_{11} + 2c_{12})(c_{11} - c_{12})} \right] \tag{2.23}$$

$$= 1 + \frac{6}{4\pi} \times \frac{168 \times 0.64}{10^2} \left[\frac{(3.2)^2 (4.1) - 4(3.2)(0.28)(1.7) + 2(2.8)^2 (2.4)}{(58)(0.7)} \right],$$

or

$$\frac{\epsilon_{cX}}{\epsilon_{cx}} \simeq 1.5,$$

where ϵ_{cX} is the permittivity at zero stress and ϵ_{cx} is the permittivity at zero strain. That is, as the crystal is clamped, the polar-direction dielectric constant is reduced by a factor of 1.5. The experimental results cited in Sec. 3 show about a twofold reduction in permittivity. This is not a bad correlation considering that the values for the Q (from which the q were calculated) given by Devonshire are fairly crude.

Applying the same constants to Eq. (2.20) yields for the crystallographic a-direction:

$$\frac{\epsilon_{aX}}{\epsilon_{ax}} = 1 + \frac{P^2 \epsilon_{aX}}{2\pi} \left[\frac{+q_{11}^2 c_{12} - 2q_{11}q_{12}c_{11} - q_{12}^2 (c_{11} - 2c_{12})}{(c_{11} - c_{12})(c_{11} + 2c_{12})} \right],$$

or (2.24)

$$\frac{\epsilon_{aX}}{\epsilon_{ax}} \simeq 1 + \frac{0.64}{2\pi} \times \frac{2900}{10^2} \left[\frac{(3.2)^2 \times (1.7) - (6.4)(0.28)(3.2) + (0.28)^2 (1)}{(58)(0.7)} \right];$$

$$\frac{\epsilon_{aX}}{\epsilon_{ax}} \simeq 2.$$

This result is almost identical with the observed data.

The following conclusion may be drawn. Relaxation of permittivity with frequency in the $BaTiO_3$-like crystals or ceramics due to mechanical clamping will not reduce the permittivity by more than a factor of about two.

This result is especially interesting in view of the data cited by Kittel, reproduced in Fig. 5, where a reduction in permittivity by a factor of ten or more is noted within a frequency range of 100:1. It was this remarkable graph which motivated the experiments on the single crystals in order to: (1) determine whether the results of Eq. (2.21) and (2.22) are experimentally verified; and (2) follow up this investigation by pursuing the question that if the clamping is indeed limited by the factor 2, then can the data of Fig. 5 be correct? A positive answer to (1) and (2) would definitely rule out an explanation of the microwave dielectric relaxation based solely on the clamping concept. This issue will be discussed after the experiments and the experimental results have been described.

It is now of interest to consider the difference between the isothermal and adiabatic permittivities. In all of the thermodynamic development up to this point, the dielectric susceptibilities have come out of terms such as $\left(\frac{\partial^2 A}{\partial P^2}\right)_{X,T}$ or $\left(\frac{\partial^2 A}{\partial P^2}\right)_{xT}$. That is, the susceptibility is taken at some fixed value of temperature while the other thermodynamic parameters are being varied. This condition strictly holds for static dielectric measurements only. For alternating fields it is the entropy which is constant, i.e., the measurement of susceptibility is taken under adiabatic conditions. The isothermal and adiabatic susceptibilities can be related to one another in the same sense that the free and clamped values are related. A consideration of the case of a free crystal will show this connection. The susceptibility is found via the free-energy function as

$$\frac{1}{\chi_T} = \left(\frac{\partial^2 A}{\partial P^2}\right)_{X,T} = a' + 3b'P^2 + \ldots, \tag{2.25}$$

the subscript T being used to indicate the isothermal condition. If the electric field is considered to be a function of polarization and temperature, that is, $E = E(P, T)$, then

$$dE = \left(\frac{\partial E}{\partial P}\right)_T dP + \left(\frac{\partial E}{\partial T}\right)_P dT,$$

from which

$$\left(\frac{\partial E}{\partial P}\right)_S = \left(\frac{\partial E}{\partial P}\right)_T + \left(\frac{\partial E}{\partial T}\right)_P \left(\frac{\partial T}{\partial P}\right)_S. \tag{2.26}$$

The subscript S indicates an isentropic process. From the definition of the Gibbs free energy one has

$$\left(\frac{\partial G}{\partial T}\right)_E = -S \quad \text{and} \quad \left(\frac{\partial G}{\partial E}\right)_T = -P,$$

from which

$$\frac{\partial^2 G}{\partial T \partial P} = \frac{\partial^2 G}{\partial P \partial T} = -\left(\frac{\partial P}{\partial T}\right)_S = -\left(\frac{\partial S}{\partial E}\right)_P. \tag{2.27}$$

Substituting this into Eq. (2.26) one obtains

$$\left(\frac{\partial E}{\partial P}\right)_S = \left(\frac{\partial E}{\partial P}\right)_T + \left(\frac{\partial E}{\partial T}\right)_P \left(\frac{\partial E}{\partial S}\right)_P . \tag{2.28}$$

Now

$$\left(\frac{\partial E}{\partial S}\right)_P = \left(\frac{\partial E}{\partial T}\right)_P \left(\frac{\partial T}{\partial S}\right)_P ,$$

and

$$\left(\frac{\partial S}{\partial T}\right)_P = \frac{C_P}{T},$$

where C_P is the heat capacity at constant polarization. Since $\frac{\partial E}{\partial P} = \frac{1}{\chi}$, one may then write Eq. (2.28) as:

$$\frac{1}{\chi_S} = \frac{1}{\chi_T} + \frac{\left(\frac{\partial E}{\partial T}\right)_P^2 T}{C_P}. \tag{2.29}$$

From the free-energy function,

$$E = \left(\frac{\partial A}{\partial P}\right)_T = a'P + b'P^3 + \ldots ;$$

and

$$\left(\frac{\partial E}{\partial T}\right)_P = P\left(\frac{\partial a'}{\partial T}\right)_P = P\frac{\partial}{\partial T}\left(\frac{T - T_0}{10^4}\right) = \frac{P}{10^4} \tag{2.30}$$

if b' is not temperature dependent. Therefore, Eq. (2.30) with Eq. (2.29) gives the result that

$$\frac{1}{\chi_S} - \frac{1}{\chi_T} = \frac{P^2 T}{10^8 C_P} . \tag{2.31}$$

The heat capacity of barium titanate is of the order of 0.9 cal/cm^3/deg. = 4 x 10^7 ergs/cm^3/deg. Taking $P = P_S = 0.78 \times 10^4$ esu and T = 400°K, one has

$$\frac{1}{\chi_S} - \frac{1}{\chi_T} \simeq \frac{0.6 \times 10^8 \times 4 \times 10^2}{10^8 \times 4 \times 10^7} = 6 \times 10^{-6},$$

or in terms of ϵ

$$\frac{1}{\epsilon_S} - \frac{1}{\epsilon_T} \simeq \frac{6}{4\pi} \times 10^{-6} \simeq 5 \times 10^{-7} ,$$

a difference which is clearly so small that it makes no practical difference in our measurements of ϵ.

This section concludes with a summary. In order to ascertain whether the reported strong microwave relaxation effect in $BaTiO_3$ ceramic could be explained on the basis of clamping, it was considered desirable to determine the theoretical magnitude of this effect based on the free-energy function of Devonshire. The calculations have shown that by clamping a $BaTiO_3$ crystal the dielectric constant is reduced roughly to one half of the "free" value. Experiments to be described in Sec. 4 completely confirm this behavior. It was further recognized that isothermal and adiabatic measurements of the permittivity do not in general lead to the same results. An estimate of this effect in $BaTiO_3$ has been made, and it was shown that for this case the difference between the adiabatic and isothermal permittivities is negligible.

2.3. SOME POLYCRYSTALLINE PROPERTIES

For many of the applications of ferroelectrics to devices which employ the nonlinearity in the permittivity with field, single crystals are unsuitable. In the first place, the single crystals are rather difficult to make, and in the second place, the properties of the crystal are somewhat different from those of a polycrystalline ceramic – especially if the ceramic contains additives. The high-permittivity perovskite mixed ceramics such as $Ba_xSr_{1-x}TiO_3$ and $Pb_xSr_{1-x}TiO_3$,[9] for example, exhibit a rather strong dependence of the incremental permittivity on electric field and temperature over a comparatively wide temperature range (compared, that is, to the single-crystal properties). The basic mechanism for the change or switching of polarization in the single crystal has been shown by many investigations to be essentially a domain growth and alignment process. However, an attempt to extend the idea of domain alignment and growth to the polycrystalline dielectric leads to some contradictions which shall be presently discussed. It is therefore of considerable practical interest to examine the mechanism of polarization for the polycrystalline ferroelectrics in light of the theory developed up to this point. First, however, it is well to review some of the properties of ceramic $Ba_xSr_{1-x}TiO_3$ which will serve as a model for all the mixed ceramics of this class of ferroelectrics.

In the polycrystalline ferroelectrics it is often necessary to consider the temperature at which the dielectric exhibits maximum permittivity. This is in contrast with the single crystal in which the Curie point is also the point of maximum permittivity as well as the transition between the ferroelectric and nonferroelectric state. For the ceramic this transition takes place gradually over a wide temperature range.

It was discovered very early by several investigators (Ref. 28 and 29) that for cation substitution in the Ba site of $BaTiO_3$, the effect is for cations, such as Sr, Ca, Mg, Fe, Sn, Pb,

[9] The value of x, of course, ranges from 0 to 1.

and others, to lower or raise the Curie temperature. Thus it is possible to have a mixed crystal or ceramic ferroelectric with a room-temperature Curie point by the inclusion of the proper amount of additive. The "proper" amount for $Ba_xSr_{1-x}TiO_3$ is x = 0.65.

Extensive experimental data have been taken in our laboratories on Ba-Sr-TiO_3 and isomorphic ferroelectrics with regard to the electric field and temperature sensitivity. In order to facilitate the handling of a large volume of routine data it was arranged to have the incremental permittivity at a fixed frequency (10,000 cps) plotted automatically as the temperature and electric field were varied. The experimental arrangement is shown in the form of a block diagram in Fig. 11. In this diagram it is seen that a small signal is fed through the specimen and a resistor R_2 whose resistance is much smaller than the reactance of the specimen. The signal voltage across R_2 will thus be proportional to the capacitance and therefore to the permittivity of the specimen. This voltage is rectified, amplified, and placed on the Y-input of a Mosely X-Y recorder. The biasing electric field is supplied through resistance R_1 by a motor-driven, high-voltage, variable power supply, the output voltage of which is sampled and fed onto the X-terminal of the X-Y recorder. With this apparatus the incremental or small-signal permittivity is plotted automatically vs. electric field with the temperature as a parameter.

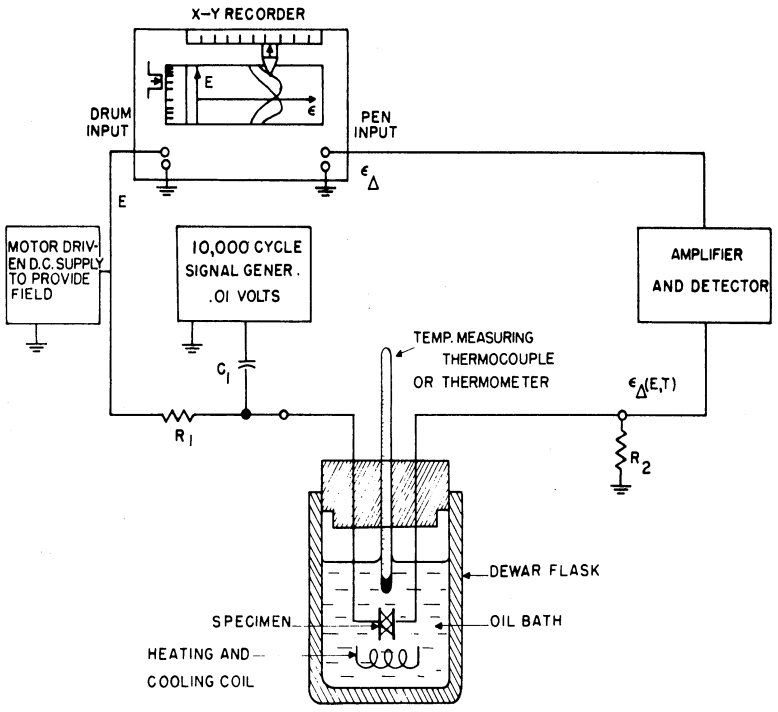

FIG. 11. AUTOMATIC RECORDING UNIT FOR MEASURING ϵ_Δ VS. E AND T

Typical results for a $Ba_{0.65}Sr_{0.35}TiO_3$ ceramic composition are shown in Fig. 12 where the display of the data is an isometric surface with the permittivity being plotted as an altitude

vs. the electric field and temperature as the independent variables. It is evident that the Curie region is extremely broad for the zero-field case and becomes even further spread out in temperature as an electric field is applied; consequently, the temperature of peak permittivity becomes difficult to measure. Nevertheless, a very definite shift in the peak toward higher temperatures is observed and has the value of about 1.4×10^{-3} °C/volt/cm, which is roughly that which is measured for a $BaTiO_3$ single crystal.

This behavior is to be compared with that of the pure $BaTiO_3$ ceramic shown in Fig. 13 and that of the $BaTiO_3$ single crystal shown for zero-bias field in Fig. 2. The pure ceramic shows a rather sharp Curie peak, and what is extremely significant, there is very little dependence of permittivity on the biasing field in the room-temperature region. This constitutes experimental evidence that ferroelectric domains are not being aligned under the action of the field, since any alignment in $BaTiO_3$ (which has such large anisotropy in its permittivities) would certainly appear as a marked decrease in the incremental permittivity. Further evidence is noted in the data shown in Fig. 12 for the mixed ceramic. It is seen that on the low-temperature side of the Curie peak, as the temperature is decreased, the large-field nonlinearity is decreasing, despite the fact that the number of domains is presumably increasing (i.e., the material has more grains becoming ferroelectric as the temperature is lowered).

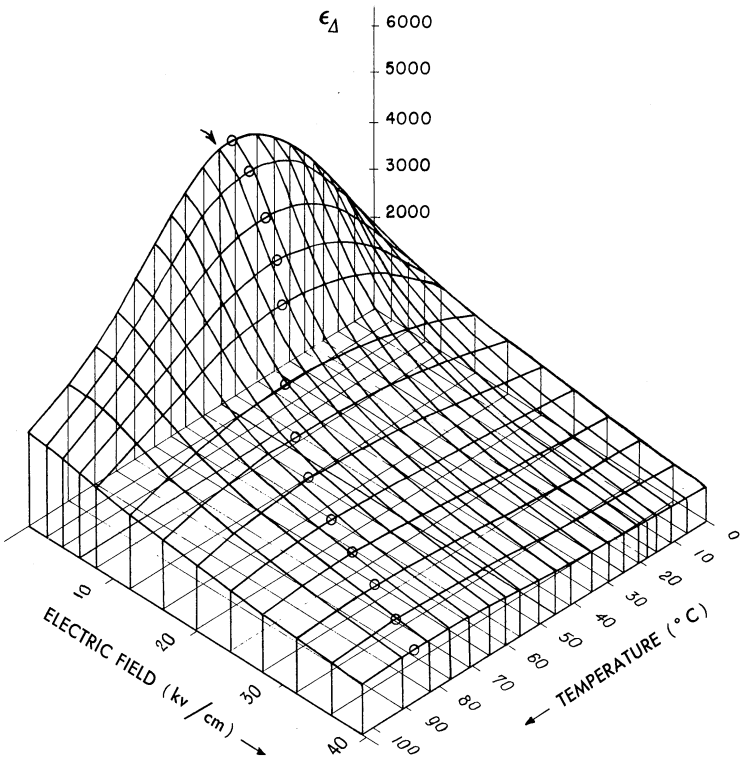

FIG. 12. ϵTE SURFACE FOR A TYPICAL $Ba_{0.65}Sr_{0.35}TiO_3$ CERAMIC

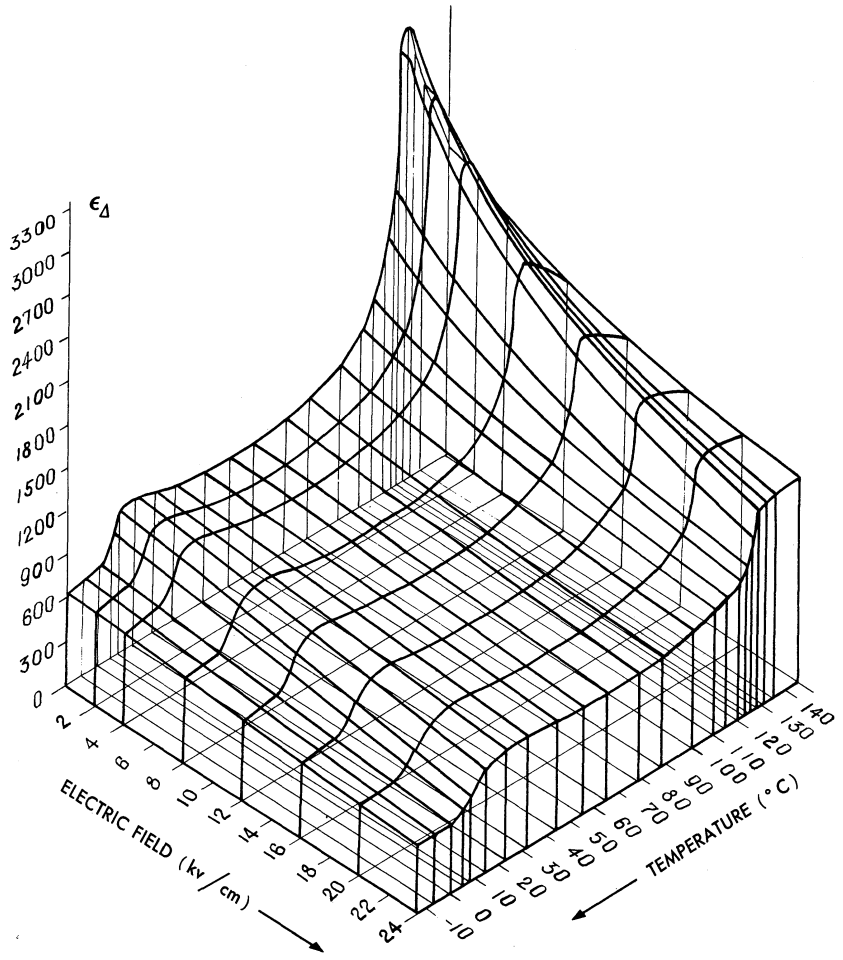

FIG. 13. ϵTE SURFACE FOR A PURE $BaTiO_3$ CERAMIC

The conclusion from these and other experiments is that the domains are "frozen in" with regard to the large electric fields. The question is then raised: what is the explanation for the large-field nonlinearity in the vicinity of the Curie region? It is tempting to postulate that there is something like an activation energy associated with the domains such that with sufficient thermal energy the domains become mobile and then align themselves with the field. A test for such a postulate can be made by the following experiment. If the incremental permittivity is measured both transverse and parallel to the large biasing field, one would expect that as the permittivity decreases when viewed parallel to the field it would increase if viewed transverse to the electric field, if domains were being aligned. An experiment of this type has been performed[10] with a $Ba_{0.65}Sr_{0.35}TiO_3$ ceramic composition, and the results are shown in Fig. 14. It is rather surprising to find that both the parallel and transverse permittivities are reduced with field. It is therefore quite evident that domains are not being aligned with the large fields, and are indeed "frozen in."

[10]These data have been kindly supplied by Mr. T. W. Butler of the Electronics Defense Group, Department of Electrical Engineering, The University of Michigan.

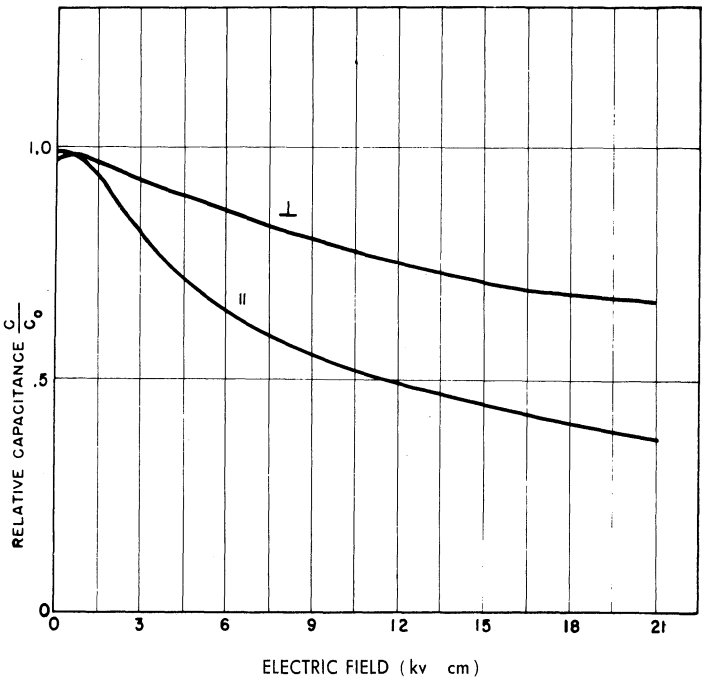

FIG. 14. RELATIVE CAPACITANCE VS. ELECTRIC FIELD. Measured transverse (⊥) and parallel (||) to the field for a $Ba_{0.65}Sr_{0.35}TiO_3$ ceramic.

The question, therefore, of the cause of the large-field nonlinearity in these mixed ceramics is still unanswered. It is at this point that we introduce the notion of an induced ferroelectric state in grains or regions which are essentially nonferroelectric in the absence of the applied field. This is the same type of effect that is observed as a shift in the Curie point of a single crystal and which is predicted from the thermodynamics and observed experimentally (cf. Fig. 9 and 10). In the ceramic or polycrystalline dielectrics, for temperatures in the vicinity of the peak permittivity, one assumes that there is a distribution of Curie points in the different crystallites and therefore that there are a significant number of grains which are actually nonferroelectric under zero-field conditions. The reason for the distribution of Curie points in the different crystallites may be taken as a result of the original processing of the polycrystalline material. For example, since the percentage of strontium in $BaTiO_3$ influences the Curie point, one could expect in preparing a Ba-Sr-TiO_3 ceramic by first mixing the components and then sintering, that the grains thus formed would not all have precisely the same composition and therefore that a distribution of Curie points would result. In fact, in preparing samples for the experiments cited here, it was noticed that the longer and harder (higher temperatures) that the samples of $(BaSr)TiO_3$ were sintered, the lower in temperature the peak permittivity was, indicating that the amount of Sr entering the $BaTiO_3$ lattice by diffusion was, of course, a function of firing time and temperature. Naturally, a distribution of percentage of Sr among the grains is expected for this situation. Also, it is possible to have a distribution

as a result of crystallite strains. The consequences of the postulate of induced ferroelectricity in the polycrystalline material will now be further explored.

3
A THEORY of LARGE-FIELD NONLINEARITY in the PEROVSKITE FERROELECTRICS

3.1. POSTULATES AND GENERAL PROPERTIES

In this section we again specify the case of $Ba_xSr_{1-x}TiO_3$ ferroelectrics, although the results could be qualitatively the same for any ferroelectric whose free-energy function allows the prediction of the shift of the Curie transition to higher temperatures with electric field. To illustrate qualitatively the consequences of our postulate of induced ferroelectricity in the mixed ceramic as the source of large-field nonlinearity, consider the idealization of the thermal behavior of the single crystal shown in Fig. 2. This is presented schematically in Fig. 15. The over-all behavior of the polycrystalline sample is then to be considered an average over many such crystallites taking into account some distribution of the Curie temperatures, T_c.

The idealization shown in Fig. 15 leads one intuitively to the following qualitative conclusions for a material operated in the vicinity of its Curie transition.

(1) The incremental permittivity would first increase for small fields and then decrease (Fig. 15c). This has been verified experimentally, and the data are shown in Fig. 16 as a butterfly loop of sample capacity vs. field.

(2) The transverse (ϵ_a in Fig. 15c) and the parallel (ϵ_c in Fig. 15c) permittivities would slightly increase for small fields and then both decrease. From the figure it is seen that one could expect that the transverse permittivity would not decrease to the same extent as the parallel permittivity. This explains the data of Fig. 14 which could not be made consistent with domain orientation, as has been previously noted.

(3) The rather peculiarly shaped butterfly loop shown in Fig. 16 and predicted by the idealization of Fig. 15(c), also implies that the P vs. E hysteresis loop would be doubled or at least constricted in the zero-field region. This follows from the fact that $\epsilon_\Delta \sim \frac{\partial P}{\partial E}$ and $\frac{\partial \epsilon_\Delta}{\partial E} \sim \frac{\partial^2 P}{\partial E^2}$. Thus where $\frac{\partial \epsilon}{\partial E} = 0$ in Fig. 16 an inflection point would be found on the P vs. E characteristic. The effect is actually observed as can be seen from the data shown in Fig. 17 and 18. Since these conclusions are based on the postulate of an induced ferroelectric state, one can expect that the hysteresis loops would be thinner than for a material in which domains were being moved about. Also, the constricted part of the loop would become longer as the temperature is increased, as can be deduced from Fig. 15. All these properties are experimentally confirmed by the butterfly and hysteresis loops for the $Ba_{0.65}Sr_{0.35}TiO_3$ ceramic shown in Fig. 16, 17, and 18. The hysteresis loop data are traced from oscillograms made with the circuit of Fig. 8.

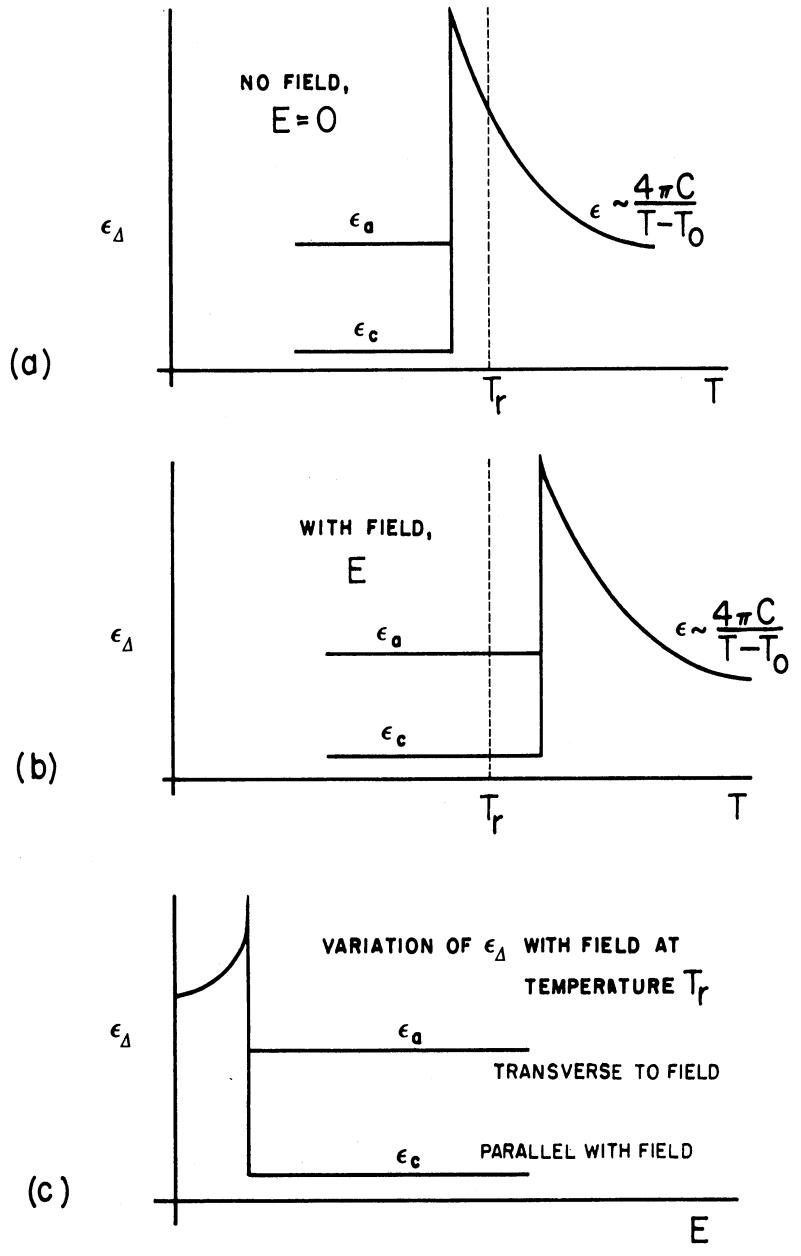

FIG. 15. IDEALIZED THERMAL BEHAVIOR OF A FERROELECTRIC CRYSTALLITE. Based on data of Fig. 2 and the free-energy function. T_r is taken as the "room temperature" or operating temperature.

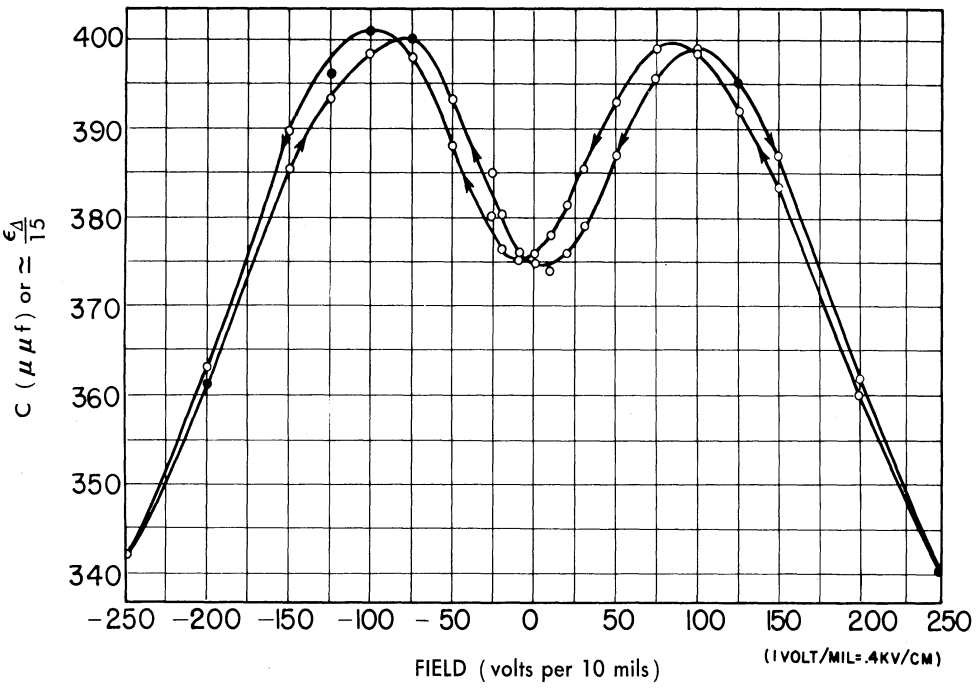

FIG. 16. THE STATIC CAPACITY VS. FIELD BUTTERFLY LOOP FOR A $Ba_{0.65}Sr_{0.35}TiO_3$ FERROELECTRIC CERAMIC AT 25°C. 1 volt/mil = 0.4 kv/cm.

(4) The application of strong fields to the polycrystalline sample would be expected to have two effects. First, as larger and larger fields are applied, more and more of the grains become ferroelectric and therefore have reduced permittivities (cf. Fig. 15), so that the resultant permittivity of the sample as a whole is reduced. Those grains that have not yet become ferroelectric under the influence of the field have rather low Curie temperatures in the distribution, and as more and more of the grains become ferroelectric under the influence of stronger and stronger electric fields, the distribution becomes increasingly weighted toward higher temperatures by those high-permittivity grains which have not yet become ferroelectric. Thus a second effect is expected as a result of the applied field, namely, a shift in the peak permittivity toward higher temperatures. Both properties are shown in the experimental data already cited in Fig. 12.

The evidence, therefore, for an explanation of the large-field nonlinearity based on an induced effect rather than domain orientation seems quite strong. In order to carry out an examination of the process of induced ferroelectricity in ceramics analytically, a model based on the following postulates is considered for a polycrystalline sample.

(1) A Gaussian distribution of Curie temperatures, T_c, is taken about some temperature, T_r. Only the cubic to tetragonal transition is to be considered.

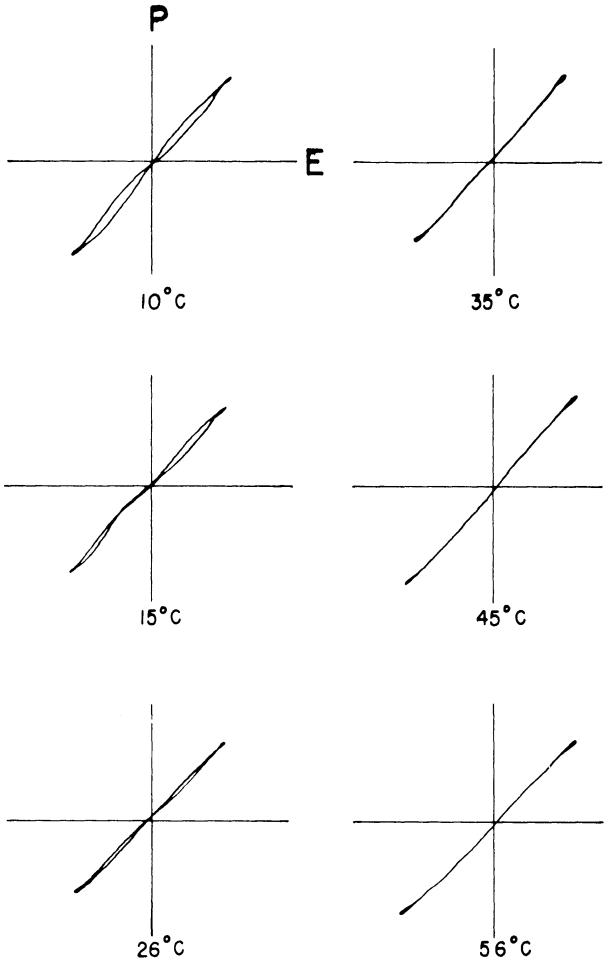

FIG. 17. DOUBLE HYSTERESIS LOOPS FOR A $Ba_{0.65}Sr_{0.35}TiO_3$ CERAMIC AT VARIOUS TEMPERATURES

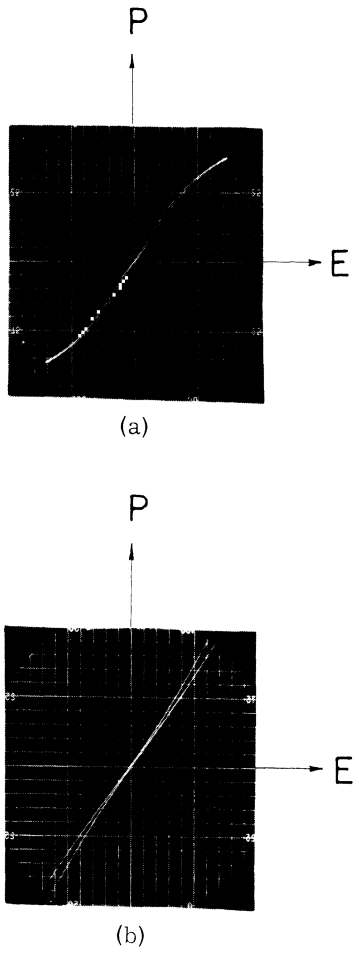

FIG. 18. 60-CYCLE HYSTERESIS LOOPS FOR A $Ba_{0.65}Sr_{0.35}TiO_3$ CERAMIC. (a) Maximum field is 20 kv/cm. Note that the loop is extremely thin. (b) With expanded oscilloscope gain in the zero-field region. Note that there is no remanent polarization at E = 0, which implies that domains are not being switched by the field in this region.

(2) For the zero-field case, each grain is presumed to have a permittivity given by a Curie-Weiss law above its Curie temperature, T_c, and some appropriate constant average value below T_c (cf. Fig. 15). The average value taken for the constant part of the permittivity would lie between ϵ_c and ϵ_a.

(3) When the tetragonal state is induced by an electric field, the c-axis tends to be aligned with the field.

(4) The shift in Curie temperature with field of any one grain is taken in accordance with the results of the thermodynamical arguments of Sec. 2.1.

The model thus chosen undoubtedly is fairly rough. However, it should contain enough of the essential features of the material to allow at least qualitative agreement with the experimental properties outlined above.

3.2. THE ZERO-FIELD CASE

First, it is necessary to determine a value for the average permittivity for the constant part of the characteristic for the ceramic grains (Fig. 19). This is to be considered as the mean value of permittivity taken out of the permittivity tensor ellipsoid. That is, from what is meant by the mean,

$$\epsilon_{av} = \frac{\int_{\phi=0}^{2\pi} \int_{\theta=0}^{\pi} \epsilon(\phi, \theta)\, d\phi\, d\theta}{\int_0^{2\pi} d\phi \int_0^{\pi} d\theta} . \tag{3.1}$$

In Fig. 19, it is assumed that the ellipsoid becomes a sphere in the Curie-Weiss region, i.e., the grain in the region $T > T_c$ is cubic and $\epsilon_a = \epsilon_c$. For $T < T_c$, ϵ_{av} is computed from Eq. (3.1) with the measured values of ϵ_a and ϵ_c for a single crystal at temperatures slightly less than T_c. For the material as a whole, T_c is taken as a Gaussian distribution about some appropriately chosen temperature T_r. The permittivity $\epsilon(\phi, \theta)$ is associated with the equation of the ellipsoid shown by Fig. 19, i.e.,

$$\frac{x^2}{\epsilon_a^2} + \frac{y^2}{\epsilon_a^2} + \frac{z^2}{\epsilon_c^2} = 1,$$

or in polar form:

$$\frac{\epsilon^2 \sin^2\theta \cos^2\phi}{\epsilon_a^2} + \frac{\epsilon^2 \sin^2\theta \sin^2\phi}{\epsilon_a^2} + \frac{\epsilon^2 \cos^2\theta}{\epsilon_c^2} = 1. \tag{3.2}$$

Then Eq. (3.2) may be written in the form:

$$\epsilon(\theta, \phi) = \frac{1}{\sqrt{\frac{\cos^2\theta}{\epsilon_c^2} + \frac{\sin^2\theta}{\epsilon_a^2}}} = \frac{\epsilon_c}{\sqrt{1 - k^2 \sin^2\theta}}, \tag{3.3}$$

where $k^2 = 1 - \epsilon_c^2/\epsilon_a^2$.

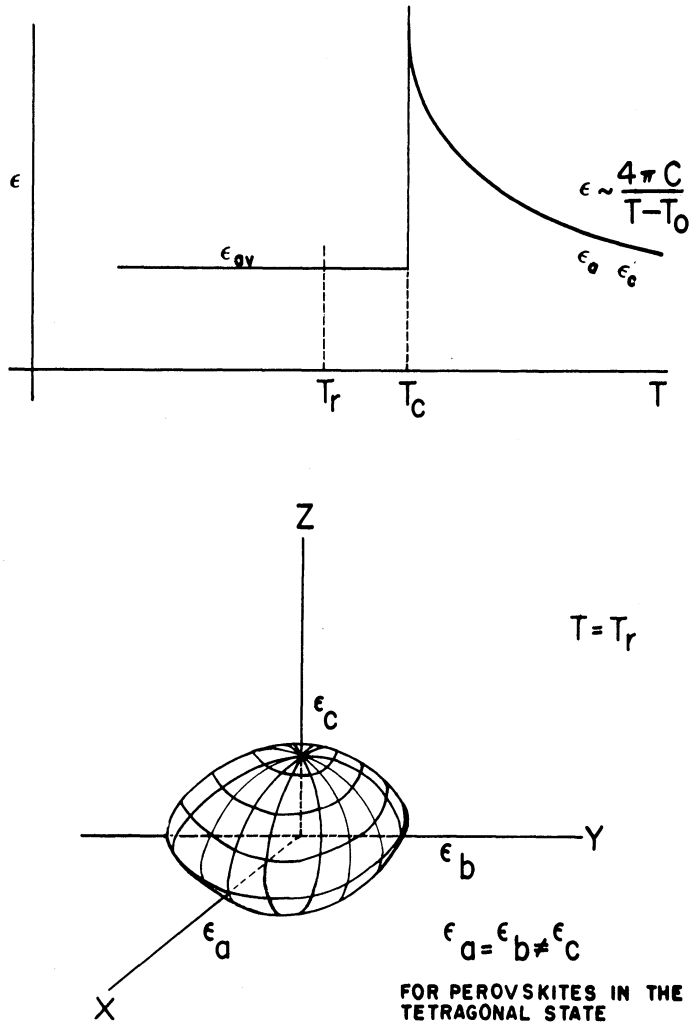

FIG. 19. THE AVERAGE CHARACTERISTIC OF A CERAMIC GRAIN AND THE PERMITTIVITY ELLIPSOID AT ZERO FIELD

By substituting Eq. (3.3) into Eq. (3.1) one obtains

$$\epsilon_{av} = \frac{\epsilon_c}{2\pi^2} \int_{\phi=0}^{2\pi} \int_{\theta=0}^{\pi} \frac{d\theta\, d\phi}{\sqrt{1 - k^2 \sin^2 \theta}} = \frac{2\epsilon_c}{\pi} \int_0^{\pi/2} \frac{d\theta}{\sqrt{1 - k^2 \sin^2 \theta}} . \qquad (3.4)$$

The latter expression is in the form of Legendre's integral of the first kind (an elliptic integral) and may be evaluated from the tables. From the experimental data for a single crystal of $BaTiO_3$ (shown in Fig. 2b) in the tetragonal form are taken:

$$\epsilon_a \cong 4000,$$

$$\epsilon_c \cong 400,$$

and

$$k^2 = 1 - \left(\frac{\epsilon_c}{\epsilon_a}\right)^2 = 0.999.$$

Applying this to Eq. (3.4) and evaluating the integral from the tables, one obtains

$$\epsilon_{av} \cong 940,$$

in excellent agreement with the experimental results for polycrystalline tetragonal $BaTiO_3$ (cf. Fig. 13 for $T < 120^oC$).

Assuming a model based on a collection of grains whose transition temperatures T_c are given according to a Gaussian distribution with a variance $\frac{\alpha^2}{2}$ about some temperature T_r, and that the dielectric behavior of any one grain is similar to that shown in Fig. 19, it is then possible, in principle at least, to compute the zero-field permittivity as a function of temperature. This is done out of the expression for the mean in a Gaussian distribution:

$$\bar{\epsilon}(T) = \frac{\int_0^\infty \epsilon(T, T_0) e^{-\frac{(T_c - T_r)^2}{\alpha^2}} dT_c}{\int_0^\infty e^{-\frac{(T_c - T_r)^2}{\alpha^2}} dT_c}, \tag{3.5}$$

where $$\epsilon(T, T_0) = \begin{cases} \epsilon_{av} \text{ for } T \leq T_c \\ \frac{4\pi C}{T - T_0} \text{ for } T > T_c \end{cases}.$$

In this expression, T_r is some chosen temperature about which the distribution is taken. This can be controlled experimentally, for example, by cation substitutions in the perovskite structure (Sr or Pb substituted for Ba in $BaTiO_3$ will lower or raise, respectively, the temperature T_r). The α determines the degree of spreading of the distribution and is another factor under experimental control. The permittivity ϵ of any given grain is assumed to be ϵ_{av} for $T \leq T_c$ and $\frac{4\pi C}{T - T_0}$ for $T > T_c$ where C is the Curie constant. It is important to point out again that T_0 is not the same at T_c. The latter factor, T_c, is the actually observed Curie transition temperature. T_0 is about 10^o lower in temperature than T_c, depending on the crystal. The fact that $T_0 \neq T_c$ results from the nature of the first-order transition at the Curie temperature (cf. Sec. 2.1).

The evaluation of the integrals in Eq. (3.5) proceeds as follows. First, consider the denominator, which is the normalizing factor.

$$D \equiv \int_0^{\infty} e^{-\frac{(T_c - T_r)^2}{\alpha^2}} dT_c, \tag{3.6}$$

and for convenience let

$$x \equiv T_c - T_r, \tag{3.7}$$

so that

$$D = \int_{-T_r}^{\infty} e^{-\frac{x^2}{\alpha^2}} dx. \tag{3.8}$$

Now T_r is the temperature of maximum for the distribution and is taken as about $300^{\circ}K$, i.e., in the room-temperature range. On the other hand, α would be of the order of about 10°. That is, experimentally the variance of transitions about the Curie peak is, very roughly, $\pm 10^{\circ}$. Therefore, one has:

$$e^{-\frac{x^2}{\alpha^2}} \Big|_{x = -T_r} \simeq \text{order of } e^{-900}.$$

It is clear then that extending the lower limit of the integral of Eq. (3.8) to $-\infty$ adds practically nothing to the integral. In this instance Eq. (3.8) becomes

$$D = \int_{-\infty}^{\infty} e^{-\frac{x^2}{\alpha^2}} dx = \alpha\sqrt{\pi}. \tag{3.9}$$

Let us now consider the numerator of Eq. (3.5).

$$N \equiv \int_0^{\infty} \epsilon(T_0, T) e^{-\frac{(T_c - T_r)^2}{\alpha^2}} dT_c, \tag{3.10}$$

and defining x as before, N becomes

$$N = \int_{-T_r}^{\infty} \epsilon(x, T) e^{-\frac{x^2}{\alpha^2}} dx, \tag{3.11}$$

$$\text{where } \epsilon(T_0, T) = \begin{cases} \epsilon_{av} & \text{for } T \leq T_c \\ \dfrac{4\pi C}{T - T_0} & \text{for } T > T_c ; \end{cases}$$

$4\pi C \cong 1.7 \times 10^5$.

It is more convenient to define $\epsilon(T_0, T)$ in terms of the variable x. Also, T_0 is strictly related to T_c by way of the free-energy function for the crystal, but for the sake of simplicity we take $T_c - T_0 = 10$. This is consistent with the results of Sec. 2.1, where it was shown that the difference between T_c and T_0 would be about $10^{\circ}C$. The value of the constant $4\pi C = 1.7 \times 10^5$ is taken from the recent experimental results of Drougard and Young (Ref. 30) for a very pure $BaTiO_3$ single crystal.

Since $x = T_c - T_r$, one can write:

$$\epsilon(x, T) = \begin{cases} \epsilon_{av} & \text{for } x \geq T - T_r \\ \dfrac{4\pi C}{T - T_c + 10} & \text{for } x < T - T_r \\ \dfrac{4\pi C}{T - T_r + 10 - x} & \text{for } x < T - T_r . \end{cases} \tag{3.12}$$

By applying the conditions of Eq. (3.12) to Eq. (3.11), it is possible to break up the integral of Eq. (3.11) into two separate intervals, viz:

$$N = \int_{-T_r}^{T-T_r} \frac{4\pi C}{T - T_r + 10 - x} e^{-\frac{x^2}{\alpha^2}} dx + \int_{T-T_r}^{\infty} \epsilon_{av} e^{-\frac{x^2}{\alpha^2}} dx. \tag{3.13}$$

The first integral in Eq. (3.13) is called N_1, and the second integral N_2. Considering N_2, one has:

$$N_2 = \epsilon_{av} \int_{T-T_r}^{\infty} e^{-\frac{x^2}{\alpha^2}} dx. \tag{3.14}$$

This integral is a standard form and is found in the tables as the conjugate error function. Thus,

$$N_2(T) = \frac{\alpha\sqrt{\pi}}{2}\epsilon_{av}\left[1 - E_2\left(\frac{T - T_r}{\alpha}\right)\right] = \frac{\alpha\sqrt{\pi}}{2}\epsilon_{av}\,\mathrm{erfc}\left(\frac{T - T_r}{\alpha}\right), \tag{3.15}$$

which may be evaluated from the tables.[11] To evaluate N_1 consider:

$$N_1(T) = \int_{-T_r}^{T-T_r} \frac{4\pi C}{(T - T_r + 10 - x)} e^{-\frac{x^2}{\alpha^2}} dx. \qquad (3.16)$$

The integrand in Eq. (3.16) will always be finite for the limits set on the integral, since the denominator can only be zero for $x = T - T_r + 10$, and x must be less than or equal to $T - T_r$ by the condition of the upper limit.

The actual integration of Eq. (3.16) was carried out on an IBM 650 electronic digital computer. The machine program consisted of a numerical procedure using Simpson's Rule with various values of α and temperature as parameters. For convenience, T_r was taken as 300°K (i.e., room temperature), although the results would be qualitatively the same for another value of T_r.

Results have been compiled for α = 2, 10, 20, 31, and 50, and for temperatures in the range of 265°K to 400°K. These results are plotted in Fig. 20 for α = 10, 20, and 50. The curves for α = 20 and 50 are very similar to those for commercial so-called K6000 and K3000 ceramic compositions. The theoretical permittivity vs. temperature curve for α = 31 is compared in Fig. 21 with the experimental data of Fig. 12 for the zero-field case. The temperature scale of the theoretical curve is shifted so that the peak permittivities occur at the same temperature for both the experimental and the theoretical data. This is permissible since the theoretical peak is set by the parameter T_r, which is an adjustable parameter. That is to say, T_r does not determine the shape of the curve but only sets the temperature of the peak permittivity. The results given in Fig. 21 show a truly remarkable fit between the theoretical and experimental data. (This result inspires a certain confidence in the theory.) However, a better test of the theory would be if it can be used to predict the experimentally observed decrease in permittivity under the influence of strong electric fields such as is shown in Fig. 12. A plot of the peak permittivities as a function of the parameter α, was made as a result of the work on the digital computer and is shown in Fig. 22.

3.3. THE LARGE-FIELD CASE

In the previous section, results were derived for the zero-field case. The effect of an electric field on the dielectric properties of polycrystalline ferroelectrics is now to be considered. The following assumptions are made in carrying out the derivations.

---

[11] Cf: the tables of Janke-Emde, p. 23, where $E_2\left(\frac{T - T_r}{\alpha}\right) = \frac{2}{\sqrt{\pi}\alpha} \int_0^{T-T_r} e^{-\frac{\mu^2}{\alpha^2}} d\mu$, a function which is tabulated.

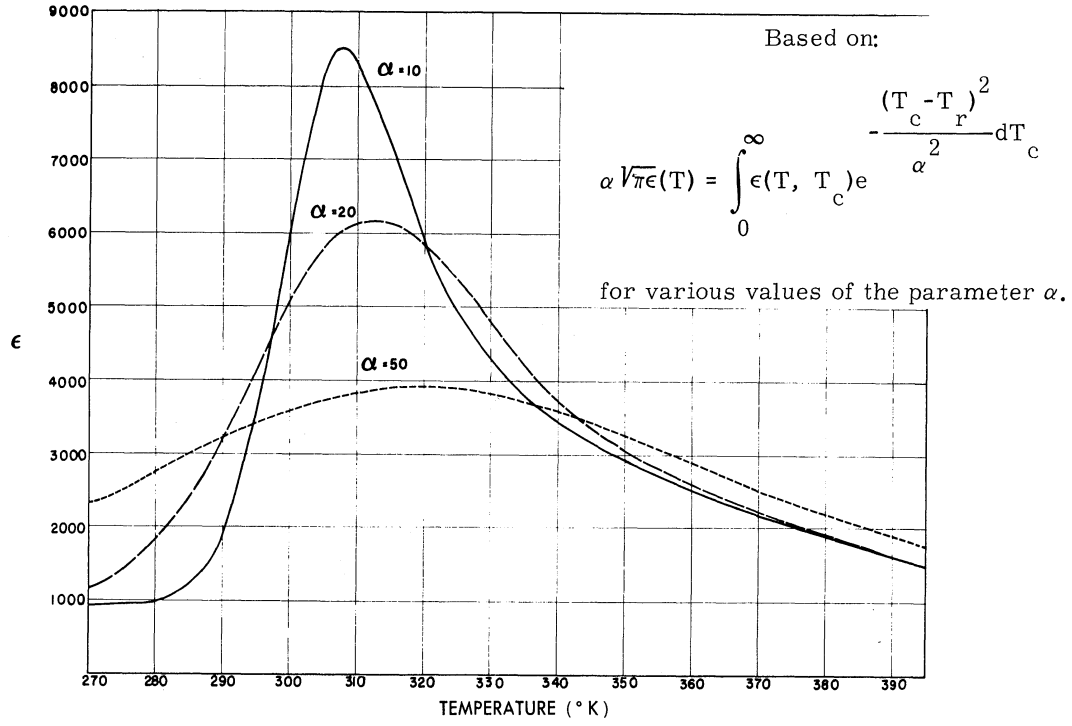

FIG. 20. THEORETICAL VALUES OF PERMITTIVITY VS. TEMPERATURE

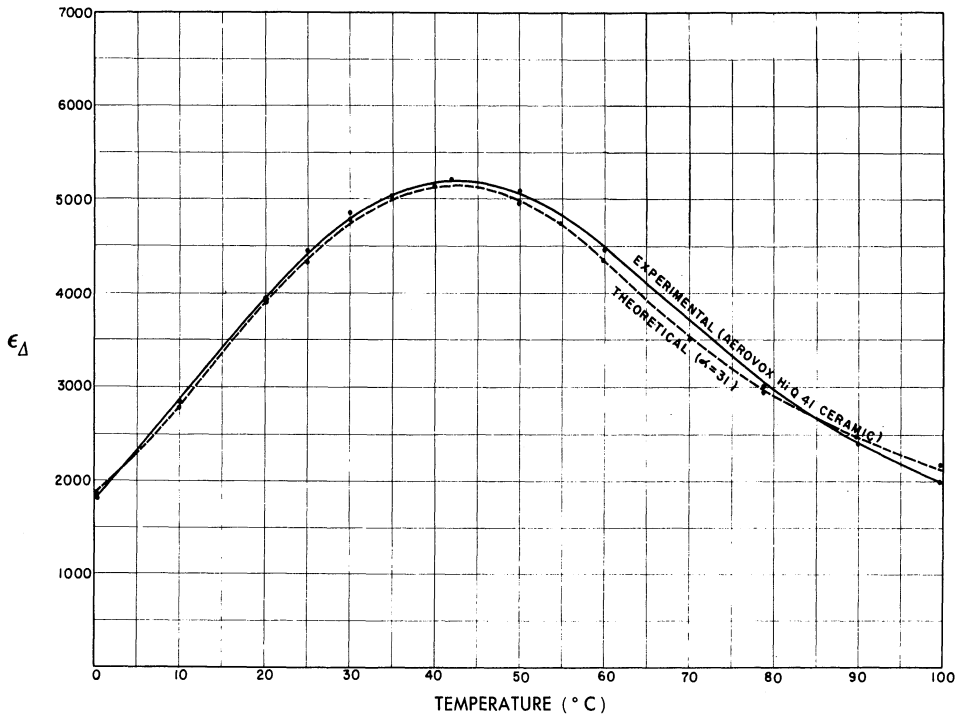

FIG. 21. COMPARISON OF EXPERIMENTAL AND THEORETICAL PERMITTIVITIES

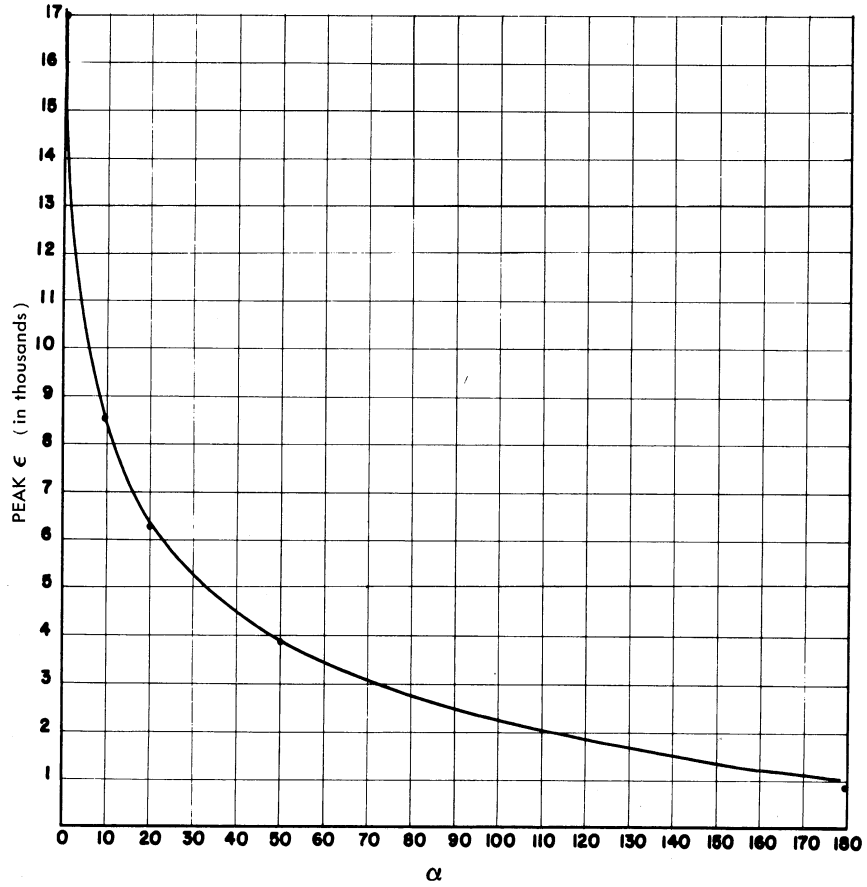

FIG. 22. PEAK PERMITTIVITY VS. THE PARAMETER α

(a) All domains are presumed "frozen in" in those grains which are ferroelectric.

(b) The shift in Curie temperature of any grain is in accordance with the thermodynamic arguments given in Sec. 2.1 which resulted in Eq. (2.13).

(c) When a ferroelectric state is induced within a crystallite by a field, a tetragonal c-axis is induced along the field direction.

(d) The distribution of Curie points, in the absence of an applied electric field, is taken as a Gaussian distribution about some arbitrary temperature, T_r.

(e) The free-energy function of an individual crystallite in a mixed ceramic (e.g., $Ba_xSr_{1-x}TiO_3$) is of the same general form as that for the single $BaTiO_3$ crystal given by Eq. (2.4).

Thus, by using arguments similar to those of Sec. 3.1, the average permittivity of a polycrystalline specimen can be written as:

$$\bar{\epsilon}(T, E) = \frac{\int_0^{\infty} \epsilon(T_c^*, E) e^{\frac{-(T_c^* - \gamma E - T_r)^2}{\alpha^2}} dT_c^*}{\int_0^{\infty} e^{\frac{-(T_c^* - \gamma E - T_r)^2}{\alpha^2}} dT_c^*}, \tag{3.17}$$

with the parameters defined as before. In accordance with the linear shift in Curie point with an applied field (cf. Eq. 2.13) one may write

and
$$\begin{cases} T_c^* = T_c + \gamma E \\ T_c = T_0 + 10, \end{cases} \tag{3.18}$$

where T_c^* is the modified Curie point, T_c is the zero-field Curie point, and γ is a parameter determined theoretically (cf., Eq. 2.13) or experimentally (cf., Fig. 10). For the experimental results shown in Fig. 10, one has

$$\gamma = 1.3^{\circ}/\text{kv/cm}; \tag{3.19}$$

also,

$$\epsilon = \begin{cases} \dfrac{4\pi C}{T - T_0} & \text{for } T > T_C^* \\ \begin{cases} \epsilon_c \text{ for } \parallel \text{ fields} \\ \epsilon_a \text{ for } \perp \text{ fields} \end{cases} & \text{for } T_c \leq T \leq T_c^* \\ \epsilon_{av} & \text{for } T < T_c. \end{cases} \tag{3.20}$$

The latter equation requires some explanation. For any grain in which $T < T_c$, $\epsilon = \epsilon_{av}$ on the basis of the assumption that the domains are frozen in the ferroelectric grains. If $T_c \leq T \leq T_c^*$ for a given grain, the field has induced a ferroelectric state in the grain. Since the induced polar axis is presumed to be aligned with the field, one takes $\epsilon = \epsilon_c$ parallel to the field, and $\epsilon = \epsilon_a$ if the grain is viewed normal to the field. For $T > T_c^*$ in a grain, a Curie-Weiss law is presumed to hold, i.e., $\dfrac{4\pi C}{T - T_0} = \dfrac{4\pi C}{T - T_c^* + 10 - \gamma E}$. It is rather interesting that the Curie-Weiss law is field dependent and that at $T = T_c^*$, where $\epsilon = \epsilon_{max}$,

$$\epsilon_{max} = \frac{4\pi C}{\gamma E + 10}, \tag{3.21}$$

which is also field dependent. These properties may be shown by the free-energy function in the following way. Considering Eq. (2.4) and (2.7) for the free energy and susceptibility, one has

$$\frac{1}{\chi} = a' + 3b'P^2 + 5c'P^4 + \ldots ;$$

also, from Eq. (2.5),

$$E = a'P + b'P^3 + c'P^5 + \ldots .$$

Then χ may be written

$$\chi \simeq \frac{\epsilon}{4\pi} \simeq \frac{1}{a' + b'P^2 + 5c'P^4 + \ldots} , \tag{3.22}$$

and $P = f(E)$ from Eq. (2.5), with

$$a' = \frac{T - T_0}{C}, \quad C \sim 10^4;$$

$$b' \simeq -10^{-12};$$

and

$$c' \simeq 10^{-22}.$$

By substituting $P \simeq \frac{E}{a'}$ from Eq. (2.5) into Eq. (3.22), one has

$$\epsilon \simeq \frac{4\pi}{a' + \frac{3b'}{a'^2}E^2} = 4\pi \left(\frac{a'^2}{a'^3 + 3b'E^2} \right) , \tag{3.23}$$

or Eq. (3.23) may be written:

$$\epsilon \simeq 4\pi \left(\frac{1}{\alpha'} - \frac{3b'E^2}{\alpha'^4} + \ldots \right) . \tag{3.24}$$

As a matter of convenience, leading to a rough approximation, only the first term will be considered, even for fields as large as 20 kv/cm. That is,

$$\frac{1}{a'} = \frac{C}{T - T_0} \simeq \frac{10^4}{40} = 250 \qquad \text{for} \begin{cases} T = T_c^* \simeq 150^\circ\text{C at 20 kv/cm} \\ T_0 = 110^\circ\text{C}, \end{cases}$$

and

$$\left(\frac{1}{a'} \right)^4 = 4 \times 10^9,$$

and

$$3b'E^2 = -3 \times 10^{-12} \times (70 \text{ kv/cm})^2.$$

Thus the second term of Eq. (2.24) is

$$\frac{3b'E^2}{a'^4} \simeq -4 \times 10^9 \times 3 \times 10^{-12} \times 5 \times 10^3$$

$$\simeq -60,$$

as compared with the value for the first term of 250. This amounts to a 20% correction to the peak permittivity. To the extent that the first approximation is valid, $\epsilon \simeq 4\pi C/T - T_0$ for $T > T_c^*$ and the property in Eq. (3.21) follows. In actual practice, it is just as easy to program the computer for the expression of Eq. (3.22) or Eq. (3.24) as it is for the first approximation.

The integration of Eq. (3.17) proceeds in a manner similar to that employed for the zero-field case. One lets

$$x \equiv T_c^* - T_r - \gamma E,$$

so that Eq. (3.17) and (3.20) become, respectively,

$$\bar{\epsilon}(T, E) = \frac{\int_{-T_r-\gamma E}^{\infty} \epsilon(x, T, E) e^{-\frac{x^2}{\alpha^2}} dx}{\int_{-T_r-\gamma E}^{\infty} e^{-\frac{x^2}{\alpha^2}} dx}, \tag{3.25}$$

with

$$\epsilon(x, TE) = \begin{cases} \dfrac{4\pi C}{T - x - T_r + 10} & \text{for } x < (T - T_r - \gamma E) \\ \left\{ \begin{matrix} \epsilon_c \text{ for } \parallel \text{ fields} \\ \epsilon_a \text{ for } \perp \text{ fields} \end{matrix} \right\} & \text{for } T - T_r > x > T - T_r - \gamma E \\ \epsilon_{av} & \text{for } x > T - T_r. \end{cases} \tag{3.26}$$

The denominator of Eq. (3.25) becomes, as before,

$$\int_{-T_r - \gamma E}^{\infty} e^{-\frac{x^2}{\alpha^2}} dx \simeq \alpha \sqrt{\pi}. \tag{3.27}$$

The numerator is broken up into three integrals, each of whose limits correspond to the intervals of Eq. (3.27).

Thus:

$$\int_{-T_r - \gamma E}^{\infty} \epsilon(x, T, E) e^{-\frac{x^2}{\alpha^2}} dx = \epsilon_{av} \int_{T-T_r}^{\infty} e^{-\frac{x^2}{\alpha^2}} dx \qquad (3.28)$$

$$+ \left\{ \begin{matrix} \epsilon_a \\ \text{or} \\ \epsilon_c \end{matrix} \right\} \int_{T-T_r-\gamma E}^{T-T_r} e^{-\frac{x^2}{\alpha^2}} dx + \int_{-T_r-\gamma E}^{T-T_r-\gamma E} \frac{4\pi C}{T - x - T_r + 10} e^{-\frac{x^2}{\alpha^2}} dx$$

$\equiv N_1 + N_2 + N_3$, respectively.

The first term on the right in Eq. (3.28) is, as for the zero-field case, the complementary error function

$$N_1 = \frac{\alpha\sqrt{\pi}}{2} \epsilon_{av} \left[1 - E_2 \left(\frac{T - T_r}{\alpha} \right) \right]. \qquad (3.29)$$

The second term, N_2, is obviously a difference of two error functions:

$$N_2 = \frac{\alpha\sqrt{\pi}}{2} \left(\begin{matrix} \epsilon_a \\ \text{or} \\ \epsilon_c \end{matrix} \right) \left[E_2 \left(\frac{T - T_r}{\alpha} \right) - E_2 \left(\frac{T - T_r - \gamma E}{\alpha} \right) \right],$$

with ϵ_c used for parallel fields or ϵ_a for transverse fields. These terms are easily evaluated from tables of error functions for specific values of the parameters, α, T, E, etc. The last term in Eq. (3.28),

$$N_3 = \int_{-T_r-\gamma E}^{T-T_r-\gamma E} \frac{4\pi C}{T - x - T_r + 10} e^{-\frac{x^2}{\alpha^2}} dx, \qquad (3.30)$$

is the same as the integral of Eq. (3.16) except for the limits of integration. Thus, with the same computer program as before, with limits of integration set by the values of the electric field, E, one may numerically evaluate Eq. (3.30).

The results for α = 31, and for various values of parallel electric fields are shown in Fig. 23. These results are to be compared with the experimental data for a commercially

prepared $Ba_{0.65}Sr_{0.35}TiO_3$ ceramic shown in Fig. 12. The agreement is both qualitatively and quantitatively excellent. Figure 24 shows the theoretical values of permittivity vs. temperature and field, for transverse fields. Theoretical "tuning" data for the temperature of zero-field peak permittivity are presented for both parallel and transverse fields in Fig. 25, and these results are in qualitative agreement with data for the parallel and transverse field experiment cited in Fig. 14. Figure 26 shows the theoretical ϵTE characteristic for the case where α = 20. Here, where the peak permittivity is large, for temperatures slightly higher than the temperature of peak permittivity, the dielectric constant exhibits a slight increase with field before finally decreasing. This is consistent with the experimental data of Fig. 16, 17, and 18.

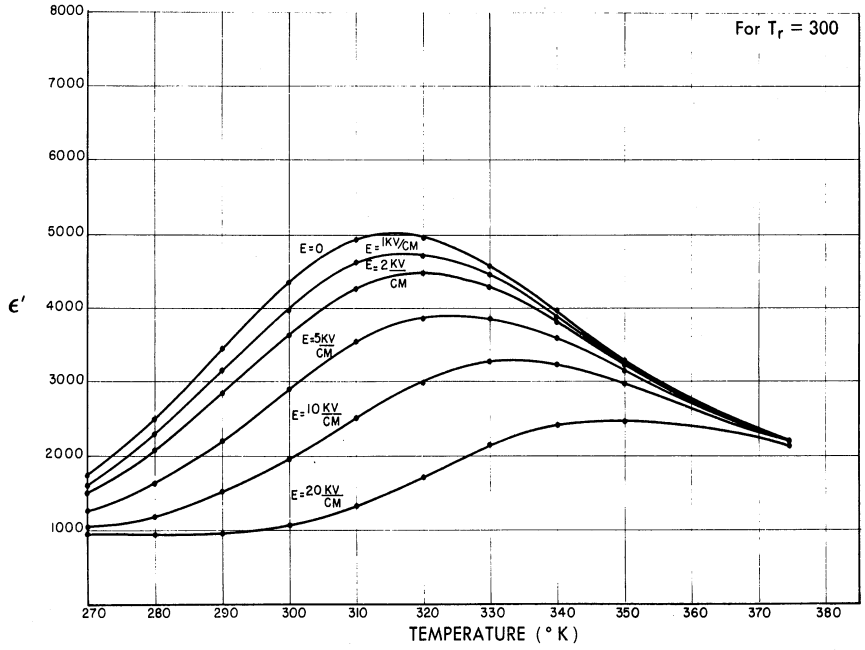

FIG. 23. THEORETICAL PARALLEL PERMITTIVITY VS. TEMPERATURE AND ELECTRIC FIELD (FOR α = 31)

The results of the theory outlined in the two preceding sections, and the excellent agreement of this theory with experimental data, indicates that the nonlinear property of ferroelectrics need not be based on a domain process. One of the many interesting implications of this result is that certain high-frequency and microwave large-signal applications of the ferroelectrics may be feasible if domain orientation and growth time constants are not involved.

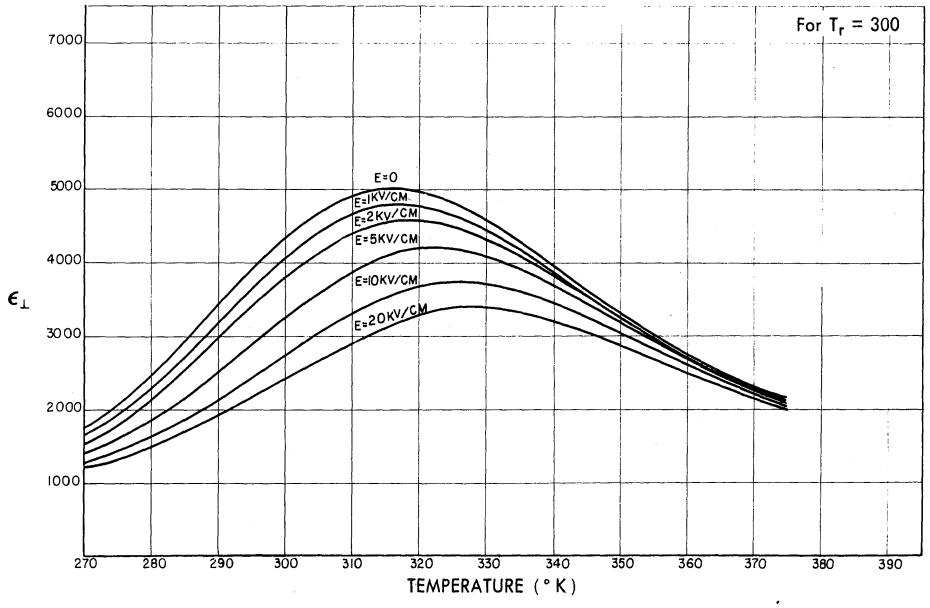

FIG. 24. THEORETICAL TRANSVERSE PERMITTIVITY VS. TEMPERATURE AND ELECTRIC FIELD (FOR α = 31)

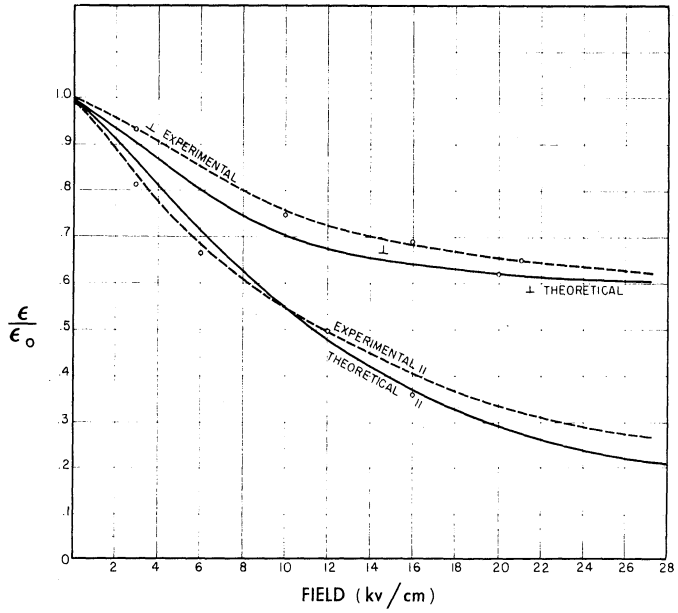

FIG. 25. THEORETICAL AND EXPERIMENTAL RELATIVE TUNABILITY FOR $Ba_{0.65}Sr_{0.35}TiO_3$

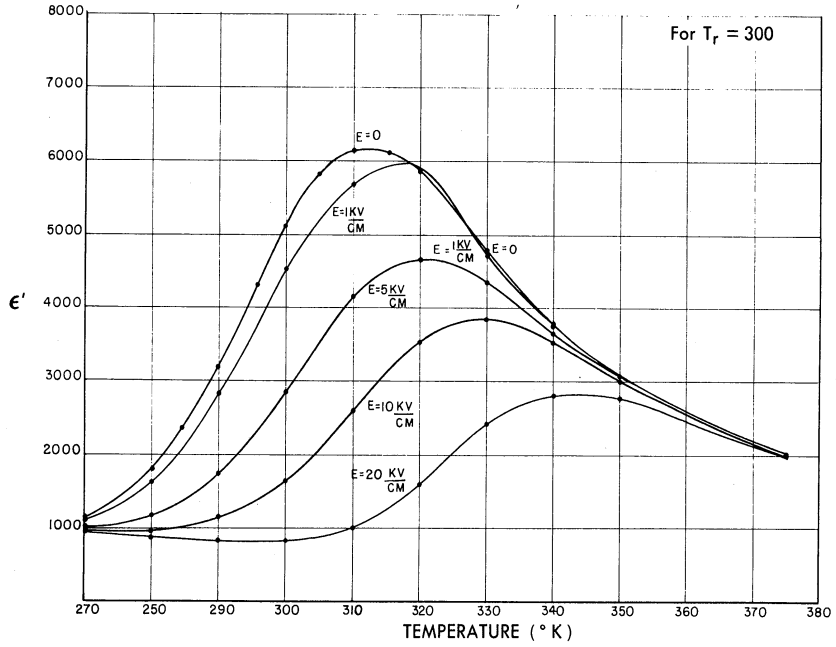

FIG. 26. THEORETICAL PARALLEL PERMITTIVITY VS. TEMPERATURE AND ELECTRIC FIELD (FOR α = 20)

4
DISPERSION PHENOMENA for HIGH-PERMITTIVITY DIELECTRICS

4.1. LOW-FREQUENCY DYNAMIC SPECTRA

As has been previously mentioned in Sec. 1.4 and 2.2 and in connection with Fig. 4 and 5, data on permittivity with frequency for a dielectric serve as a means of separating mechanisms of polarization. The results cited by Kittel (Ref. 20), which are shown in Fig. 5, for ceramic $BaTiO_3$ show almost a tenfold decrease in permittivity over a frequency range of 0.1 mc to 10,000 mc, and the question naturally arises as to what is the cause of such strong dispersion. This report has presented the following possibilities for explaining such behavior: (a) a polar relaxation effect, such as is found for water at microwave frequencies, (b) an effect due to clamping of the ceramic grains at sufficiently high frequencies, and (c) a relaxation primarily caused by the action of dielectric losses which would then affect the real permittivity through the Hilbert Transform relations of Eq. (1.37). Ferroelectric domain processes are being discounted as an explanation here, since it has been shown in Sec. 3 that domain orientation and growth do not substantially affect even the large-field polarizability, and thus one certainly would not expect the domains to move about under very weak signal fields.

The polar relaxation, if present, may be thought of as the microwave dispersion of some molecular association within the perovskite structure such as strong molecular binding between Ti and O_I along the polar direction (Fig. 1). If a relaxation due to the molecular group were to exist, it would be expected that the effect would be very pronounced in a single crystal for

a signal field transverse to the polar direction. As will be shown in the succeeding sections, experiments on single crystals at uhf and microwave frequencies have failed to reveal any substantial dispersion behavior other than effects due to dimensional resonances, and therefore molecular relaxation is not a likely mechanism for the observed dispersion effects in the polycrystalline samples.

In Sec. 2.2 the relationship between the permittivity of a $BaTiO_3$ crystal which is free to strain and that for a mechanically clamped crystal is derived. It has been shown that the free permittivity is roughly twice that of the clamped value, both for the "a" and the "c" crystallographic directions. For frequencies higher than the dimensional resonant modes for a given crystal, one would expect that the substance would behave as if it were mechanically constrained. Therefore, if the dispersion observed for ceramic $BaTiO_3$ were caused solely by a clamping effect, one would expect a reduction in the permittivity by a factor of about two.

It has been noted in Sec. 1.3 that for a linear dielectric the real and imaginary parts of a complex permittivity are not independent if one part can be specified as a function of frequency. Although ferroelectrics of the perovskite type are strikingly nonlinear with regard to large fields, the point of view has been adopted here that for very small signal fields the incremental permittivity is linear. The incremental signal fields used in the experiments are of the order of 10 volts/cm as compared with coercive fields of about 10^3 volts/cm. If one were to assume large frictional losses at, say, grain boundaries or domain interfaces in a polycrystalline aggregate, then these losses would lead to a relaxation spectrum which could easily account for a tenfold reduction in the real permittivity. For high-permittivity substances such as the perovskites, one may expect large electrostrictive and piezoelectric effects as a consequence of the very large polarizability, and hence it would not be unreasonable for large frictional losses to exist in these ferroelectric ceramics.

In order to examine further the notions presented above, experiments covering from low frequencies to the microwave region have been designed. The substances investigated include both single crystal and ceramic $BaTiO_3$, ceramic $Ba_{0.65}Sr_{0.35}TiO_3$, $Pb_{0.40}Sr_{0.60}TiO_3$, and $Cd_2Nb_2O_7$. Because measurements were made over a very wide frequency range, it was necessary to employ three separate experimental techniques. For frequencies from 0.5 mc to 150 mc a special low-frequency dielectric spectrometer has been constructed. In the range from 20 mc to 250 mc a Boonton Corporation Type 190-A high-frequency Q-meter was employed. A slotted coaxial transmission-line technique was used in the frequency region from 300 mc to 4000 mc. In this section the low-frequency spectra will be considered.

For piezoelectric $BaTiO_3$, the dimensional resonances are expected to occur in the 0.5-mc to 150-mc range. In order to best display permittivity vs. frequency in a region where rather sharp resonant peaks are expected, a dynamic method of obtaining data must be employed. To

this end, a low-frequency dielectric spectrometer has been constructed. The block diagram for this instrument is shown in Fig. 27. The operation of the unit depends upon mechanically sweeping a series of General Radio Corporation unit oscillators with a General Radio Type 1750-A drive motor. The output of the oscillator is sampled with a crystal diode, D_1 in the figure, and the rectified voltage is used to control an electronically regulated oscillator power supply (General Radio Type 1263-A) which adjusts the plate voltage of the swept oscillator in such a way that a constant output is assured. The oscillator output is placed across two capacitors in series, C_x and C. C_x is the sample and C is a calibrated variable capacitor. The value of C is much greater than that of C_x, i.e., its reactance is smaller, so that the voltage appearing across C is approximately proportional to the value of C_x. The high-frequency voltage appearing across C is rectified by a crystal diode D_2 and filtered by C_2. The resultant d-c, which is proportional to the value of C_x, is placed on the Y terminals of an oscilloscope. A potentiometer, which is placed on the drive shaft of the same motor that sweeps the unit oscillator, provides the X drive for the oscilloscope. The oscilloscope trace is photographed with the aid of a Polaroid Land camera attachment. While this method of displaying dynamic spectra is extremely simple, it has nonetheless proven to be very effective. What is actually measured with this method is the magnitude of C_x, which is proportional to the magnitude of the complex permittivity. However, for substances whose Q is of the order of 10 or greater,[12] the magnitude of the permittivity is approximately equal to the real part. The spectrometer has been calibrated through the use of rutile (TiO_2) standards which were in turn calibrated on a Q-meter.

The ceramic samples are prepared in the following manner. A thin section, 0.5 mm thick, of the ceramic is sliced out of a larger bar or rod by means of a diamond cutting wheel. The faces of this section are painted with a silver conducting paste. The unit is then baked in a furnace at 650°C for one-half hour in order to remove the organic binders from the silver conducting paint. The ceramic section is then sliced into squares, 1 mm on a side, with a diamond wheel. The small ceramic plate thus formed has electrodes on two faces. The samples are held in a sample holder between a pair of phosphor bronze spring clips which are adjusted to provide only enough pressure to hold the sample in place. This is done in order to minimize mechanical loading.

The basic ceramic stock is prepared in the laboratory by mixing the constituent oxide powders with a binder, such as methyl cellulose, and a stearate lubricant. Water is then added to form a slurry which is ball-milled for 8 hr. The mix is then dried in a drying oven at 85°C. The dry powder is screened through a 100-mesh screen and pressed into cylindrical shape with a hydraulic press at pressures from 5000 to 10,000 psi. The cylinders are then

[12] The Q is defined as $Q = \frac{1}{\tan \delta} = \frac{\mathrm{Im}(Z)}{\mathrm{Re}(Z)}$, where Z is the complex impedance.

fired at a temperature which depends on the composition; for the $BaTiO_3$-$SrTiO_3$ series the firing is done at 1350°C for 2 hr. All the ceramics have been fired in a Harper 5-kw glow-bar furnace, which is provided with an automatic temperature control and programer.

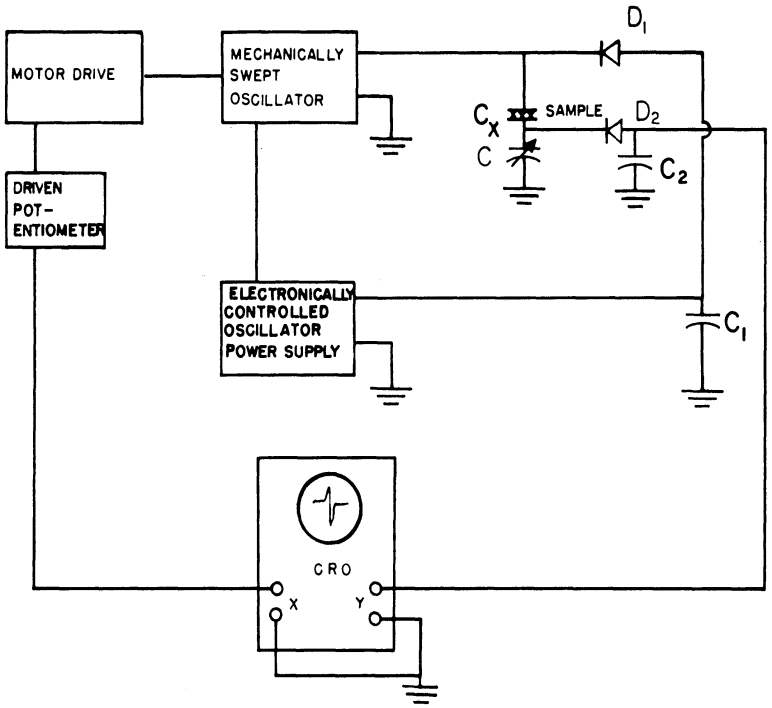

FIG. 27. DYNAMIC DIELECTRIC SPECTROMETER

Preparation of the single crystals of $BaTiO_3$ is somewhat more difficult than that for ceramics. The crystals are formed by a method discovered by J. P. Remeika of the Bell Telephone Laboratories. In this method, $BaTiO_3$ powder is mixed with potassium fluoride in a covered platinum crucible which is placed in a furnace at 1400°C and held at this temperature for 10 hr. This allows a quantity of the barium titanate to dissolve in the fluoride flux. At the end of the 10-hr hold period the temperature is lowered at a rate of about 30°C per hour until a temperature of 950°C is reached. The furnace is then allowed to cool rapidly at its natural rate. The crystals precipitate out of the molten flux in the form of thin plate-like crystals, roughly 1 cm on a side and about 0.2 mm thick.

At first an attempt was made to cut these crystals into smaller squares with a diamond wheel using the method employed for ceramics, but this was unsuccessful. A method later adopted consists of first determining the directions of the atomic planes by observing the orientation of the domains with the aid of a polarizing microscope. (The domains tend to line up along the (1, 0, 0) planes). The crystal is then cleaved by striking a sharp edge (e.g., that of a razor blade) against the crystal and along the (1, 0, 0) direction. By this technique, samples of about 1 mm square and 0.2 mm thick are formed. In order to insure that the crystals

are untwinned and single domain, an electrical polarizing technique is employed. Polarizing is accomplished by placing the cleaved sample on a piece of electrically conducting glass to which one terminal of a 300-volt battery is attached. The sample on the conducting glass is placed under a polarizing microscope, and while one observes the crystal through the microscope, a probe, which is attached to the other battery terminal, is touched onto the crystal at those areas in which domains are seen to exist. As this is done, the domains flip perpendicularly to the plane of the plate until the whole crystal becomes essentially a single domain. Copper electrodes are then applied to the appropriate sample faces by means of vacuum evaporation. If the electrodes are placed parallel to the direction of the spontaneous polarization, the sample is called a c plate; and if the electrodes are perpendicular to the spontaneous polarization, one has an a plate. This is shown in Fig. 28. One measures ϵ_a for an a plate and ϵ_c for a c plate.

Typical results are shown for $BaTiO_3$ single crystal a and c plates in Fig. 29, 30, and 31. Figure 29 shows data taken in the region 0.5 mc to 150 mc. The resonant peaks observed are dimensional resonances, and the frequencies and character of the peaks vary widely from crystal to crystal. The resonances can be substantially diminished or even made to disappear by mechanically clamping the crystal. The particular modes of vibration for the resonances have not been specifically identified in these spectra, since it is the purpose of these data to determine the reduction in permittivity as a result of increasing the frequency beyond the range of dimensional resonances. It has been found that the ratio of low-frequency permittivity to high-frequency permittivity varies from crystal to crystal. Most a crystals have ratios from 1.2:1 to about 2:1, averaging around 1.5:1, and most of the c crystals have ratios of about 2:1. This is in complete agreement with the theory developed in Sec. 2.2 where the relationship between the free and clamped permittivities is derived. The theoretical ratios were shown to be 1.5:1 and 2:1 for the a and c crystals, respectively. Figure 30 shows spectra for other $BaTiO_3$ crystals for the frequency range from 0.5 mc to 150 mc. The effect of clamping on reducing the mechanical resonances is shown. In Fig. 31 a $BaTiO_3$ ceramic spectrum is displayed both with a biased sample and an unbiased sample. Originally, in the absence of an electric field, no resonance is observed. When a biasing field is applied, a dimensional resonance appears and in fact remains after the field is removed. The latter phenomenon is due to the remanent polarization of the $BaTiO_3$ sample (i.e., it has become "poled"). The ratio of low-frequency to high-frequency permittivity for the ceramic in this case is about 1.2:1.

The conclusion to be drawn from this section is that a reduction in permittivity in $BaTiO_3$ due to mechanical clamping or dimensional resonance effects would, at most, be of the order of a ratio of 2:1. The ratio for ceramics measured on the dielectric spectrometer is closer to 1.2:1. Therefore, as a result of both theory and experiment, it would seem that the tenfold

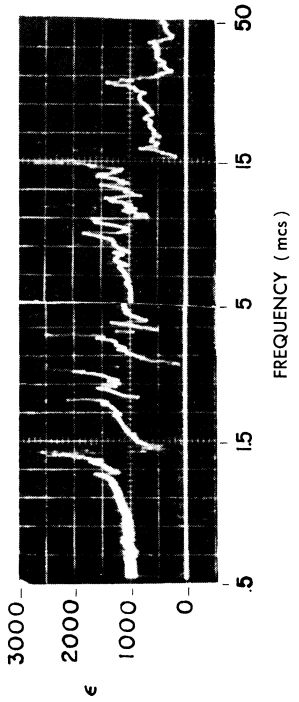

a Plate

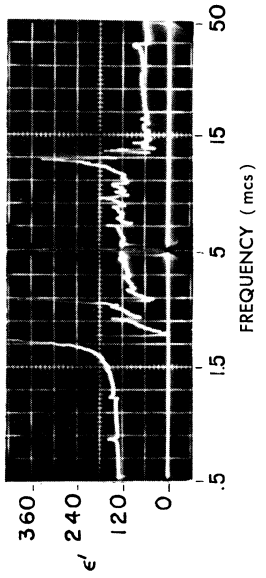

c Plate

FIG. 29. DYNAMIC SPECTRA FOR a AND c PLATES OF $BaTiO_3$ SINGLE CRYSTALS (T = 25°C)

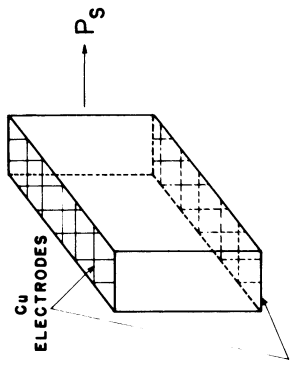

a Plate

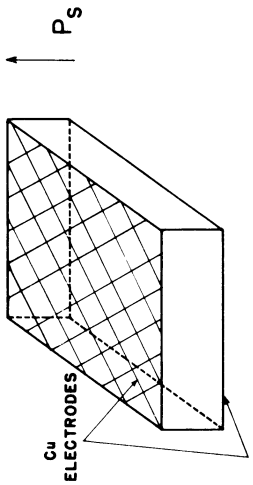

c Plate

FIG. 28. $BaTiO_3$ SINGLE CRYSTALS. a- and c-oriented $BaTiO_3$ single crystals showing orientation of spontaneous polarization direction as compared to electrodes.

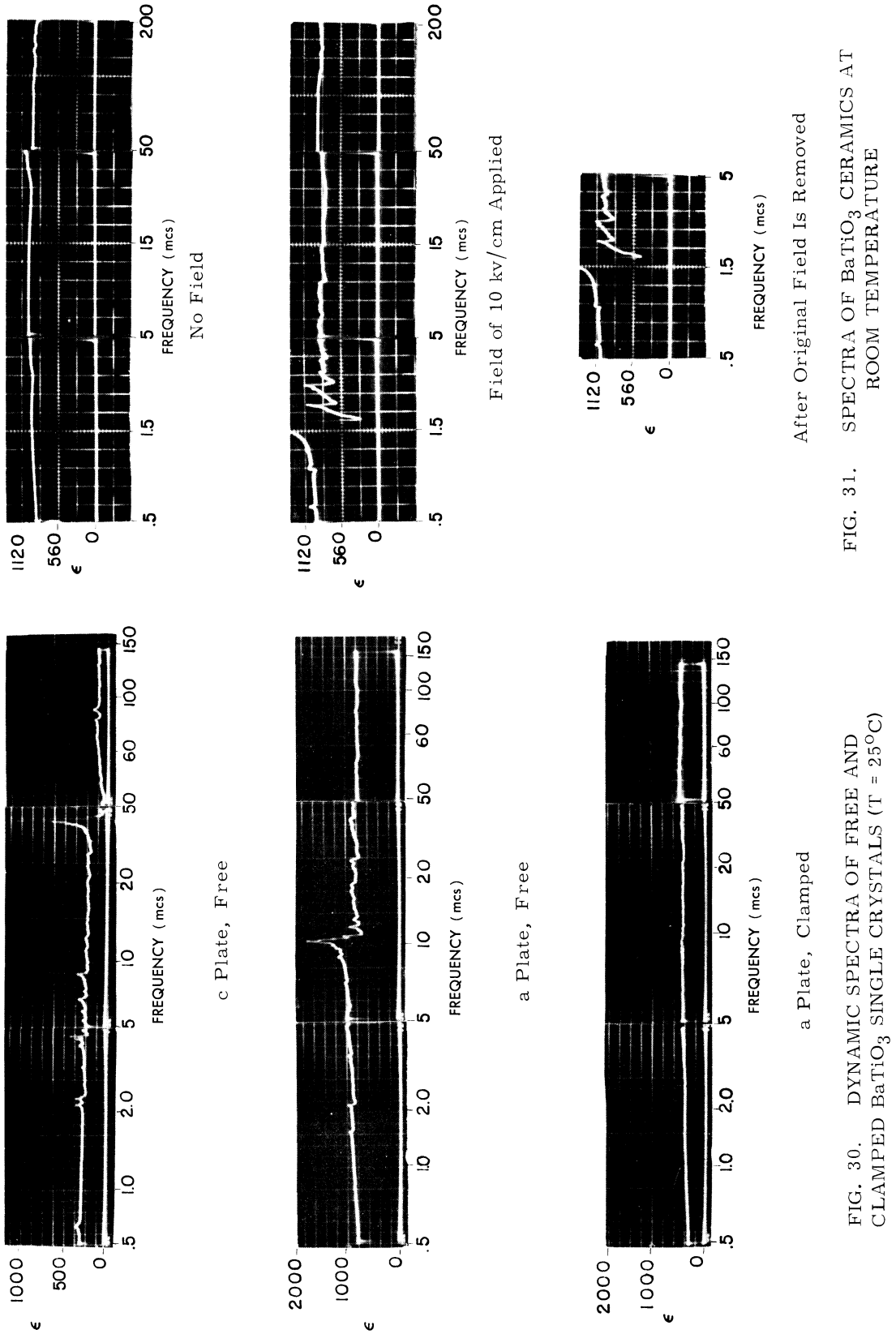

FIG. 30. DYNAMIC SPECTRA OF FREE AND CLAMPED $BaTiO_3$ SINGLE CRYSTALS (T = 25°C)

FIG. 31. SPECTRA OF $BaTiO_3$ CERAMICS AT ROOM TEMPERATURE

reduction in permittivity for a $BaTiO_3$ ceramic as reported by Kittel (see Fig. 5) cannot be explained on the basis of dimensional resonances and clamping effects alone.

4.2. MICROWAVE PROPERTIES

Measurements have been made of permittivity vs. frequency in the microwave region for both ceramic and single crystals of ferroelectrics. A slotted transmission line and probe technique has been employed for the measurements. The schematic of the experimental arrangement is shown in Fig. 32. The ferroelectric specimen is treated as a lumped element terminating a transmission line. Appropriate corrections are necessary for the effects of fringing fields at the sample and for discontinuities introduced by the sample holder. The sample holder is diagrammed in Fig. 33. An additional correction is required to take into account wave propagation within the specimen. Since permittivities of the perovskite ferroelectrics are of the order of thousands, even small samples can have an appreciable fraction of a wavelength within the medium at the higher frequencies.

The sample holder is calibrated in the following manner. First at a given frequency a copper "specimen" of the same dimensions as the sample is used to short-circuit the line and a reference nul in the standing wave pattern on the slotted section is established. The line is then open-circuited by removing the copper short and replacing the empty sample holder, and the open-circuit reference nul is established. Then a rutile (TiO_2) standard of known capacitance is placed in the sample holder and another reference nul is found. The above reference positions are presumed lossless since the standing wave ratios are very much greater than for the case of a real sample. (The voltage standing wave ratio for the open and short-circuited line is of the order of several hundred as compared to tens for the samples measured). From the above data the following equivalent circuit is deduced for the sample holder.

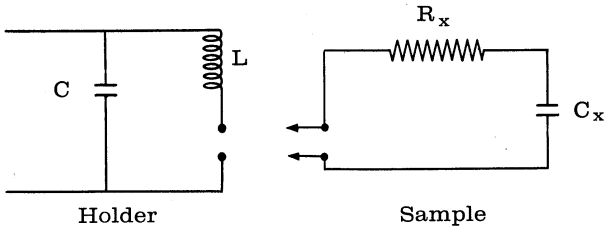

The values for L and C are remarkably constant over a very wide frequency range (500 mc to 3000 mc) and are numerically: $L \cong 0.9 \times 10^{-9}$ henry and $C = 0.2 \times 10^{-13}$ farad. In actually reducing the data, the slight variations in these values at a given frequency point are taken into account. R_x and C_x, respectively, are the lossy part and the reactive part of the sample.

The correction for the propagation effect within the sample is dependent on the dimensions and shape of the sample as well as upon the permittivities. It is therefore necessary to develop a correction formula which allows these factors to enter as parameters. The crystals

and ceramic samples used in the experiments were of rectangular cross section so that the correction formula involves solving the wave equation under boundary conditions imposed by this geometry. Jaynes and Varenhorst (Ref. 31) have obtained a correction factor for a one-dimensional sample (infinitely wide sheet), but these results are not applicable to the problem under consideration. A summary of the analysis leading to the correction factor for a rectangular parallelepiped and a cylindrical disc follows.

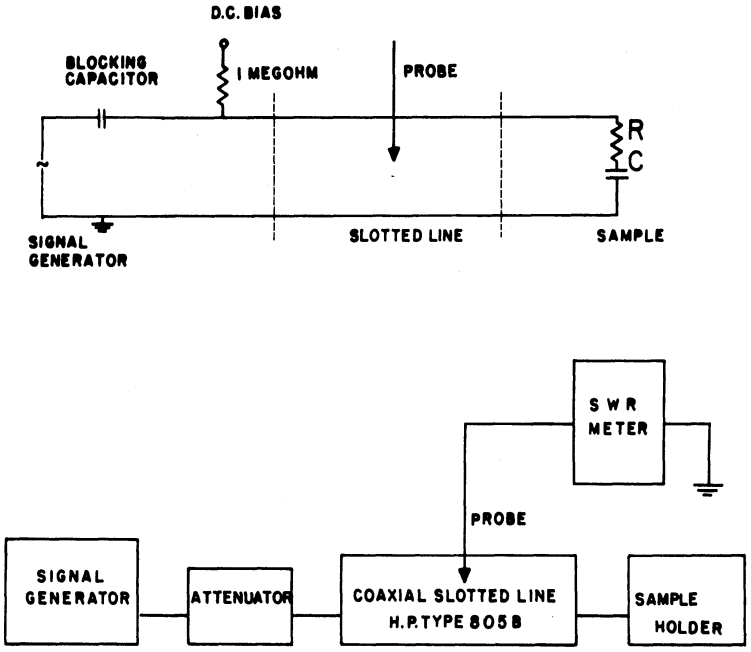

FIG. 32. EXPERIMENTAL ARRANGEMENT FOR UHF AND MICROWAVE MEASUREMENTS

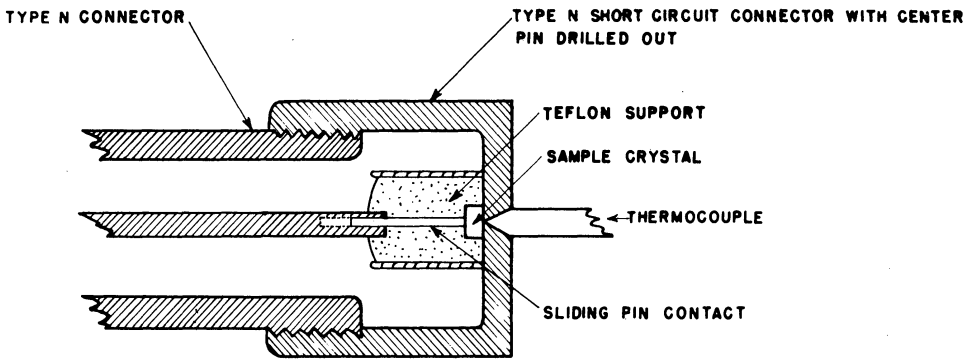

FIG. 33. DIELECTRIC SAMPLE HOLDER FOR LINE

The electric field in the sample must, at all frequencies, satisfy the wave equation:

$$\nabla^2 E + k^2 E = 0, \tag{4.1}$$

where $k^2 = \omega^2 \mu\epsilon$, and the factor $d^{i\omega t}$ is understood. The mks system of units is employed. In general ϵ is a tensor; that is,

$$\epsilon = \begin{pmatrix} \epsilon_{11} & 0 & 0 \\ 0 & \epsilon_{22} & 0 \\ 0 & 0 & \epsilon_{33} \end{pmatrix}$$

The dielectric constant takes this form for the case where a principal axis coordinate system is used for a tetragonal single crystal. For the case of an isotropic ceramic one takes $\epsilon_{11} = \epsilon_{22} = \epsilon_{33} = \epsilon$. The coordinate system for the rectangular sample is shown below.

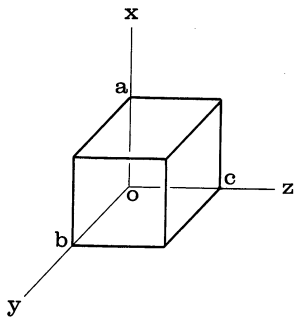

The z-direction corresponds to the axial dimension of the coaxial line. The metal electrodes are at the planes z = 0 and z = c and the following assumptions are made.

(a) In the neighborhood of, and within the sample, the electric field is entirely z directed.

(b) The wavelength in air is much greater than the length of the sample c. (The sample lengths used were 1 mm or less.)

(c) The sample is considered lossless to a first approximation.

Assumption (a) appears reasonable on the basis that parallel plane electrodes are employed on a high-permittivity sample. Therefore, most of the flux would be inside the sample and parallel to the z-axis. Jaynes and Varenhorst have shown in the paper noted above (Ref. 31) that the cavity resonant modes within the dielectric that are associated with the z-direction are not excited when assumption (b) is valid. Assumption (c) is not expected to lead to difficulty because of the relative independence of the dielectric constant measurement upon the loss tangent in this method. If this proves not to be the case, a first-order correction can be made to account for the effect of loss in the sample. With these assumptions,

$$E(0, y) = E(a, y) = E(c, 0) = E(x, b) \equiv E_1, \tag{4.2}$$

and

$$E \equiv E_z, \quad k^2 = \omega^2 \mu \epsilon, \tag{4.3}$$

where E_1 is the applied field at the sample boundaries. The apparent value of the dielectric constant, ϵ_{ap}, is given by

$$\epsilon_{ap} = \frac{I}{\omega A E_1}, \tag{4.4}$$

where A is the cross-sectional area of the sample and I is the total current (displacement) flowing through it, that is,

$$I = \iint J \, dA = \iint \omega \epsilon E(x, y) \, dx \, dy. \tag{4.5}$$

The solutions of Eq. (4.1), E(x, y), and Eq. (4.4) and (4.5) give the desired relationship between ϵ_{ap}, and ϵ.

To obtain the solution to the differential equation most conveniently, the following transformations are made:

$$E - E_1 \equiv E'; \quad u \equiv \frac{\pi x}{a}. \tag{4.6}$$

Then the wave equation restated becomes:

$$\frac{\pi^2}{a^2}\left(\frac{\partial^2 E'}{\partial y^2}\right) + \frac{\partial^2 E'}{\partial y^2} + k^2(E' + E_1) = 0, \tag{4.7}$$

with the boundary conditions

$$E'(0, y) = E'(\pi, y) = E'(u, 0) = E'(u, b) = 0, \tag{4.8}$$

and

$$E' = E'(u, y).$$

The solution proceeds by taking a finite Fourier sine transformation[13] of Eq. (4.7) and (4.8) on u for the interval $0 \leq u \leq \pi$. This leads to a transformed differential equation:

$$\frac{d^2}{dy^2} e(n, y) - \alpha^2 e(n, y) + \beta = 0, \tag{4.9}$$

[13] See, for example, R. V. Churchill, Modern Operational Mathematics, McGraw-Hill, 1944, Chap. X.

where

$$\alpha^2 = \frac{n^2\pi^2}{a^2} - k^2, \quad n = 1, 2, 3, \ldots,$$

$$\beta = k^2 E_1 S\left\{1\right\}, \quad S\left\{1\right\} = \frac{1 - (-1)^n}{n}$$

and

$$e(n, y) = S\left\{E(u, y)\right\} = \int_0^{\pi} E(u, y) \sin nu \, du.$$

The differential Eq. (4.9) has the solution:

$$e(n, y) = c_1 e^{\alpha y} + c_2 e^{-\alpha y} + \frac{\beta}{\alpha^2}, \tag{4.10}$$

where

$$c_1 = \frac{\beta}{\alpha^2} \frac{e^{-\alpha b} - 1}{e^{\alpha b} - e^{-\alpha b}}$$

and

$$c_2 = \frac{-\beta}{\alpha^2} \frac{e^{-\alpha b} - 1}{e^{\alpha b} - e^{-\alpha b}}.$$

The inverse transformation is given by

$$E'(u, y) = \frac{2}{\pi} \sum_{n=1} e(n, y) \sin nu, \tag{4.11}$$

which, when combined with Eq. (4.4), (4.5), and 4.6) yields

$$\epsilon_{ap} = \frac{\epsilon}{ab\, E_1} \int_0^b \int_0^a \frac{2}{\pi} \sum_{n=1} \left(e(n, y) \sin \frac{n\pi x}{a} + E_1 \right) dx \, dy. \tag{4.12}$$

From Eq. (4.10) there results,

$$\epsilon_{ap} = \epsilon \left[1 + \frac{4k^2}{\pi^2} \sum_{n=1} \frac{1 - (-1)^n}{\alpha^2 n^2} \left(1 - \frac{2}{\alpha b} \tanh \frac{\alpha b}{2} \right) \right], \tag{4.13}$$

where

$$\alpha^2 = \frac{n^2\pi^2}{a^2} - k^2, \quad \text{and } n = 1, 2, 3, \ldots.$$

$$k^2 = \omega^2 \mu \epsilon,$$

and where a and b are the cross-sectional dimensions of the sample. This latter formula relates the apparent value of permittivity (ϵ_{ap}) with the "true" value, ϵ. In the derivation it was assumed that the media was lossless. If the use of the formula is limited to about 10% corrections or less, and if there is about a 10% error in the correction formula itself due to the assumption of lossless media, the total error would be of the order of 1%.

If a sample is in the form of a disc of radius a, with the coordinate system as shown below, the calculation of the correction is very much simpler than for the rectangular case.

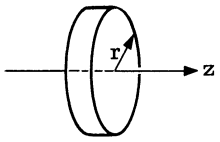

The sample is again assumed to be immersed in a uniform z-directed field, E_1, and the other assumptions used for the previous case are again applied. The wave equation in cylindrical coordinates, assuming no angular dependence of E_z, is

$$\frac{\partial^2 E_z}{\partial r^2} + \frac{1}{r}\frac{\partial E_z}{\partial r} + k^2 E_z = 0, \tag{4.14}$$

which, for positive and real k, has the solution,

$$E_z = E_o J_o(kr), \tag{4.15}$$

where

$$E_1 = E_z(a) = E_o J_o(ka),$$

and

$J_o(kr)$ is a zeroth order Bessel function of argument kr.

Applying the same arguments as in the previous case,

$$I = 2\pi E_o \omega\epsilon \int_o^a r J_o(kr)\, dr, \tag{4.16}$$

and

$$\epsilon_{ap} = \epsilon \frac{2}{ka}\frac{J_1(ka)}{J_o(ka)}, \tag{4.17}$$

which is the desired correction formula for the disc-shaped sample. Equation (4.17) can be expanded in a series, which may be a more useful form:

$$\epsilon_{ap} = \epsilon \left[1 + \frac{(ka)^2}{8} + \frac{(ka)^4}{48} + \cdots\right]. \tag{4.18}$$

Typical of the results for measurements on the single crystals in the uhf and microwave-frequency regions are shown in Fig. 34 and 35. Figure 34 shows the data of ϵ' and ϵ'' for a single crystal c plate of $BaTiO_3$ for the frequency range of 20 mc to 4000 mc. Figure 35 displays similar data but for a single crystal a plate. The results for both the a- and c-oriented crystals show that there is a decrease in ϵ' at the lower frequency end of the spectrum but that the permittivity in the 400-mc to 4000-mc range is relatively constant. The decrease in

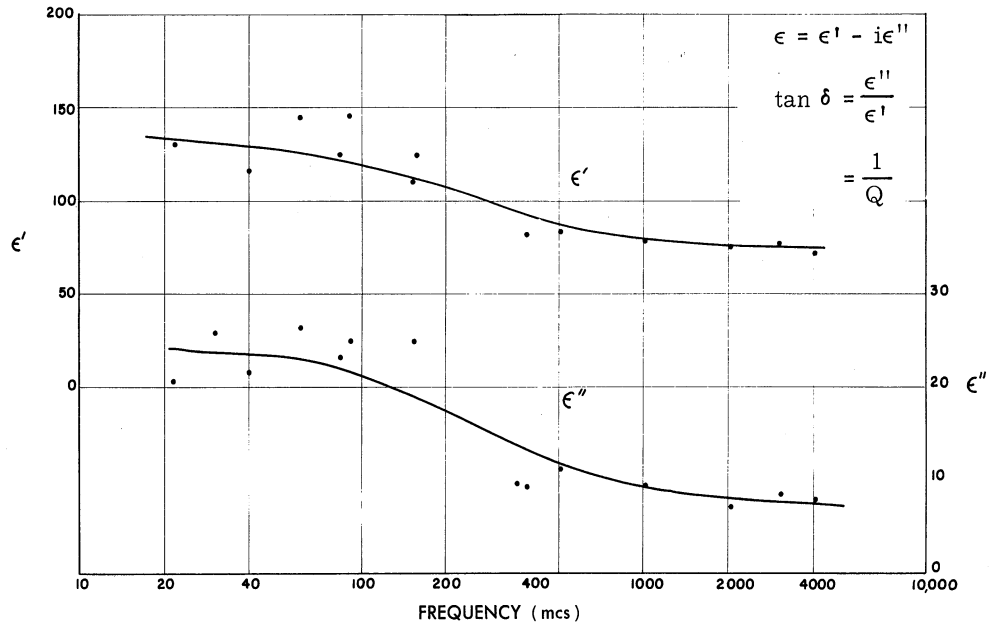

FIG. 34. FREQUENCY DATA FOR CRYSTAL OF $BaTiO_3$ c PLATE (AT 23°C)

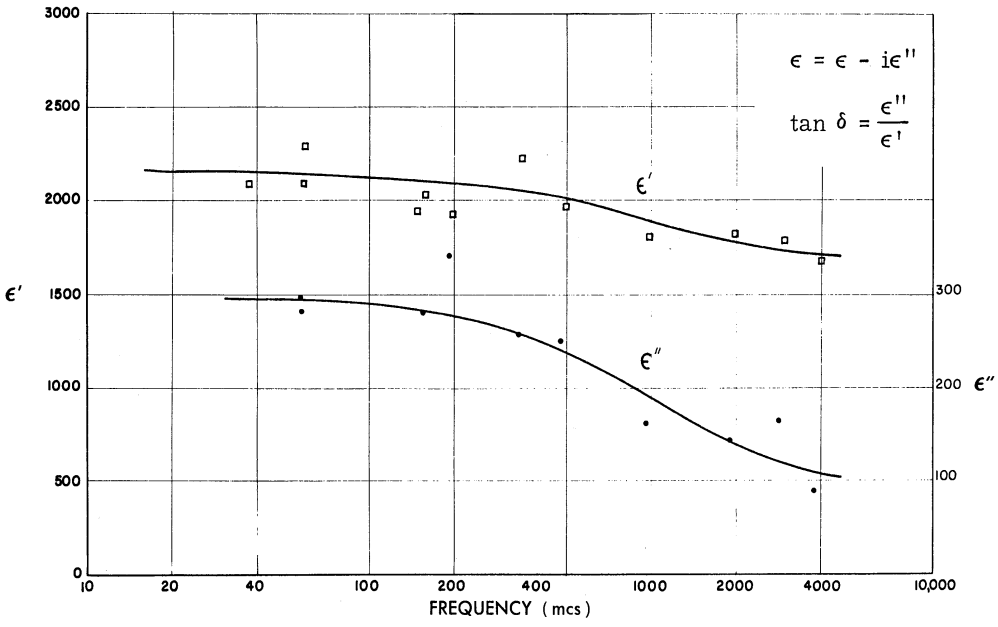

FIG. 35. FREQUENCY DATA FOR CRYSTAL OF $BaTiO_3$ a PLATE (AT 23°C)

the low-frequency region may possibly be due to the same type of dimensional effects as have been observed in the dynamic spectra, but which are not resolved here because the data are taken point by point. This would further explain the relatively large scatter of the data points in the low-frequency region.

The important thing from the point of view of the purposes of this experiment is that no strong relaxation or resonance effect has been observed for the $BaTiO_3$ single crystals at microwave frequencies (up to 4000 mc for this experiment). A total of eight crystals have been measured and each crystal exhibits data similar to those displayed in Fig. 34 and 35. A very recent measurement of the permittivity of single crystals of $BaTiO_3$ at 24,000 mc and 56,000 mc has been reported by Benedict and Durand (Ref. 32) with the same conclusion drawn, namely, there is no substantial relaxation of the permittivity of $BaTiO_3$ single crystals at microwave frequencies (i.e., to 56,000 mc).

On the other hand, the data for the ceramics does show a tendency for dispersion at microwave frequencies. Figures 36 and 37 show microwave data for a $BaTiO_3$ ceramic composition containing a small (0.5%) Fe_2O_3 additive. The Fe_2O_3 is added as a fluxing agent, enabling one to obtain a high-density ceramic with a moderate firing schedule (1350°C for two hours). The results of the measurement are compared in Fig. 36 with those cited by Kittel in Fig. 5, and it is seen that these data do show a dispersion at high frequencies but that this is not as pronounced as the data shown by Kittel. Similar results are shown for other $BaTiO_3$ ceramic preparations such as is shown in Fig. 38 and 39. It is not clear why the initial permittivity of the hot-pressed ceramic[14] (Fig. 38) is as high as 2000, a value twice as great as is usually encountered for $BaTiO_3$ ceramic. The answer may be that the hot-pressing technique produces an unusually high-density ceramic or that hot pressing produces a large number of a domains (high-permittivity direction) in the plane of the pressed disc. The hot-pressing method of preparation consists of firing the ceramic under a pressure of about 5000 psi for one-half hour. The heating is accomplished with the aid of an induction heater with a metal sleeve about a ceramic die.

The data for hot-pressed $Cd_2Nb_2O_7$ ferroelectric ceramic is shown in Fig. 40. It is noted that the decrease in the real permittivity with frequency is very slight to 3000 mc and that the losses are relatively low ($Q = \epsilon'/\epsilon'' = 25$ at 3000 mc). The permittivity and loss for a typical $Ba_{0.65}Sr_{0.35}TiO_3$ ceramic are presented in Fig. 41 and the dispersion appears very similar to that of the pure $BaTiO_3$ ceramic. The data for $PbTiO_3$ and $Pb_{0.35}Sr_{0.65}TiO_3$ ceramics for frequencies between 1800 and 4000 mcs have been very kindly supplied by C. B. Sharpe and

[14]The hot-pressed sample for this experiment and samples of $Cd_2Nb_2O_7$ ceramic were supplied through the kind offices of Dr. Alex deBrettville of the Signal Corps Engineering Laboratories, Fort Monmouth, New Jersey.

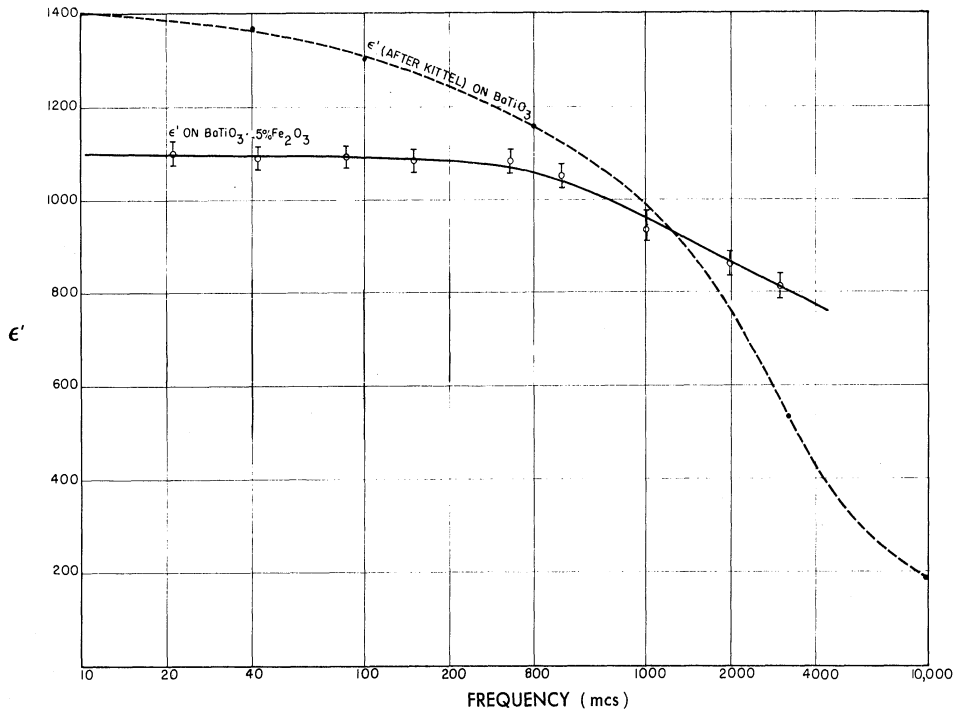

FIG. 36. ϵ VS. FREQUENCY FOR A $BaTiO_3$ + 0.5% Fe_2O_3 CERAMIC

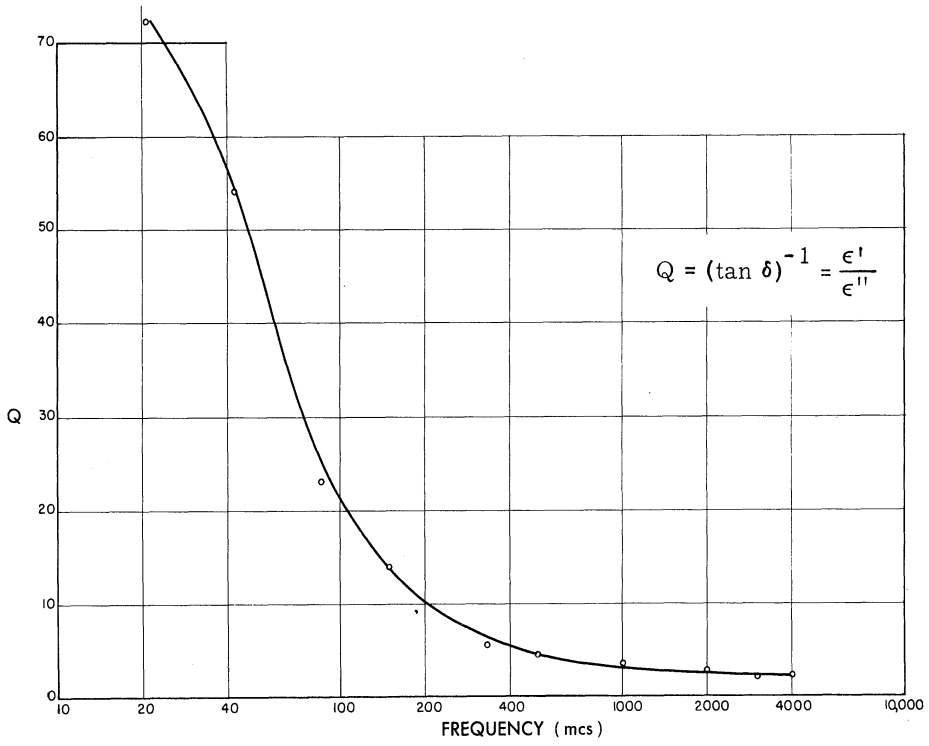

FIG. 37. Q VS. FREQUENCY FOR A $BaTiO_3$ +0.5% Fe_2O_3 CERAMIC

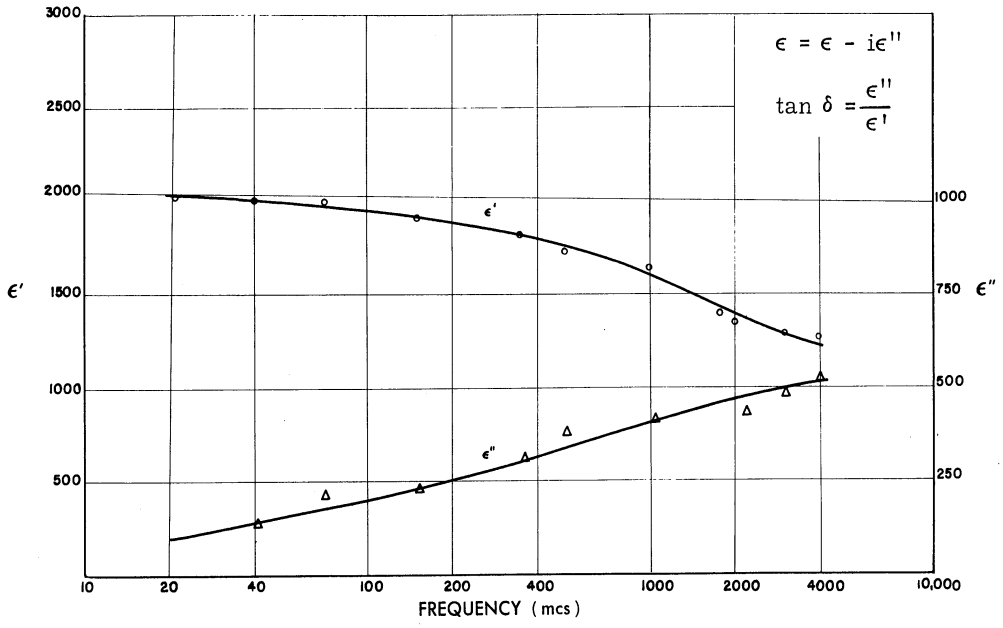

FIG. 38. DATA FOR HOT-PRESSED $BaTiO_3$ CERAMIC (AT 23°C)

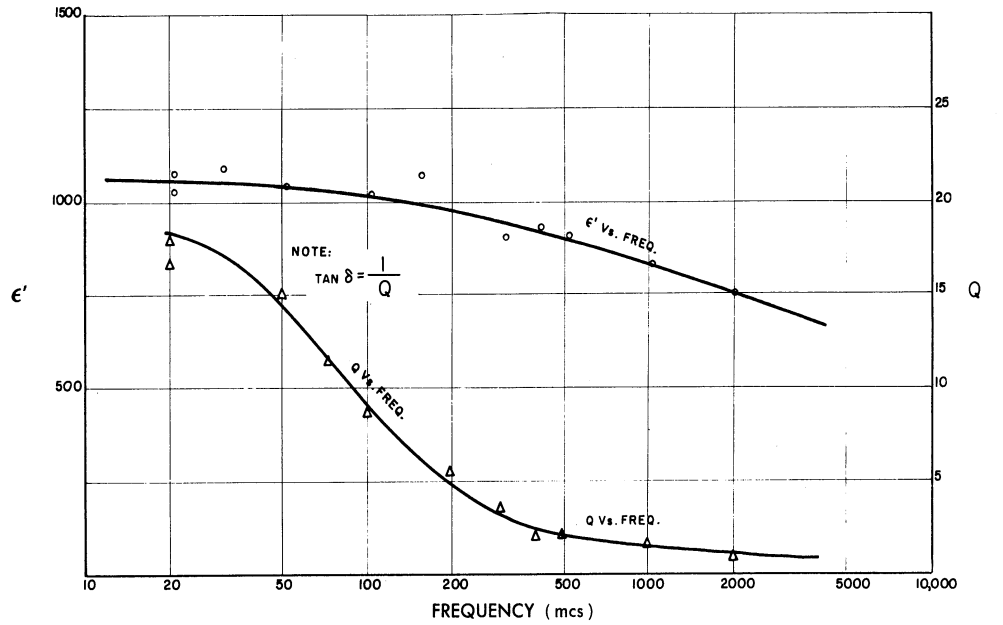

FIG. 39. $BaTiO_3$ CERAMIC WITH EXCESS TiO_2. ϵ and Q vs. frequency (23°C)

G. Brockus (Ref. 22) and are shown in Fig. 42 and 43, respectively. Here again, no unusual dispersive effects are observed. The particular composition $Pb_{0.35}Sr_{0.65}TiO_3$ was chosen because this ceramic has its peak permittivity in the room-temperature region and is therefore similar to the $Ba_{0.65}Sr_{0.35}TiO_3$ ceramic.

In Fig. 44, data are presented for the variation in the 1000-mc permittivity and Q as a function of a d-c biasing field for a $Ba_{0.65}Sr_{0.35}TiO_3$ ceramic. It is noted that the decrease in permittivity (parallel permittivity, in this case) is the same as for lower frequencies (Fig. 14). An extremely interesting feature of these data is the increase in Q as a d-c field is applied. This does not mean, however, that the absolute losses necessarily decrease, since, if even the approximate validity of the Debye equations (1.41) and (1.42) may be assumed, one may write:

$$Q = \frac{\epsilon'}{\epsilon''} = \frac{\epsilon_s' - \epsilon_\infty \omega^2 \tau^2}{(\epsilon_s' - \epsilon_\infty)\omega\tau} \simeq \frac{1}{\omega t} \text{ for } \epsilon_s >> \epsilon_\infty . \tag{4.19}$$

In terms of an equivalent electrical circuit the Debye equations amount to:

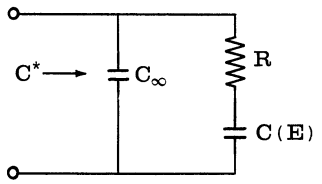

where $C^* = C' - jC''$

and

$$\begin{aligned} \epsilon_\infty &\rightarrow C_\infty \\ \tau &\rightarrow RC \\ \epsilon_s' &\rightarrow C + C_\infty . \end{aligned} \tag{4.20}$$

Thus Eq. (4.19) becomes:

$$Q = \frac{C'}{C''} = \frac{C + C_\infty(1 - \omega^2 R^2 C^2)}{\omega RC^2} \simeq \frac{1}{\omega RC} \tag{4.21}$$

for $C >> C_\infty$. Therefore, if C alone would decrease by the application of a field (as it would for a $Ba_{0.65}Sr_{0.35}TiO_3$ ceramic, (Sec. 3), then Q increases inversely as C decreases, and the dissipative element R need not change with field in order to effect the increase in Q. This general behavior in Q is noted from Fig. 44. Much better data on this inverse behavior in Q

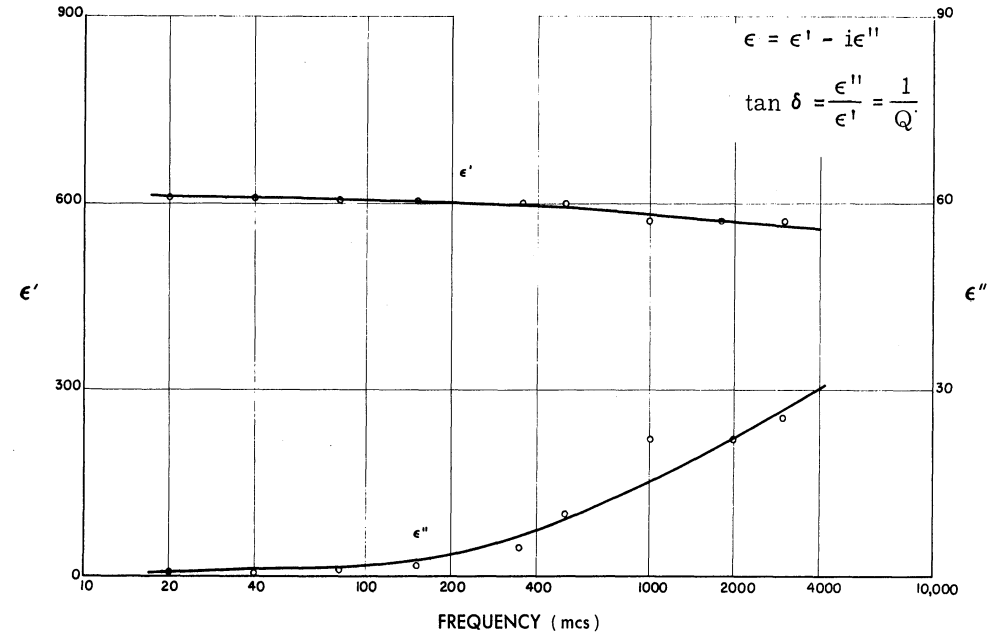

FIG. 40. DATA FOR HOT-PRESSED $Cd_2Nb_2O_7$ (AT 23°C)

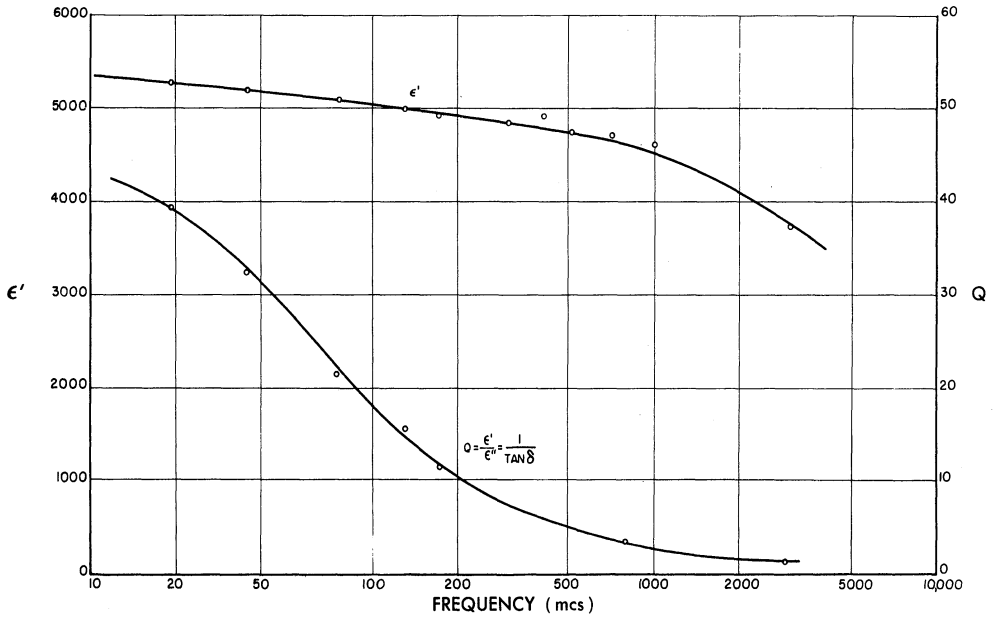

FIG. 41. ϵ' AND Q VS. FREQUENCY FOR $Ba_{0.65}Sr_{0.35}TiO_3$ CERAMIC

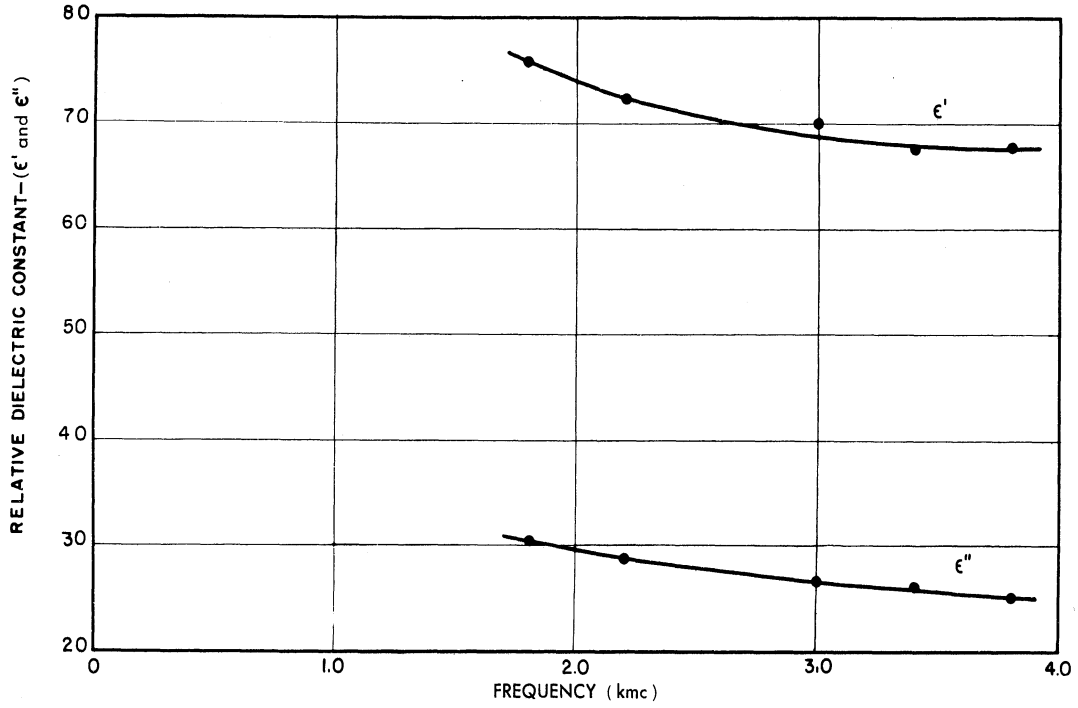

FIG. 42. DIELECTRIC CONSTANTS VS. FREQUENCY FOR $PbTiO_3$. Bias field = 0; ambient temperature = 26°C. [After Sharpe and Brockus (Ref. 22).]

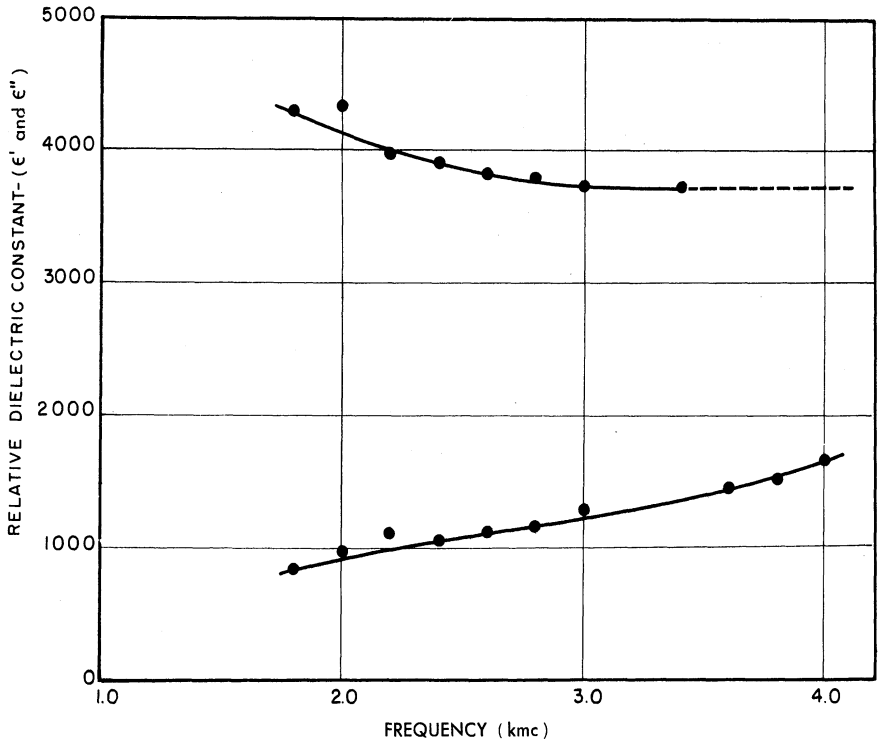

FIG. 43. DIELECTRIC CONSTANTS VS. FREQUENCY FOR $Pb_{0.35}Sr_{0.65}TiO_3$. Bias field = 0; ambient temperature = 26°C. [After Sharpe and Brockus (Ref. 22).]

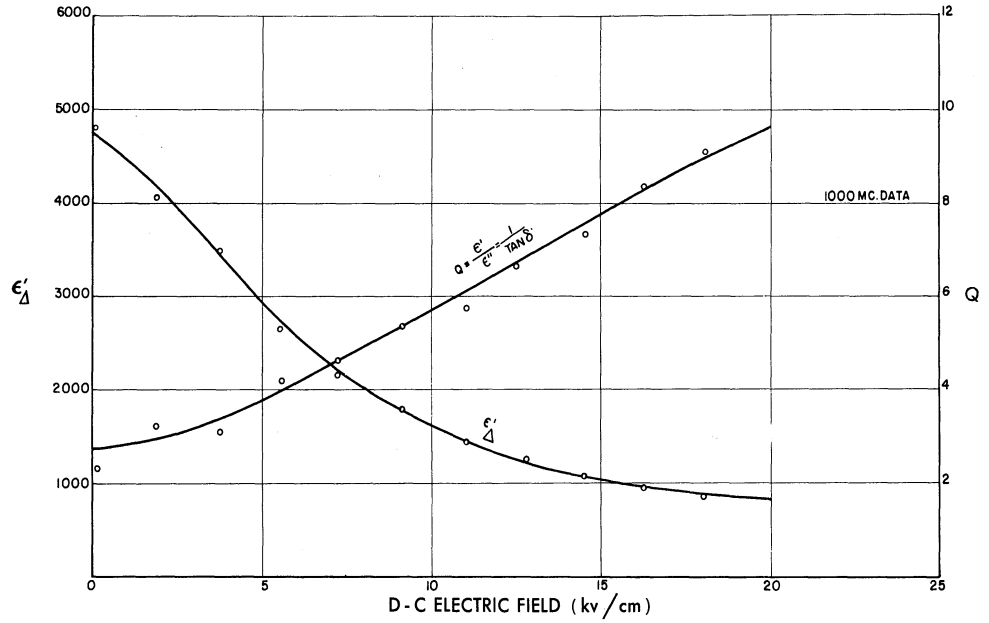

FIG. 44. TUNING DATA FOR $Ba_{0.65}Sr_{0.35}TiO_3$ CERAMIC. ϵ'_Δ MEASURED WITH 1000-mc signal.

are obtained at lower frequencies where more accurate data are obtainable for this and similar ceramics.

The data for the a-oriented and c-oriented single crystals of $BaTiO_3$ fail to show microwave relaxation; therefore, on the basis of these data it is concluded that atomic or molecular relaxation does not exist at microwave frequencies. The explanation of the observed microwave relaxation of the permittivities for polycrystalline samples rests on: (a) dimensional resonances which, due to the small sizes of the crystallites making up the ceramics, would occur in the microwave range; (b) domain growth or orientation time constants; and (c) an apparent relaxation produced by a loss mechanism.

Dimensional resonances would not be able to occur within the crystallites of a ceramic, since these would undoubtedly be effectively clamped by the bulk of the material. The effect of clamping has been discussed in previous sections, and Fig. 30 shows experimentally that, for a clamped crystal, the dimensional resonances are reduced or even disappear. It has also been shown in Sec. 3 that domain orientation or growth does not substantially contribute to the incremental permittivity, so that it would be unreasonable to postulate that the permittivity is reduced at microwave frequencies by domain-motion time constants when the domains do not even contribute to the permittivity. On the other hand, since all materials are to some extent electrostrictive, and for ferroelectrics they are piezoelectric, the mechanical compliance of the material to the signal fields would result in frictional effects at grain and domain boundaries. Thus domains may enter into the relaxation indirectly, i.e., by means of a loss mechanism.

This type of loss and its effect on the high-frequency properties of these ferroelectrics is to be discussed in the following section.

4.3. LOSSES AND DISPERSION

In previous sections it was shown that the Debye equations lead to a particularly simple equivalent circuit and that expressions for $Q = \left(\frac{1}{\tan \delta}\right)$ are given in Eq. (4.19) or (4.20). It was also mentioned in regard to dispersion effects in dielectrics of the high-permittivity type, that in addition to effects such as molecular relaxation and dimensional resonances, dispersion may be a direct consequence of a loss mechanism. In Sec. 3 it has been shown that excellent correlation with various experimental data for permittivities is obtained if one assumes that domain motion and orientation do not contribute to the susceptibility. Thus, domain orientation and growth processes have been ruled out as a direct relaxation mechanism, but domain effects, due to the existence of domain walls, may very well enter into a mechanism of dielectric loss, which in turn would produce the observed relaxation. A direct molecular mechanism of dielectric relaxation is being ruled out, at least to frequencies of 56,000 mc, on the basis of the experimental results with the single crystals.

In a recent paper (January 1959) Lewis (Ref. 33) has investigated energy-loss processes in ferroelectric ceramics, particularly that of pure $BaTiO_3$, and has concluded that although domains do not enter into the small-field polarization they do play a role in the loss mechanism. I have arrived at the same conclusion about the polarization, and in fact found it necessary to assume no domain motion at all in deriving the theoretical models of Sec. 3. Lewis attributes the small-field losses to a so called "microhysteresis," which he feels is due to "... the switching of individual atomic moments in successive lattice planes traversed by the moving boundary." With this I do not agree. Any "switching of atomic moments" in a $BaTiO_3$ ceramic amounts to, in the tetragonal state (cf. Fig. 1 and 2) moving an ion, say Ti^{+4}, from one potential minimum to another. This would involve an activation energy of the order of

$$\Delta E = k\Delta T,$$

where k is Boltzman's constant and ΔT is the difference between the Curie temperature and room temperature at which the measurement is assumed to be made. For $\Delta T = 100^{\circ}K$,

$$E \cong 0.009 \text{ electron-volts.}$$

If we consider the Ti^{+4} ion in a double potential well, then the distance between minima is of the order of 2 angstroms and Ti^{+4} has four electronic charges. Thus to attain an activation energy of 0.009 volts, an electric field of the order of

$$E \cong \frac{\frac{0.009}{4}\text{volts}}{2 \times 10^{-8}\text{ cm}} \sim 10^5 \text{ volts/cm}$$

is required. This figure is very rough, of course, but even if one allows several orders of magnitude for local-field "amplification" the resultant field is very much larger than the small-signal fields. This is one of the reasons why the theory of "microhysteresis" based on a local switching effect appears to be a rather untenable explanation for the high losses observed in the ferroelectrics. Moreover, ferroelectrics are known to be somewhat lossy at temperatures above their Curie points where domains are assumed not to exist. Some experimental evidence does show a reduction in the losses as a ferroelectric is heated through its Curie point, but even at the reduced value, the losses are still somewhat high. Typical data for a ceramic are shown in Fig. 45 where the signal frequency is 1 mcs. A possible explanation for this behavior is to be discussed presently.

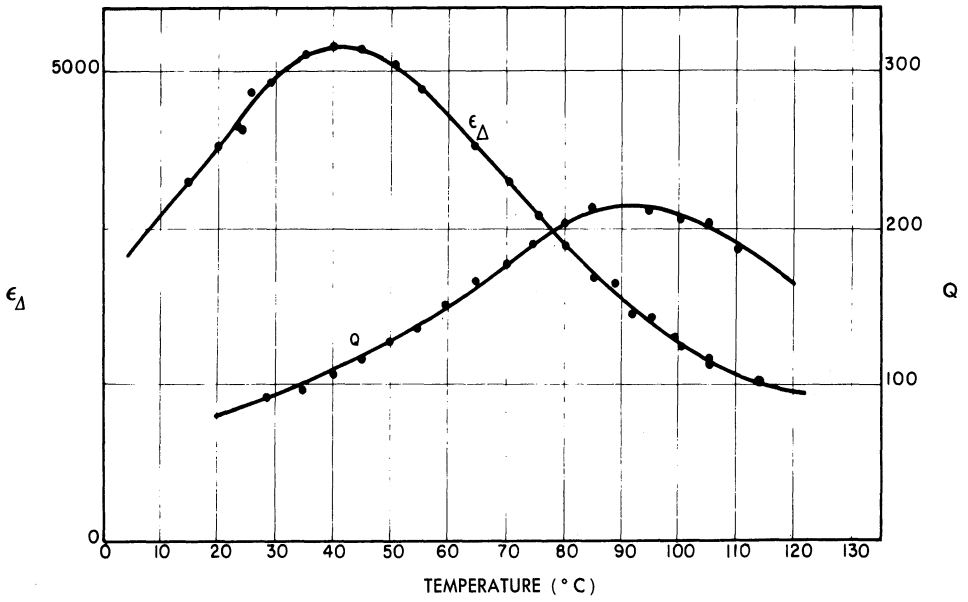

FIG. 45. ϵ_Δ AND LOSS DATA FOR A TYPICAL $Ba_{0.65}Sr_{0.35}TiO_3$ CERAMIC

One of the most fundamental characteristics of ferroelectrics is their piezoelectric property. By this it is meant that a field will produce a linear strain in a single crystal or domain, and if the field is reversed, a strain of opposite sign will result (e.g., if a field in the direction of the polar axis produces an extension, a field in the opposite direction would cause a compression). This is to be distinguished from electrostriction, which is a quadratic effect. In electrostriction the material has an extension along the field direction, and this extension is independent of the sign of the field. Due to the quadratic behavior, electrostrictive effects would be much smaller than piezoelectric effects at small fields.

Although it is felt that domain motion of the type in which atomic moments are switched is not a particularly good model for dielectric losses for the reasons cited above, it is not unreasonable to assume that domains make themselves felt in the piezoelectric or electrostric-

tive interactions (effects which are completely ignored by Lewis's paper). To illustrate, consider the example of a 180° domain wall under the influence of an applied field. This example is shown in the schematic below.

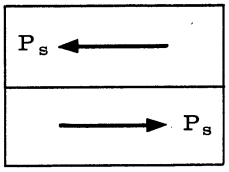

180° wall in the absence of a field

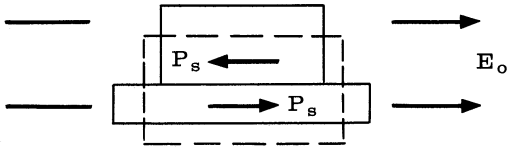

180° wall in the presence of a parallel applied field, E_o

In the absence of an external field, the two domains have opposite directions of spontaneous polarization, and a 180° wall is formed between them. When an external field is applied, the piezoelectric interaction causes a linear extension in the domain which has its spontaneous polarization parallel with the field. The domain in which the spontaneous polarization is antiparallel undergoes a compression. Thus at a 180° domain wall there would be a rather large relative motion of one set of atomic planes over another whenever an electric field is applied, so that a loss mechanism involving what amounts to "wall friction" may be conceived. This mechanism does not require an actual switching of atomic moments. Since there would also be, to a smaller extent, relative motion at 90° walls in the presence of a field, these types of domain walls would also affect the loss. In addition, there would be the possibility of relative motion of the ceramic grain boundaries due to electrostriction, so that this frictional type loss could contribute to the dielectric losses even above the Curie temperatures.

In presuming a piezoelectric and electrostrictive loss mechanism in the ferroelectrics, it is assumed that the frequency is sufficiently high that joule heat losses due to conduction may be ignored. On the other hand, the frequency must be sufficiently low that the wavelengths are not of the order of magnitude of sample dimensions (a few millimeters), so that radiation does not take place from the sample. Frequencies of the order of 10^6 to 10^{10} cps would be the rough range of validity for these assumptions.

Good quantitative data for an attempt to verify any particular loss model are, to date, lacking. It is considered to be a major part of the future research in ferroelectrics at this laboratory to develop models of dielectric loss and to attempt quantitative experimental tests of these models. The concept of piezoelectric and electrostrictive activity being responsible for the dielectric losses can be examined only qualitatively in the light of our present data.

An observation of Q vs. temperature for a typical $Ba_{0.65}Sr_{0.35}TiO_3$ ceramic shown in Fig. 45 shows that as the temperature is increased through the peak-permittivity range, Q is increasing. This would be consistent with the concept that as the individual ceramic grains become heated they undergo a ferroelectric to paraelectric transition, and the domains disappear. Thus piezoelectric activity ceases above the Curie temperature of a given grain. It

is also noted that the Q shows an apparent decrease at the high-temperature limit. This may be due to the fact that the $BaTiO_3$-type ceramics become very conductive at elevated temperatures, so that the high-temperature reduction in Q may be due to conduction losses (the Q vs. temperature data were taken at 1 mc). If one compares the data for $Cd_2Nd_2O_7$ (Fig. 40), which is nonferroelectric at room temperature, with that of the $BaTiO_3$ ceramics (Fig. 38, 39, and 41), which are ferroelectric at room temperature, it is noted that the losses are somewhat smaller in the $Cd_2Nd_2O_7$. An even more interesting observation can be made by comparing the loss behavior of a $BaTiO_3$ single crystal with that of the ceramic. It is seen that the losses in the crystals, which have been prepared as single domain and hence contain no domain walls, actually decrease with frequency, whereas the data for the $BaTiO_3$ ceramic, which presumably contains a large number of domains, shows increasing losses with frequency. It is recalled that at the low-frequency end of the spectrum, $BaTiO_3$ single crystals undergo rather striking dimensional resonances. As the frequency is increased, the dimensional effects cease, and since there are no domains in the crystal, the losses would be expected to decrease. On the other hand, the ceramic contains many domains. It is not necessary to assume dimensional resonances for the individual domains; even highly damped relative motion of the domains in accordance with their piezoelectric behavior would be sufficient to produce losses which would increase with frequency.

The ideas set forth in this section are only qualitative, to be sure. It remains for a future research program to produce a more formal loss model and resultant analysis. Very carefully controlled experiments leading to quantitative data on the number, sizes and types of domains and their possible effects on dielectric losses are required. Such a large-scale experimental program has been beyond the scope of the present study. However, it has been one of the results of this study to suggest this particular direction for future research.

5
CONCLUSIONS

The conclusions stated in this section will be itemized concisely. For a more detailed discussion of a particular point, the reader is referred to the preceding sections in the text. On the basis of the experimental and analytical investigations of the polarization, microwave dispersion, and losses in high-permittivity ferroelectrics, especially those of the $BaTiO_3$ type, the following conclusions may be drawn.

(1) According to the experimental work described in Sec. 4, little or no microwave dispersion has been observed for the permittivity of either a- or c-oriented barium titanate single crystals. On the other hand, experiments on high-permittivity ceramics, both of the pure barium titanate and mixed composition types, show that there is a definite microwave relax-

ation effect for most of the ceramics. Since this effect was absent in the barium titanate single crystals, it is concluded that a polar or molecular mechanism for relaxation is not present. It is further concluded that the observed dispersion for the ceramic composition must be due either to a mechanism of dielectric loss, which is characteristic of ceramic grain and domain properties, or due to a reduction in the permittivity as a result of mechanical clamping of the ceramic grains at microwave frequencies. It has been shown analytically and with high-frequency spectra that this latter effect could account for only a twofold reduction in permittivity through the microwave region.

(2) The ceramic dispersion observed in the experiments is not as strong as that reported by Kittel (Fig. 5 and 36). In order to explain the extremely large reduction in permittivity over two decades in frequency as reported by Kittel, one must adopt a point of view that dielectric losses play a significant role in the microwave relaxation effect in high-permittivity ferroelectrics. These losses may come about as a result of piezoelectric and electrostrictive action at domain boundaries and at the interfaces of ceramic grains.

(3) It has been shown that if domain alignment, orientation, and growth are assumed responsible for the nonlinearity in the permittivity of the ferroelectrics, then one is led to a conflict with the experimental data. In order to describe analytically the observed nonlinear effects, a phenomenological model has been postulated. This model presumes that the domains are "frozen" in the ceramic grains which are ferroelectric and are not moved about by the electric field. The ceramic material is thought to consist of a collection of grains, each of which has a Curie temperature which is given by a Gaussian distribution about some appropriately chosen temperature. In this way the ceramic composition, at the temperature about which the Gaussian distribution is taken, has half of its grains in a paraelectric (nonferroelectric) state. The electric field acts on the nonferroelectric grains in such a way as to induce a ferroelectric state in them. This effect is consistent with the predictions of a free-energy function postulated by Devonshire. The theory developed on the basis of this model leads to results which correlate remarkably well with the experimental data.

(4) On the basis of the model described above, all nonlinear effects in the barium titanate-type ferroelectrics must be accompanied by strong thermal sensitivity; therefore, the present activity in some circles in seeking a ferroelectric of the barium titanate or perovskite class which is sensitive to electric fields but which is insentitive to temperature changes would appear to be unfruitful. This is simply because the free-energy function demands that the thermal and electric-field effects go hand in hand.

(5) Since excellent correlation between experimental and theoretical data has resulted from the assumption of ferroelectric domains being "frozen in" with regard to large electric fields, it is doubtful whether domain effects could contribute to the small signal incremental

permittivities at high frequencies. The large value of permittivity observed in the perovskite ferroelectrics could then be thought of as coming about as a result of the action of the local field in the perovskite structure. Calculations on the local field in $BaTiO_3$ by Slater (Ref. 13) and Triebwasser (Ref. 14) seem to bear this out. In order to account for the large anisotropy in the permittivities for the perovskites in the ferroelectric state, it is interesting to speculate about the possibility of a directed bond between ions in the structure such as Ti and O_I (Fig. 1). For such a case the large transverse permittivity could be thought of as resulting from torsional motion of the directed bond pairs, T_i-O_I. Although measurements on single crystals of $BaTiO_3$ at frequencies up to 56,000 mc have failed to indicate such a polar association, this does not mean that one cannot exist. It may well be that millimeter-wave spectra would reveal this mechanism. Investigations along these lines are to be left for a future program.

APPENDIX

A. 1. This section of the Appendix presents a proof that superposition in the time domain follows from the statement of linearity in the following form:

$$D(\omega) = \epsilon(\omega)E(\omega)$$

or

$$P(\omega) = \chi(\omega)E(\omega),$$

where ϵ or χ has a unique value at a given frequency.

By the Fourier integral, let

$$D_1(t) = \int_{-\infty}^{\infty} D_1(\omega)e^{i\omega t}\,d\omega = \int_{-\infty}^{\infty} \epsilon(\omega)E_1(\omega)e^{i\omega t}\,d\omega, \tag{A. 1}$$

where

$$E_1(\omega) = \frac{1}{2\pi}\int_{-\infty}^{\infty} E_1(t)e^{-i\omega t}\,dt. \tag{A. 2}$$

When Eq. (A. 2) is substituted into Eq. (A. 1), one can say that given an $E_1(t)$ one can predict the $D_1(t)$. Similarly, given an $E_2(t)$ one gets $D_2(t)$ via

$$D_2(t) = \int_{-\infty}^{\infty} \epsilon(\omega)E_2(\omega)e^{i\omega t}\,d\omega, \tag{A. 3}$$

where

$$E_2(\omega) = \frac{1}{2\pi}\int_{-\infty}^{\infty} E_2(t)e^{-i\omega t}\,dt. \tag{A. 4}$$

Superposition in the time domain means that $D_3(t) = D_1(t) + D_2(t)$ is produced by $E_3(t) = E_1(t) + E_2(t)$. By adding Eq. (A. 1) and (A. 3) one gets:

$$D_3(t) = D_1(t) + D_2(t) = \int_{-\infty}^{\infty} \epsilon(\omega)E_1(\omega)e^{i\omega t}\,d\omega + \int_{-\infty}^{\infty} \epsilon(\omega)E_2(\omega)e^{i\omega t}\,d\omega, \tag{A. 5}$$

or

$$D_3(t) = \int_{-\infty}^{\infty} \epsilon(\omega)e^{i\omega t}\left[E_1(\omega) + E_2(\omega)\right]d\omega.$$

But by the property of Eq. (A. 2) and (A. 4) one may write

$$E_3(\omega) = E_1(\omega) + E_2(\omega) = \frac{1}{2\pi} \int \left[E_1(t) + E_2(t)\right] e^{-i\omega t} dt. \tag{A. 6}$$

Thus by substituting $E_1(\omega) + E_2(\omega) = E_3(\omega)$ into Eq. (A. 5) and interpreting property (A. 1)(using the subscript 3), one gets the result that $D_3(t) = D_1(t) + D_2(t)$ is produced by $E_3(t) = E_1(t) + E_2(t)$. It is important to note that this result would not follow if the ϵ were a function of the electric field, since ϵ could then not have been factored from $E_1(\omega)$ and $E_2(\omega)$ in Eq. (A. 5).

A. 2. This section of the Appendix presents a derivation of the relationship between the free and the clamped coefficients in Devonshire's free-energy function for $BaTiO_3$.

Let the Helmholtz free energy for the crystal at some temperature be given by the following expansion in terms of the polarizations (P_i) and strains (x_i).

$$\begin{aligned} A = A_0 &+ \tfrac{1}{2}a''\left(P_1^2 + P_2^2 + P_3^2\right) + \tfrac{1}{4}b''_{11}\left(P_1^4 + P_2^4 + P_3^4\right) \\ &+ \tfrac{1}{2}b''_{12}\left(P_1^2P_2^2 + P_1^2P_3^2 + P_2^2P_3^2\right) + \tfrac{1}{2}c_{11}\left(x_1^2 + x_2^2 + x_3^2\right) \\ &+ c_{12}(x_1x_2 + x_1x_3 + x_2x_3) + \tfrac{1}{2}c_{44}\left(x_4^2 + x_5^2 + x_6^2\right) \\ &+ q_{11}\left(x_1P_1^2 + x_2P_2^2 + x_3P_3^2\right) + q_{12}\left[x_1\left(P_2^2+P_3^2\right)\right. \\ &\left. + x_2\left(P_1^2 + P_3^2\right) + x_3\left(P_1^2 + P_2^2\right)\right] \\ &+ q_{44}(x_4P_2P_3 + x_5P_1P_3 + x_6P_1P_2) + \ldots . \end{aligned} \tag{A. 7}$$

Here the double primes indicate that the coefficients are for the clamped crystal. Subscripts 1, 2, and 3 refer to the coordinates x, y, and z. The strains with subscripts 4, 5, and 6 are shears. For the cubic to tetragonal transition there is only one polar axis, although strains may exist along the three crystallographic axes. The assumption may be made that no shear strains exist for this geometry. Therefore, we set

$$P_2 = P_3 = x_4 = x_5 = x_6 = 0.$$

Also by the geometry of the crystal there are two equivalent a-axes in the tetragonal state so that we take $x_2 = x_3$ along the a-axis. Setting the stresses $X_i = -\frac{\partial A}{\partial x_i}$ equal to zero, one has

$$c_{11}x_1 + 2c_{12}x_2 + q_{11}P_1^2 = 0,$$

and (A.8)

$$c_{11}x_2 + c_{12}(x_1+x_2) + q_{12}P_1^2 = 0.$$

From these equations one may solve for the strains x_1 and x_2 in terms of the polarization and electrostrictive coefficients, obtaining

$$x_1 = \frac{(2q_{12} - q_{11})c_{12} - q_{11}c_{11}}{(c_{11} + 2c_{12})(c_{11} - c_{12})}P_1^2 \equiv \alpha P_1^2,$$

and (A.9)

$$x_2 = x_3 = \frac{q_{11}c_{12} - q_{12}c_{11}}{(c_{11} + 2c_{12})(c_{11} - c_{12})}P_1^2 \equiv \beta P_1^2,$$

where α and β are defined as a matter of convenience. Substituting these values for the strains into Eq. (A.7) gives the free energy the form:

$$A = A_0 + \frac{1}{2}a''P_1^2 + \frac{1}{4}b''_{11}P_1^4 + \frac{1}{2}c_{11}(\alpha^2 + 2\beta^2)P_1^4 + c_{12}(2\alpha\beta + \beta^2)P_1^4 + q_{11}\alpha P_1^4 + 2q_{12}\beta P_1^4 . \quad (A.10)$$

On the other hand, it has already been noted in Eq. (2.4) that the free energy expressed in terms of the "free" coefficients is written as

$$A = A_0 + \frac{1}{2}a'P_1^2 + \frac{1}{4}b'_{11}P_1^4 + \ldots . \quad (A.11)$$

Equating the coefficients on the same powers of P_1 in Eq.(A.10) and (A.11) yields

$$a' = a'' = \frac{T - T_0}{10^4},$$

and

$$b'_{11} = b''_{11} + 2\left[\frac{-q_{11}^2(c_{12} + c_{11}) - 2q_{12}^2c_{11} + 4q_{11}q_{12}c_{12}}{(c_{11} + 2c_{12})(c_{11} - c_{12})}\right], \quad (A.12)$$

etc., for the higher-order coefficients. This gives the relationship between the free and the clamped coefficients in the Helmholtz free energy.

REFERENCES

1. Valasek, J., Phys. Rev., 1921, Vol. 17, p. 475.
2. Von Hippel, A., et al., Cambridge, Mass., Massachusetts Institute of Technology, Laboratory for Insulation Research, NDRC Report 14-300, 1944, and NDRC Report 14-540, 1945.
3. Wul, B., J. Phys. (USSR), 1946, Vol. 10, p. 95.
4. Frazer, B. C., Danner, H., and Pepinsky, R., Phys. Rev., Oct. 1955, Vol. 100.
5. Kay, H. F., and Vousden, P., Phil. Mag., 1949, Vol. 40.
6. Merz, W. J., Phys. Rev., 1949, Vol. 76, p. 1221.
7. Merz, W. J., Phys. Rev., 1952, Vol. 88, p. 421.
8. Jaynes, E. T., Proc. IRE, 1955, Vol. 43, No. 12.
9. Butler, T. W., Quarterly Progress Report No. 18, Ann Arbor, Mich., The University of Michigan Research Institute, July 1958.
10. Lorentz, H. A., The Theory of Electrons, Tuebner, 1909.
11. Onsager, L., J. Am. Chem. Soc., 1936, Vol. 58.
12. Jaynes, E. T., Ferroelectricity, Princeton, N. J., Princeton University Press, 1953.
13. Slater, J. C., Phys. Rev., 1950, Vol. 78, p. 748.
14. Triebwasser, S., J. Phys. and Chem. Solids, 1957, Vol. 3, No. 1 and 2.
15. Born, M., and Von Karman, T., Physik Z., 1912, Vol. 13.
16. Fröhlich, H., The Theory of Dielectrics, London, Oxford University Press, 1958, second edition.
17. Toupin, R. A., and Lax, M., J. Chem. Phys., 1957, Vol. 27, No. 2.
18. Powles, J. G., Jackson, W., Proc. Inst. Elec. Engrs. (London), 1949, Vol. 96, p. 383.
19. Von Hippel, A., Rev. Mod. Phys., 1950, Vol. 22, p. 221.
20. Kittel, C., Introduction to Solid State Physics, New York, Wiley, 1956, 2nd ed.
21. Von Hippel, A., Dielectrics and Waves, New York, Wiley, 1954.
22. Sharpe, C. B., and Brockus, G., Microwave Properties of Ferroelectric Materials, Ann Arbor, Mich., The University of Michigan Research Institute, March 1959, Final Report.
23. Devonshire, A. F., "Theory of Ferroelectrics," Advances in Phys., April 1954, Vol. 3, No. 4.
24. Merz, W. J., Phys. Rev., 1953, Vol. 91, p. 513.
25. Huibregtse, E. J., and Young, D. R., Phys. Rev., 1956, Vol. 103, p. 1705.
26. Diamond, H., and Orr, L. W., Ann Arbor, Mich., The University of Michigan, Engineering Research Institute, 1954, Technical Report No. 31.
27. Berlincourt, D., and Jaffe, H., Phys. Rev., 1958, Vol. 109, No. 1.

28. Shelton, G. R., Bunting, E. N., and Kopell, L., Dielectrics for Ceramic Components, National Bureau of Standards, July 1953, Report No. 4.

29. High Dielectric Ceramics, Niagara Falls, N. Y., Titanium Alloy Manufacturing Co., 1950.

30. Drougard, M. E., and Young, D. R., Phys. Rev., 1954, Vol. 95, p. 1152.

31. Jaynes, E. T., and Varenhorst, V., Stanford, Calif., Stanford University Microwave Laboratory, Technical Report No. 287.

32. Benedict, T. S., and Durand, J. L., Phys. Rev., February 1958, Vol. 109, No. 4.

33. Lewis, B., Proc. Phys. Soc. (London), January 1959, Vol. 73.

DISTRIBUTION LIST 6, PROJECT MICHIGAN REPORTS
1 January 1960 – Effective Date

Copies — Addressee

1 Office, Chief of Research and Development
Department of the Army
Washington 25, D. C.

ATTN: Army Research Office

1 Office, Assistant Chief of Staff for Intelligence
Department of the Army, Washington 25, D. C.

ATTN: Chief, Combat Developments /G-2 Air Branch

1 Commanding General, U. S. Continental Army Command
Fort Monroe, Virginia

ATTN: ATSWD-G

2 Commanding General, U. S. Army Combat Surveillance Agency
1124 N. Highland Street, Arlington 1, Virginia

1 Chief, Research and Development Division
Office of the Chief Signal Officer
Department of the Army, Washington 25, D. C.

25 Commanding Officer
U. S. Army Signal Research and Development Laboratory
Fort Monmouth, New Jersey

ATTN: SIGFM/EL-DR

1 Commanding General, U. S. Army Electronic Proving Ground
Fort Huachuca, Arizona

ATTN: Technical Library

1 Office of the Director, Defense Research and Engineering
Technical Library, Department of Defense
Washington 25, D. C.

1 Chief of Engineers, Department of the Army
Washington 25, D. C.

ATTN: Research and Development Division

1 Office, Chief of Ordnance, Research and Development Division
Department of the Army, Washington 25, D. C.

ATTN: ORDTB, Research and Special Projects

1 Commanding General
Quartermaster Research and Engineering Command, U. S. Army
Natick, Massachusetts

2 Chief, U. S. Army Security Agency
Arlington Hall Station, Arlington 12, Virginia

2 Commander, Army Rocket and Guided Missile Agency
Redstone Arsenal, Alabama

ATTN: Technical Library, ORDXR-OTL

4 Director, U. S. Army Engineer Research and Development Laboratories
Fort Belvoir, Virginia

(1) ATTN: Chief, Topographic Engineer Department
(2) ATTN: Chief, Electrical Engineering Department
(1) ATTN: Technical Documents Center

1 Commanding General
U. S. Army Combat Development Experimentation Center
Fort Ord, California

1 Commandant, U. S. Army Command and General Staff College
Fort Leavenworth, Kansas

ATTN: Archives

Copies — Addressee

2 Assistant Commandant, U. S. Army Artillery and Missile School
Fort Sill, Oklahoma

3 Assistant Commandant, U. S. Army Air Defense School
Fort Bliss, Texas

1 Commandant, U. S. Army Engineer School
Fort Belvoir, Virginia

ATTN: Combat Developments Group

1 Commandant, U. S. Army Signal School
Fort Monmouth, New Jersey

ATTN: SIGFM/SC-DO

1 Commandant, U. S. Army Aviation School
Fort Rucker, Alabama

3 President, U. S. Army Artillery Board
Fort Sill, Oklahoma

1 President, U. S. Army Air Defense Board
Fort Bliss, Texas

1 President, U. S. Army Airborne and Electronics Board
Fort Bragg, North Carolina

1 Commanding Officer, U. S. Army Signal Electronic Research Unit
Post Office Box 205, Mountain View, California

2 Office of Naval Operations
Department of the Navy, Washington 25, D. C.

(1) ATTN: OP-37
(1) ATTN: Op-07T

1 Office of Naval Research, Department of the Navy
17th and Constitution Avenue, N. W.
Washington 25, D. C.

ATTN: Code 463

2 Director, U. S. Naval Research Laboratory
Washington 25, D. C.

ATTN: Code 2027

1 Commanding Officer, U. S. Navy Ordnance Laboratory
Cornona, California

ATTN: Library

1 Commanding Officer and Director, U. S. Navy Electronics Laboratory
San Diego 52, California

ATTN: Library

4 Department of the Air Force
Headquarters, USAF, Washington 25, D. C.

(1) ATTN: AFOIN-1B1
(1) ATTN: AFOAC-E/A
(1) ATTN: AFDRD
(1) ATTN: Directorate of Requirements

3 Commander in Chief, Headquarters, Strategic Air Command
Offutt Air Force Base, Nebraska

(1) ATTN: DINC
(2) ATTN: DORQP

DISTRIBUTION LIST 6 1 January 1960 – Effective Date

Copies — Addressee

3 Headquarters, Tactical Air Command
Langley Air Force Base, Virginia
(1) ATTN: TOOA
(2) ATTN: TORQ

1 Commander, Air Technical Intelligence Center
Wright-Patterson Air Force Base, Ohio
ATTN: AFCIN-4B/a

10 ASTIA (TIPCR)
Arlington Hall Station, Arlington 12, Virginia

10 Commander, Wright Air Development Center
Wright-Patterson Air Force Base, Ohio
(9) ATTN: WCLROR
(1) ATTN: WCOSI-Library

2 Commander, Rome Air Development Center
Griffiss Air Force Base, New York
(1) ATTN: RCVSL-1
(1) ATTN: RCWIR

1 Director, Air University Library
Maxwell Air Force Base, Alabama
ATTN: AUL-7971

1 Commandant of the Marine Corps, Headquarters, U. S. Marine Corps
Washington 25, D. C.
ATTN: Code AO4E

4 Central Intelligence Agency
2430 E. Street, N. W., Washington 25, D. C.
ATTN: OCR Mail Room

5 National Aeronautics and Space Administration
1520 H. Street, Northwest, Washington 25, D. C.

2 Combat Surveillance Project, Cornell Aeronautical Laboratory, Inc.
Box 168, Arlington 10, Virginia
ATTN: Technical Library

1 The RAND Corporation
1700 Main Street, Santa Monica, California
ATTN: Library

Copies — Addressee

1 Chief Scientist, Research and Development Division
Office of the Chief Signal Officer
Department of the Army, Washington 25, D. C.

1 Stanford Research Institute, Document Center
Menlo Park, California
ATTN: Acquisitions

1 Operations Research Office, The Johns Hopkins University
6935 Arlington Road, Bethesda, Maryland, Washington 14, D. C.
ATTN: Chief Intelligence Division

1 Columbia University, Electronics and Research Laboratories
632 W. 125th Street, New York 27, New York
ATTN: Technical Library
THRU: Commander, Rome Air Development Center
Griffiss Air Force Base, New York
ATTN: RCSSTL-1

2 Cornell Aeronautical Laboratory, Inc.
4455 Genesee Street, Buffalo 21, New York
ATTN: Librarian
THRU: Bureau of Aeronautics Representative
4455 Genesee Street, Buffalo 21, New York

1 Control Systems Laboratory, University of Illinois
Urbana, Illinois
ATTN: Librarian
THRU: ONR Resident Representative
1209 W. Illinois Street, Urbana, Illinois

1 Polytechnic Institute of Brooklyn
55 Johnson Street, Brooklyn 1, New York
ATTN: Microwave Research Institute Library

1 The U. S. Army Aviation HRU
P. O. Box 428, Fort Rucker, Alabama

1 U. S. Continental Army Command Liaison Officer
Project MICHIGAN, Willow Run Laboratories, Ypsilanti, Michigan

1 Commanding Officer, U. S. Army Liaison Group
Project MICHIGAN, Willow Run Laboratories, Ypsilanti, Michigan

AD   Div. 14/2

Willow Run Laboratories, U. of Michigan, Ann Arbor
POLARIZATION, MICROWAVE DISPERSION, AND LOSS IN HIGH-PERMITTIVITY FERROELECTRICS by Howard Diamond. Rept. of Project MICHIGAN. Jan 60. 95 p. incl. illus., tables, 33 refs.
(Rept. no. 2900-121-T)
(Contract DA-36-039 SC-78801)   Unclassified report

The purpose of this study is to investigate, by analysis of experimental data, polarization, dispersion, and loss processes in high-permittivity ferroelectrics. The study proceeds from the observation that, according to published data, polycrystalline $BaTiO_3$ and similar compositions show strong relaxation in permittivity at microwave frequencies. This phenomenon is shown to be generally related to polarization and loss properties of the dielectric. Processes of particular interest in accounting for the microwave relaxation are: (a) domain effects, (b) possible dipolar or molecular polarization, and (c) mechanical effects produced by piezoelectric and electrostrictive coupling.

(over)

UNCLASSIFIED

1. Ferroelectric crystals – Analysis
2. Ferroelectric crystals – Polarization
3. Ferroelectric crystals – Dispersion
4. Ferroelectric crystals – Properties
5. Ferroelectric crystals – Processes
6. Ceramic materials – Dielectric properties
7. Ceramic materials – Polarization

I. Title: Project MICHIGAN
II. Diamond, Howard
III. U. S. Army Signal Corps
IV. U. S. Air Force Office of Scientific Research
V. The National Science Foundation
VI. Contract DA-36-039 SC-78801

Armed Services Technical Information Agency
UNCLASSIFIED

AD   Div. 14/2

Willow Run Laboratories, U. of Michigan, Ann Arbor
POLARIZATION, MICROWAVE DISPERSION, AND LOSS IN HIGH-PERMITTIVITY FERROELECTRICS by Howard Diamond. Rept. of Project MICHIGAN. Jan 60. 95 p. incl. illus., tables, 33 refs.
(Rept. no. 2900-121-T)
(Contract DA-36-039 SC-78801)   Unclassified report

The purpose of this study is to investigate, by analysis of experimental data, polarization, dispersion, and loss processes in high-permittivity ferroelectrics. The study proceeds from the observation that, according to published data, polycrystalline $BaTiO_3$ and similar compositions show strong relaxation in permittivity at microwave frequencies. This phenomenon is shown to be generally related to polarization and loss properties of the dielectric. Processes of particular interest in accounting for the microwave relaxation are: (a) domain effects, (b) possible dipolar or molecular polarization, and (c) mechanical effects produced by piezoelectric and electrostrictive coupling.

(over)

UNCLASSIFIED

1. Ferroelectric crystals – Analysis
2. Ferroelectric crystals – Polarization
3. Ferroelectric crystals – Dispersion
4. Ferroelectric crystals – Properties
5. Ferroelectric crystals – Processes
6. Ceramic materials – Dielectric properties
7. Ceramic materials – Polarization

I. Title: Project MICHIGAN
II. Diamond, Howard
III. U. S. Army Signal Corps
IV. U. S. Air Force Office of Scientific Research
V. The National Science Foundation
VI. Contract DA-36-039 SC-78801

Armed Services Technical Information Agency
UNCLASSIFIED

AD   Div. 14/2

Willow Run Laboratories, U. of Michigan, Ann Arbor
POLARIZATION, MICROWAVE DISPERSION, AND LOSS IN HIGH-PERMITTIVITY FERROELECTRICS by Howard Diamond. Rept. of Project MICHIGAN. Jan 60. 95 p. incl. illus., tables, 33 refs.
(Rept. no. 2900-121-T)
(Contract DA-36-039 SC-78801)   Unclassified report

The purpose of this study is to investigate, by analysis of experimental data, polarization, dispersion, and loss processes in high-permittivity ferroelectrics. The study proceeds from the observation that, according to published data, polycrystalline $BaTiO_3$ and similar compositions show strong relaxation in permittivity at microwave frequencies. This phenomenon is shown to be generally related to polarization and loss properties of the dielectric. Processes of particular interest in accounting for the microwave relaxation are: (a) domain effects, (b) possible dipolar or molecular polarization, and (c) mechanical effects produced by piezoelectric and electrostrictive coupling.

(over)

UNCLASSIFIED

1. Ferroelectric crystals – Analysis
2. Ferroelectric crystals – Polarization
3. Ferroelectric crystals – Dispersion
4. Ferroelectric crystals – Properties
5. Ferroelectric crystals – Processes
6. Ceramic materials – Dielectric properties
7. Ceramic materials – Polarization

I. Title: Project MICHIGAN
II. Diamond, Howard
III. U. S. Army Signal Corps
IV. U. S. Air Force Office of Scientific Research
V. The National Science Foundation
VI. Contract DA-36-039 SC-78801

Armed Services Technical Information Agency
UNCLASSIFIED

AD   Div. 14/2

Willow Run Laboratories, U. of Michigan, Ann Arbor
POLARIZATION, MICROWAVE DISPERSION, AND LOSS IN HIGH-PERMITTIVITY FERROELECTRICS by Howard Diamond. Rept. of Project MICHIGAN. Jan 60. 95 p. incl. illus., tables, 33 refs.
(Rept. no. 2900-121-T)
(Contract DA-36-039 SC-78801)   Unclassified report

The purpose of this study is to investigate, by analysis of experimental data, polarization, dispersion, and loss processes in high-permittivity ferroelectrics. The study proceeds from the observation that, according to published data, polycrystalline $BaTiO_3$ and similar compositions show strong relaxation in permittivity at microwave frequencies. This phenomenon is shown to be generally related to polarization and loss properties of the dielectric. Processes of particular interest in accounting for the microwave relaxation are: (a) domain effects, (b) possible dipolar or molecular polarization, and (c) mechanical effects produced by piezoelectric and electrostrictive coupling.

(over)

UNCLASSIFIED

1. Ferroelectric crystals – Analysis
2. Ferroelectric crystals – Polarization
3. Ferroelectric crystals – Dispersion
4. Ferroelectric crystals – Properties
5. Ferroelectric crystals – Processes
6. Ceramic materials – Dielectric properties
7. Ceramic materials – Polarization

I. Title: Project MICHIGAN
II. Diamond, Howard
III. U. S. Army Signal Corps
IV. U. S. Air Force Office of Scientific Research
V. The National Science Foundation
VI. Contract DA-36-039 SC-78801

Armed Services Technical Information Agency
UNCLASSIFIED

AD

The conclusions that may be drawn from this work are as follows. (1) The field sensitivity of the incremental permittivity of polycrystalline ferroelectrics is not a domain effect, but results from an induced ferroelectric state in nonferroelectric grains. (2) Nonlinear permittivity under electric fields must necessarily be accomplished by substantial thermal sensitivity. (3) Orientation of the domains does not contribute to microwave dispersion. (4) Molecular or dipolar relaxation does not occur at microwave frequencies for $BaTiO_3$ single crystals. Therefore, this is not a mechanism for dispersion in the ceramic. (5) Dielectric loss as well as piezoelectric and electrostrictive activity would result in microwave dispersion in high-permittivity ferroelectrics.

UNCLASSIFIED

UNITERMS

Polarization
Dispersion
Loss processes
Polycrystalline
$BaTiO_3$
Relaxation
Permittivity
Frequency
Microwave
Dielectric
Domain
Dipolar
Molecular
Electrostrictive
Coupling
Hysteresis
Ceramic
Free energy
Curie
Ferroelectric
Nonferroelectric
Crystals

UNCLASSIFIED

AD

The conclusions that may be drawn from this work are as follows. (1) The field sensitivity of the incremental permittivity of polycrystalline ferroelectrics is not a domain effect, but results from an induced ferroelectric state in nonferroelectric grains. (2) Nonlinear permittivity under electric fields must necessarily be accomplished by substantial thermal sensitivity. (3) Orientation of the domains does not contribute to microwave dispersion. (4) Molecular or dipolar relaxation does not occur at microwave frequencies for $BaTiO_3$ single crystals. Therefore, this is not a mechanism for dispersion in the ceramic. (5) Dielectric loss as well as piezoelectric and electrostrictive activity would result in microwave dispersion in high-permittivity ferroelectrics.

UNCLASSIFIED

UNITERMS

Polarization
Dispersion
Loss processes
Polycrystalline
$BaTiO_3$
Relaxation
Permittivity
Frequency
Microwave
Dielectric
Domain
Dipolar
Molecular
Electrostrictive
Coupling
Hysteresis
Ceramic
Free energy
Curie
Ferroelectric
Nonferroelectric
Crystals

UNCLASSIFIED

AD Div. 14/2

Willow Run Laboratories, U. of Michigan, Ann Arbor
POLARIZATION, MICROWAVE DISPERSION, AND LOSS IN HIGH-PERMITTIVITY FERROELECTRICS by Howard Diamond. Rept. of Project MICHIGAN. Jan 60. 95 p. incl. illus., tables, 33 refs.
(Rept. no. 2900-121-T)
(Contract DA-36-039 SC-78801) Unclassified report

The purpose of this study is to investigate, by analysis of experimental data, polarization, dispersion, and loss processes in high-permittivity ferroelectrics. The study proceeds from the observation that, according to published data, polycrystalline $BaTiO_3$ and similar compositions show strong relaxation in permittivity at microwave frequencies. This phenomenon is shown to be generally related to polarization and loss properties of the dielectric. Processes of particular interest in accounting for the microwave relaxation are: (a) domain effects, (b) possible dipolar or molecular polarization, and (c) mechanical effects produced by piezoelectric and electrostrictive coupling.

(over)

UNCLASSIFIED

1. Ferroelectric crystals — Analysis
2. Ferroelectric crystals — Polarization
3. Ferroelectric crystals — Dispersion
4. Ferroelectric crystals — Properties
5. Ferroelectric crystals — Processes
6. Ceramic materials — Dielectric properties
7. Ceramic materials — Polarization

I. Title: Project MICHIGAN
II. Diamond, Howard
III. U. S. Army Signal Corps
IV. U. S. Air Force Office of Scientific Research
V. The National Science Foundation
VI. Contract DA-36-039 SC-78801

Armed Services Technical Information Agency
UNCLASSIFIED

AD Div. 14/2

Willow Run Laboratories, U. of Michigan, Ann Arbor
POLARIZATION, MICROWAVE DISPERSION, AND LOSS IN HIGH-PERMITTIVITY FERROELECTRICS by Howard Diamond. Rept. of Project MICHIGAN. Jan 60. 95 p. incl. illus., tables, 33 refs.
(Rept. no. 2900-121-T)
(Contract DA-36-039 SC-78801) Unclassified report

The purpose of this study is to investigate, by analysis of experimental data, polarization, dispersion, and loss processes in high-permittivity ferroelectrics. The study proceeds from the observation that, according to published data, polycrystalline $BaTiO_3$ and similar compositions show strong relaxation in permittivity at microwave frequencies. This phenomenon is shown to be generally related to polarization and loss properties of the dielectric. Processes of particular interest in accounting for the microwave relaxation are: (a) domain effects, (b) possible dipolar or molecular polarization, and (c) mechanical effects produced by piezoelectric and electrostrictive coupling.

(over)

UNCLASSIFIED

1. Ferroelectric crystals — Analysis
2. Ferroelectric crystals — Polarization
3. Ferroelectric crystals — Dispersion
4. Ferroelectric crystals — Properties
5. Ferroelectric crystals — Processes
6. Ceramic materials — Dielectric properties
7. Ceramic materials — Polarization

I. Title: Project MICHIGAN
II. Diamond, Howard
III. U. S. Army Signal Corps
IV. U. S. Air Force Office of Scientific Research
V. The National Science Foundation
VI. Contract DA-36-039 SC-78801

Armed Services Technical Information Agency
UNCLASSIFIED

AD Div. 14/2

Willow Run Laboratories, U. of Michigan, Ann Arbor
POLARIZATION, MICROWAVE DISPERSION, AND LOSS IN HIGH-PERMITTIVITY FERROELECTRICS by Howard Diamond. Rept. of Project MICHIGAN. Jan 60. 95 p. incl. illus., tables, 33 refs.
(Rept. no. 2900-121-T)
(Contract DA-36-039 SC-78801) Unclassified report

The purpose of this study is to investigate, by analysis of experimental data, polarization, dispersion, and loss processes in high-permittivity ferroelectrics. The study proceeds from the observation that, according to published data, polycrystalline $BaTiO_3$ and similar compositions show strong relaxation in permittivity at microwave frequencies. This phenomenon is shown to be generally related to polarization and loss properties of the dielectric. Processes of particular interest in accounting for the microwave relaxation are: (a) domain effects, (b) possible dipolar or molecular polarization, and (c) mechanical effects produced by piezoelectric and electrostrictive coupling.

(over)

UNCLASSIFIED

1. Ferroelectric crystals — Analysis
2. Ferroelectric crystals — Polarization
3. Ferroelectric crystals — Dispersion
4. Ferroelectric crystals — Properties
5. Ferroelectric crystals — Processes
6. Ceramic materials — Dielectric properties
7. Ceramic materials — Polarization

I. Title: Project MICHIGAN
II. Diamond, Howard
III. U. S. Army Signal Corps
IV. U. S. Air Force Office of Scientific Research
V. The National Science Foundation
VI. Contract DA-36-039 SC-78801

Armed Services Technical Information Agency
UNCLASSIFIED

AD Div. 14/2

Willow Run Laboratories, U. of Michigan, Ann Arbor
POLARIZATION, MICROWAVE DISPERSION, AND LOSS IN HIGH-PERMITTIVITY FERROELECTRICS by Howard Diamond. Rept. of Project MICHIGAN. Jan 60. 95 p. incl. illus., tables, 33 refs.
(Rept. no. 2900-121-T)
(Contract DA-36-039 SC-78801) Unclassified report

The purpose of this study is to investigate, by analysis of experimental data, polarization, dispersion, and loss processes in high-permittivity ferroelectrics. The study proceeds from the observation that, according to published data, polycrystalline $BaTiO_3$ and similar compositions show strong relaxation in permittivity at microwave frequencies. This phenomenon is shown to be generally related to polarization and loss properties of the dielectric. Processes of particular interest in accounting for the microwave relaxation are: (a) domain effects, (b) possible dipolar or molecular polarization, and (c) mechanical effects produced by piezoelectric and electrostrictive coupling.

(over)

UNCLASSIFIED

1. Ferroelectric crystals — Analysis
2. Ferroelectric crystals — Polarization
3. Ferroelectric crystals — Dispersion
4. Ferroelectric crystals — Properties
5. Ferroelectric crystals — Processes
6. Ceramic materials — Dielectric properties
7. Ceramic materials — Polarization

I. Title: Project MICHIGAN
II. Diamond, Howard
III. U. S. Army Signal Corps
IV. U. S. Air Force Office of Scientific Research
V. The National Science Foundation
VI. Contract DA-36-039 SC-78801

Armed Services Technical Information Agency
UNCLASSIFIED

AD

The conclusions that may be drawn from this work are as follows. (1) The field sensitivity of the incremental permittivity of polycrystalline ferroelectrics is not a domain effect, but results from an induced ferroelectric state in nonferroelectric grains. (2) Nonlinear permittivity under electric fields must necessarily be accomplished by substantial thermal sensitivity. (3) Orientation of the domains does not contribute to microwave dispersion. (4) Molecular or dipolar relaxation does not occur at microwave frequencies for $BaTiO_3$ single crystals. Therefore, this is not a mechanism for dispersion in the ceramic. (5) Dielectric loss as well as piezoelectric and electrostrictive activity would result in microwave dispersion in high-permittivity ferroelectrics.

UNCLASSIFIED

UNITERMS

Polarization
Dispersion
Loss processes
Polycrystalline
$BaTiO_3$
Relaxation
Permittivity
Frequency
Microwave
Dielectric
Domain
Dipolar
Molecular
Electrostrictive
Coupling
Hysteresis
Ceramic
Free energy
Curie
Ferroelectric
Nonferroelectric
Crystals

UNCLASSIFIED

AD

The conclusions that may be drawn from this work are as follows. (1) The field sensitivity of the incremental permittivity of polycrystalline ferroelectrics is not a domain effect, but results from an induced ferroelectric state in nonferroelectric grains. (2) Nonlinear permittivity under electric fields must necessarily be accomplished by substantial thermal sensitivity. (3) Orientation of the domains does not contribute to microwave dispersion. (4) Molecular or dipolar relaxation does not occur at microwave frequencies for $BaTiO_3$ single crystals. Therefore, this is not a mechanism for dispersion in the ceramic. (5) Dielectric loss as well as piezoelectric and electrostrictive activity would result in microwave dispersion in high-permittivity ferroelectrics.

UNCLASSIFIED

UNITERMS

Polarization
Dispersion
Loss processes
Polycrystalline
$BaTiO_3$
Relaxation
Permittivity
Frequency
Microwave
Dielectric
Domain
Dipolar
Molecular
Electrostrictive
Coupling
Hysteresis
Ceramic
Free energy
Curie
Ferroelectric
Nonferroelectric
Crystals

UNCLASSIFIED